Copyright Warning & Restrictions

The copyright law of the United States (Title 17, United States Code) governs the making of photocopies or other reproductions of copyrighted material.

Under certain conditions specified in the law, libraries and archives are authorized to furnish a photocopy or other reproduction. One of these specified conditions is that the photocopy or reproduction is not to be "used for any purpose other than private study, scholarship, or research." If a, user makes a request for, or later uses, a photocopy or reproduction for purposes in excess of "fair use" that user may be liable for copyright infringement,

This institution reserves the right to refuse to accept a copying order if, in its judgment, fulfillment of the order would involve violation of copyright law.

Please Note: The author retains the copyright while the New Jersey Institute of Technology reserves the right to distribute this thesis or dissertation

Printing note: If you do not wish to print this page, then select "Pages from: first page # to: last page #" on the print dialog screen

NJIT New Jersey's Science & Technology University

The Van Houten library has removed some of the personal information and all signatures from the approval page and biographical sketches of theses and dissertations in order to protect the identity of NJIT graduates and faculty.

ABSTRACT

MOTION COORDINATION AND CONTROL IN THE DEVELOPMENT OF A GAIT REHABILITATION SYSTEM

by
Yazan Ahmad Manna

While most take their ability to walk for granted, some are unable to walk due to any number of pathologies, such as traumatic brain injury (TBI), spinal cord injury (SCI), and Parkinson's disease. Decreased activity has been shown to be associated with rapidly deconditioning. Rehabilitation techniques that afford patients the ability to begin reconditioning through walking sooner may ultimately enhance their return to a better quality of life. To assist the functional recovery of such patients, an appropriate afferent input to the spinal cord will help in the therapy of the patient. Manual training is labor intensive, costly, and ergonomically unfavorable and tiring to the trainer, which will make training sessions short. Task-specific exercises delivered by robotic devices have registered success in reducing impairment and increasing motor power. Advantages of using robotic devices over the manual training include: reproducibility of the movement in a physiological manner, prolongation of the training sessions. However, several shortcomings exist in the existing devices. The reliability of the hardware and software is critical for their safe operation. These devices are expensive and only available in some large rehabilitation research institutions, which limit many disabled people to get the therapy they require.

A gait pattern generation system was developed, which uses close-chain linkage mechanisms to guide the legs with coordinated movement of the leg joints to follow normal physiological gait pattern. The natural kinematics constraints of the mechanisms produce trajectories that limit the joints' range of motion (ROM) thus improving the gait training safety. The movement of the input links of gait generation mechanisms must be controlled to provide proper timing of both stance and swing phases during a training session. This research describes the development of two methods for the motion control and coordination of the linkage mechanisms. First, the desired motion profile of the input crank of the linkage mechanism is obtained in the form of continuous function of time. The first method controls the input crank of the linkage mechanism directly with a servomotor based on the derived continuous motion profile. The coordination of the mechanisms for the two legs is carried out in the motion control software. The second method proposes to achieve both timing and coordination through mechanical means so that the system works under a simple speed control. A combination of cam and planetary gear mechanisms is synthesized for this approach. The procedures for obtaining the gears ratio of the planetary mechanism, the follower motion profile and the cam profile of the cam mechanism are discussed. Computer simulation is used to demonstrate the correct timing of the ankle movements on the closed path with the two methods. It also shows that the corresponding hip and knee joints follow normal physiological gait pattern.

MOTION COORDINATION AND CONTROL IN THE DEVELOPMENT OF A GAIT REHABILITATION SYSTEM

by
Yazan Ahmad Manna

A Dissertation
Submitted to the Faculty of
New Jersey Institute of Technology
in Partial Fulfillment of the Requirements for the Degree of
Doctor of Philosophy in Mechanical Engineering

Department of Mechanical and Industrial Engineering

January 2010

Copyright © 2010 by Yazan Ahmad Manna

ALL RIGHTS RESERVED

APPROVAL PAGE

MOTION COORDINATION AND CONTROL IN THE DEVELOPMENT OF A GAIT REHABILITATION SYSTEM

Yazan Ahmad Manna

Dr. Zhiming Ji, Dissertation Advisor — Date
Associate Professor of Mechanical Engineering, NJIT

Dr. Rajpal Sodhi, Committee Member — Date
Professor of Mechanical Engineering, NJIT

Dr. Bernard Koplik, Committee Member — Date
Professor of Mechanical Engineering, NJIT

Dr. Ian Fischer, Committee Member — Date
Professor of Mechanical Engineering, NJIT

Dr. Richard A. Foulds, Committee Member — Date
Associate Professor of Biomedical Engineering, NJIT

BIOGRAPHICAL SKETCH

Author: Yazan Ahmad Manna

Degree: Doctor of Philosophy

Date: January 2010

Undergraduate and Graduate Education:

- Doctor of Philosophy in Mechanical Engineering,
  New Jersey Institute of Technology, Newark, NJ, 2010
- Master of Science in Mechanical Engineering,
  New Jersey Institute of Technology, Newark, NJ, 2005
- Bachelor of Science in Mechatronics Engineering,
  The Hashemite University, Zarqa, Jordan, 2003

Major: Mechanical Engineering

Presentations and Publications:

Manna, Yazan A. and Ji, Zhiming, "Motion Control and Coordination in the Development of a Gait Rehabilitation System", in preparation.

Ji, Zhiming and Manna, Yazan, Sep. 2008, "Synthesis of a Pattern Generation Mechanism for Gait Rehabilitation", Journal of Medical Devices, Volume 2, Number 3, Paper # 031004.

Ji, Zhiming and Manna, Yazan A., Dec. 2008, "Size Minimization of Disk Cams with Roller-Followers under Pressure Angle Constraint", Journal of Mechanical Engineering Science, Vol. 222, No C12, ISSN 0954-4062.

بسم الله الرحمن الرحيم

(وَمَآ أُوتِيتُم مِّنَ ٱلْعِلْمِ إِلَّا قَلِيلًا ﴿٨٥﴾)

صدق الله العظيم

إهداء إلى

أمي و أبي العزيزين اللذين رعاني و أحباني منذ ولادتي

وأحبهما ولن تكفي كلماتي لأشكرهما مهما كتبت

أختي و أخي الحبيبين اللذين أحبهما

زوجتي وابني أحمد الحبيبين اللذين أحبهما

In the name of Allah the most Beneficent the most Merciful

(Of knowledge it is only a little that is communicated

to you, (O men!)) Surah Isra 'a, 85.

Allah the Almighty has spoken the truth

Dedicated to:

My Dear Mother and Father: who took care of me, loved me since I was born, and whom I love. I will not be able to thank you no matter what I write.

My beloved sister and brother whom I love.

My beloved wife and my son Ahmad whom I love.

ACKNOWLEDGMENT

I would like to express my deepest appreciation to Dr. Zhiming Ji who served as my research advisor and who constantly gave me the support and help to finish my dissertation. I acquired many skills through working closely with him.

Special thanks are given to Dr. Rajpal Sodhi, Dr. Bernard Koplik, Dr. Ian Fischer and Dr. Richard Foulds for participating in my committee.

I thank my university, New Jersey Institute of Technology, and my Mechanical Engineering Department for supporting me during my study.

I thank my mother, my father, my sister, my little brother, and my wife who all constantly gave me all the support and help to finish my PhD's degree.

I also thank Magdy Mahmoud, Ammar Abdo, Dr. Riad Abdo, Ahmad Okasha, Yahia Al Smadi and Nabeel Al Saber for their support and help during my PhD study.

TABLE OF CONTENTS

TABLE OF CONTENTS
(Continued)

Chapter **Page**

LIST OF TABLES

LIST OF FIGURES

LIST OF FIGURES
(Continued)

LIST OF FIGURES
(Continued)

LIST OF FIGURES
(Continued)

LIST OF FIGURES
(Continued)

LIST OF SYMBOLS

a_i	"i^{th}" coefficient of the polynomial function
apd	Ankle plantar flexion and dorsi-flexion angles
$Beta_1$	Angle from the coupler line to coupler point
cr_1	Coupler point length or radius
d_i	Offset of link i, (meters)
hfe	Hip Flexion and Extension angles
i	Index of the coefficients of the polynomial function
j	Index of the discrete displacement point
k	Denotes the index of the corresponding coefficient that we are taking the partial derivative of "F" with respect to
kfe	Knee flexion and extension angles
n	Degree of the polynomial function
N	Number of total points
N_S	Number of teeth of the sun gear
N_P	Number of teeth of the planet gear
P_j	Approximated value of the discrete displacement point with index j
P_0	The polynomial function value at x_0
P'_0	The slope of the polynomial function at x_0
Q_1	Frame angle

${}^{base}R_0$	Orientation matrix that defines the cosine directions of frame {0} relative to the *base* frame
r_1	Frame length
r_2	Crank length
r_3	Coupler length
r_4	Rocker length
w_i	Weighting factor
x	Angular position of the gait points (in degrees)
x_c	Cam angle (in degrees)
x_{c0}	Cam angle at the start point (in degrees)
x_{cN}	Cam angle at the end point (in degrees)
x_0	The angular position of the gait point at the start of the gait cycle
x_N	The angular position of the gait point at the end of the gait cycle
X_0	X-axis of frame {0}.
X_1	X-axis of frame {1}.
X_2	X-axis of frame {2}.
X_3	X-axis of frame {3}.
y	Fitted value or approximated amount of crank rotation
y_j	Approximated value of crank rotation of the point with index j in the discrete points.
Y_0	Y-axis of frame {0}.
Y_1	Y-axis of frame {1}.

Y_2	Y-axis of frame {2}.
Y_3	Y-axis of frame {3}.
a_{i-1}	Length of link $i-1$, (meters)
α_{i-1}	Twist angle of link $i-1$, (degrees)
α_j	True value of the discrete displacement point with index j
β_l	True value of the hip/knee angle with index "l" in the discrete points
θ_i	Angle of joint i , (degree)
θ_{in}	Angular position of the gait points
θ_l	Hip/Knee angle value that results from the Inverse kinematics of the fitting with index "l" in the discrete points
θ_{ref}	The crank angle or crank position corresponding to the first point in the gait cycle
$C\theta$	Shorthand for $Cos\,\theta$
$S\theta$	Shorthand for $Sin\,\theta$
ω_{cam}	Angular velocity of the cam with respect to the global system
$\omega_{cam/carrier}$	Angular velocity of the cam with respect to the carrier link
$\omega_{carrier}$	Angular velocity of the carrier link with respect to the global system
ω_{SC}	The angular velocity of the sun gear in the gear train relative to the carrier link
ω_{PC}	The angular velocity of the planet gear in the gear train relative to the carrier link
ζ_j	True value of the point with index j in the discrete points

CHAPTER 1

INTRODUCTION

1.1 Background

Accidents from motor vehicles, sports, and falls may cause Traumatic Brain Injury (TBI), or Spinal Cord Injury (SCI) that in most cases might lead to a loss of movement (paralysis). Paralysis that involves the majority of the body, including the arms and legs, is called quadriplegia. When a spinal cord injury affects only the lower body, the condition is called paraplegia [1]. The resulting damage to the spinal cord is known as a *lesion*. There are two types of SCI; complete and incomplete injuries. A complete type of injury means the person is completely paralyzed below their lesion, whereas an incomplete injury means only part of the spinal cord is damaged. A person with an incomplete injury may have sensation below their lesion but no movement. Stroke is another leading cause of permanent disability despite continued advances in prevention strategies such as controlling the blood pressure, cessation of smoking, attention to weight control and modest exercise regiments [2]. To assist the functional recovery of people with spinal cord injury or stroke, an appropriate afferent input to the spinal cord will help in the therapy of the patient [3]. Regular manual treadmill training accomplished with the help of physiotherapists, has been shown by recent studies, can improve *walking capabilities* in *incomplete* spinal cord-injured subjects [3]. The main goal of treadmill training is to "teach" the patient to walk again [3], where the leg movements of the patients have to be assisted by physiotherapists on a moving treadmill, as shown in Figure 1.1 [4].

Figure 1.1 Treadmill training with physiotherapists [4].

The assistance of at least three therapists is needed to move the patient's legs in manual treadmill training; two therapists assist in legs movement, while the third therapist assists in torso movement. This type of trainings is labor intensive and costly. For therapists, the moving of a patient's legs during the treadmill training represents ergonomically unfavorable and tiring work and thus not attractive work [3]. Training sessions are usually short because they cause fatigue to the therapist when training one patient after another [5]. Also, a patient's gait (manner of walking) can become asymmetrical since his/her legs are moved by two therapists, each trains based on his/her individual experience [6]. The performance of a single therapist may even differ from day to day [3]. So, no reproducible or constant afferent inputs are provided, and patients are not optimally profiting from manually training, and *learning* to walk again is a slow process. The variability in training sessions makes it difficult to assess the outcome of the trainings.

It was shown by Volpe [2] that results from several groups have registered success in reducing impairment and increasing motor power with task-specific exercise delivered by *robotic devices*. In this therapy, actuators move joints of the patient in a physiological way by imposing joint movements known from recordings in healthy subjects [3] while the patient is held by a body weight support system. Use of the robotic gait trainers has several advantages. First is the reproducibility of the leg movement in a *physiological manner*, which provides an *optimal afferent input to the spinal cord* [3, 6]. Another advantage is that the locomotor training sessions can be prolonged and the walking speed can be adjusted. The third advantage is that it will be possible to examine the effects of different gait parameters (speed, step length) [3]. Several gait trainers were designed, such as Driven Gait Orthosis (DGO) [3], Supported Treadmill Ambulation Training (STAT) [7], Robotic Orthosis Lokomat [8], Haptic Walker [5], and Mechanized Gait Trainer [6]. Some of these gait trainers are shown in Figure 1.2 below.

Robotic Orthosis Lokomat

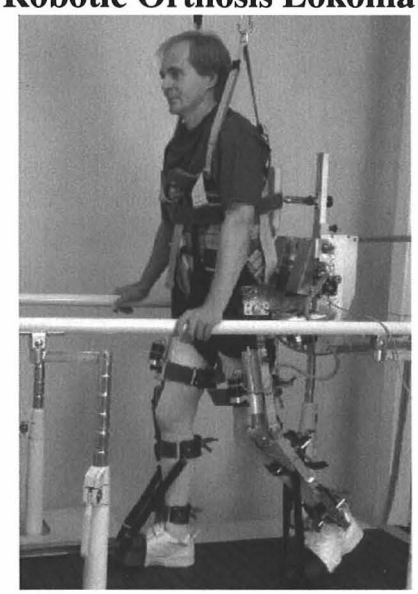

Haptic Walker

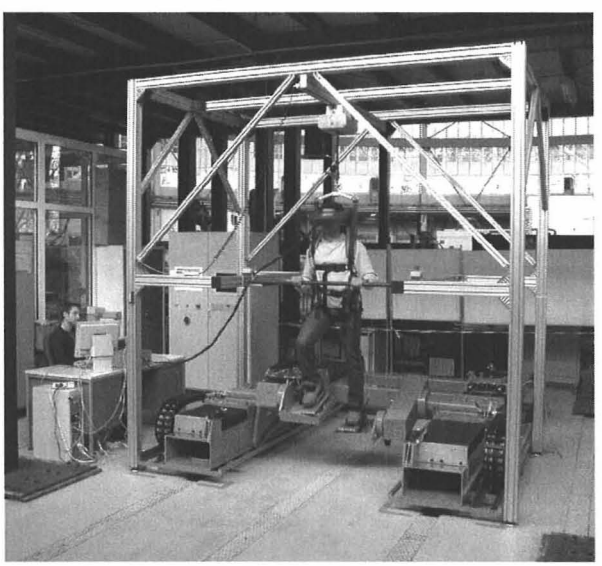

Figure 1.2 Examples of some robotic devices [5, 7].

In the DGO, the orthosis is adjustable in size so different patients can use it. Actuators at the knee and hip joints are controlled by position controllers [3]. In the STAT, the program of therapy involves simultaneously supporting a portion of the patient's weight while gait training on a treadmill [7]. In the Robotic Orthosis Lokomat, an exoskeletal orthosis is attached to patient's legs to assist the person in walking on a treadmill. In Haptic Walker, a multi-degrees-of-freedom mechanism generates foot pedal motions to simulate regular walking on an even floor, up/down staircase, and rough ground. The multiple joints in these devices must be individually and precisely controlled in order to achieve physiological gait patterns. Thus reliability of the hardware and software that control the powered joints is critical for their safe operation. Although these systems must always be operated within safety procedures, operators could become complacent and cause a mismatch between procedure and practice. There might be a gap in maintaining the system and accounting for wear and drift in use. Users' trust in powered devices with direct body contact can be a major social-technical challenge for such devices. A device with robust simplicity tends to make patients feel more comfortable and safe, thus has better chance to gain their acceptance. Currently these robotic devices are expensive and only available in some large rehabilitation research institutions. Thus, many disabled people do not get the therapy they require. The orthotic devices used in these trainers to move the legs are placed in parallel to the physical legs, which a presents a problem since they could affect the actual amount of body weight support designed for the training.

1.2 Research Objectives

The main objective of this research is to design a gait training system that is safer than the existing trainers while still move the legs in a physiological manner. Another objective is to make the new system easy to use and affordable and not limited to few rehabilitation institutions so patients can use this new system to train at home.

1.3 Research Methodology

It was observed during manual gait training, similar to the training shown in Figure 1.1, that the movement of therapists' hands that guide patients' legs forms closed-loop trajectories during each gait cycle, (a gait cycle is defined as the time interval between two successive occurrences of one of the repetitive events of walking [9]). While the trajectory formed by the subject's ankle is not exactly planar due to the motion of the trunk and abduction at the hip joint, the successful clinical trials of devices such as Lokomat show that it is practical to treat the ankle trajectories as planar in the sagittal plane. With Haptic Walker, training is performed in the sagittal plane since all major foot movements occur in this plane [5]. Similar to the development of the Lokomat and Haptic Walker shown in Figure 1.2, the design of our gait generation mechanism is based on the fact that the leg movements occur essentially in the sagittal plane [9].

The closed trajectories formed by movement of therapists' hands in Figure 1.1, could be produced by path-generation mechanisms. Such mechanisms may be used to guide the legs to produce coordinated movement of the leg joints. These trajectories can also limit the joints' range of motion (ROM) due to their natural kinematics constraints,

thus improves *safety of the gait training*. Assuming that the walking gait cycle is bilaterally symmetric, the coordination between the left and right legs can be achieved with two identical, but phase shifted, mechanisms. Hesse and Uhlenbrock used a modified crank and rocker mechanism in a mechanized gait trainer [6], where a planetary gear system replaced the crank to simulate 60/40 percent split of stance (the period when the leg is on the ground supporting the body, which is roughly 60% of gait cycle) and swing phases (the period when the leg is off the ground, which is roughly 40% of the gait cycle). It is not clear what is the resulted gait pattern generated during the entire gait cycle by this device. Since the coordination of joints motion and limitation of joints range are achieved directly through the closed trajectories of the generation mechanism, safety and reliability of the training should be greatly improved when compared with a robotic system based on open-loop mechanisms.

To achieve the objective of a gait rehabilitation system based on a simple trajectory guidance mechanism, two critical issues must be addressed. One is to define the timed trajectory for the entire gait cycle and the other is to find a proper mechanism to carry out the guidance function. This device should have both passive and active modes of operation. That is, it can be automatically controlled to manipulate affected legs in desired speed (passive mode for the user), or be programmed to have adjustable resistance to user's own movement (active mode for the user), according to the purpose and level of training. The approach towards synthesizing a four-bar mechanism to be used in such a gait training system is described in Chapter two. A conceptual design of the gait generation mechanism was developed using a computer-aided design (CAD) software.

While the mechanism alone can be used with patients to produce the desired gait movement, the timing of the mechanism must also be controlled so the movement follow the normative gait pattern during the entire gait cycle. Two approaches are presented in Chapter 3 for control of the timing in the gait generation mechanism. One will require control elements such as motion controllers, transducers, amplifiers, etc. to control the motion of the four-bar mechanism. This approach relies on the reliability of the hardware and software to control the motion of the four-bar mechanism and the coordination of the left and right legs. In order to simplify the control for ease of use, a mechanism based on the combination of cam, cam-follower and planetary gear train is proposed for the timing and coordination of the gait generation mechanisms during the entire gait cycle (i.e. during both the stance and swing phases). With this mechanism, the control of the system is no longer dependent on any servo control software and hardware. Instead, it can be activated simply with a motor running at constant speed when used in passive mode or with an input from user's unaffected leg or hand.

CHAPTER 2

MECHANISM FOR GENERATING PHYSIOLOGICAL GAIT PATTERN

2.1 Introduction

Since the gait generation mechanism should produce physiological gait pattern in the leg joints, a timed trajectory for the entire gait cycle must be defined. Then a mechanism for generating the desired trajectory must be synthesized. This chapter presents the definition of the desired trajectory and the synthesis of a four bar mechanism whose coupler curve matches closely with this desired trajectory.

2.2 Gait Kinematics Data

Understanding physiological gait patterns is critical to the definition of the desired trajectories for leg guidance. Human gait is the subject of many studies, for example [9], and data on kinematics and kinetics of human gait can be found from the Clinical Gait Analysis Normative Gait Database [10]. Since joint angles are more scalable, gait data are commonly presented in the form of the statistical average and standard deviation of different sets of measured values, normalized to full gait cycle in 50 equal time intervals. This research focuses on the gait in the sagittal plane since the leg movements occur essentially in the sagittal plane [9]. To generate ankle trajectory in the sagittal plane, hip flexion and extension (hfe) angles, knee flexion and extension (kfe) angles, and ankle plantar flexion and dorsi-flexion (apd) angles are required since these are the data that are relative to the movement in the sagittal plane. The definition and sign convention of these angles are shown in Figure 2.1.

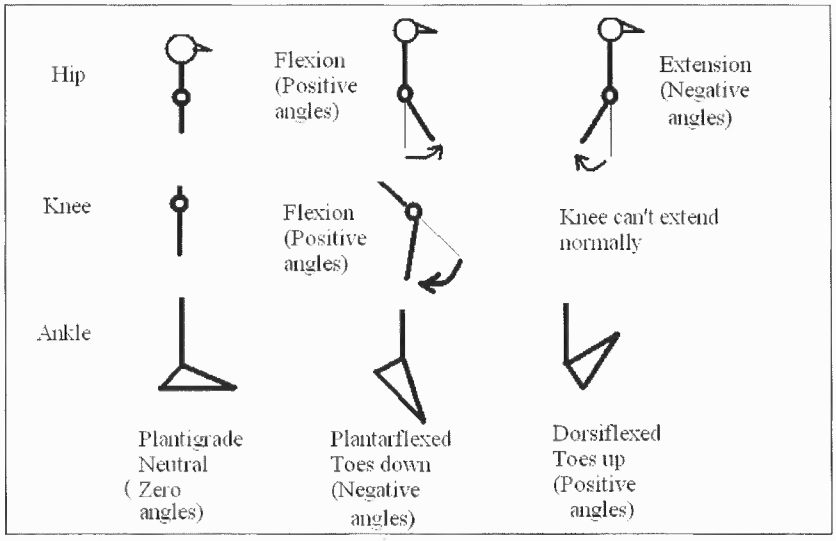

Figure 2.1 Definition and sign convention of hip flexion and extension angles, knee flexion and extension angles, and ankle plantar flexion and dorsi-flexion angles.

A gait cycle is defined as the time interval between two successive occurrences of one of the repetitive events of walking [9]. The hip and knee flexion and extension angles during a complete gait cycle are taken from Clinical Gait Analysis Normative Gait Database [10], where the initial contact is the occurrence that the gait cycle starts and ends with. Although other occurrences such as the heel rise, the toe off could be used to define the start and end of the gait cycle, the term "start of the gait cycle" refers to the initial contact event in this research.

An example set of the hip, knee, and ankle joint angles are shown in Figures 2.2 through 2.4, where they are presented in the form of the statistical average and standard deviation of different sets of measured values, normalized to full gait cycle in 50 equal time intervals.

There are 51 data points and each interval represents 2% of the whole cycle. The numerical values of these angles and their standard deviations are shown in Tables A.1, A.2 and A.3 of appendix A. Due to variation in measurement techniques and subject

selections used by different research groups, there are differences among the reported data sets. While one arbitrarily selected set of data (from the file Young.gcd by Dr. Chris Kirtley [10]) is used to illustrate the design approach in this study, the same methodology applies to the other data sets.

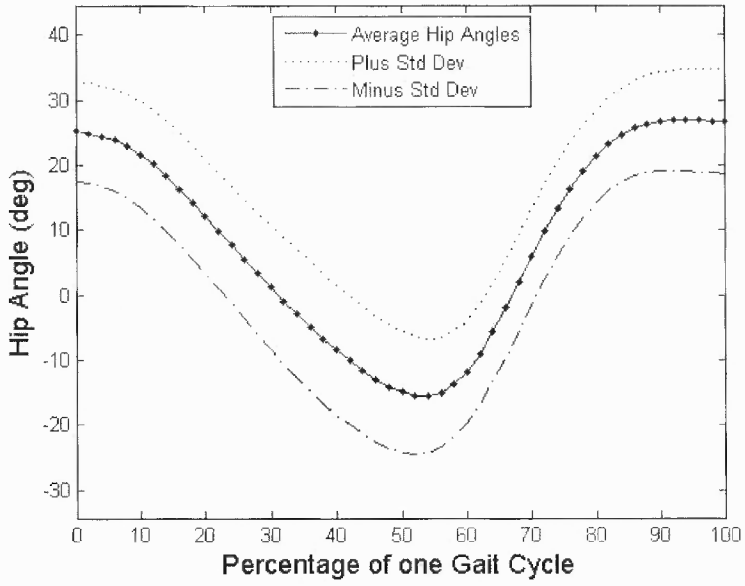

Figure 2.2 Hip flexion and extension angles in one gait cycle.

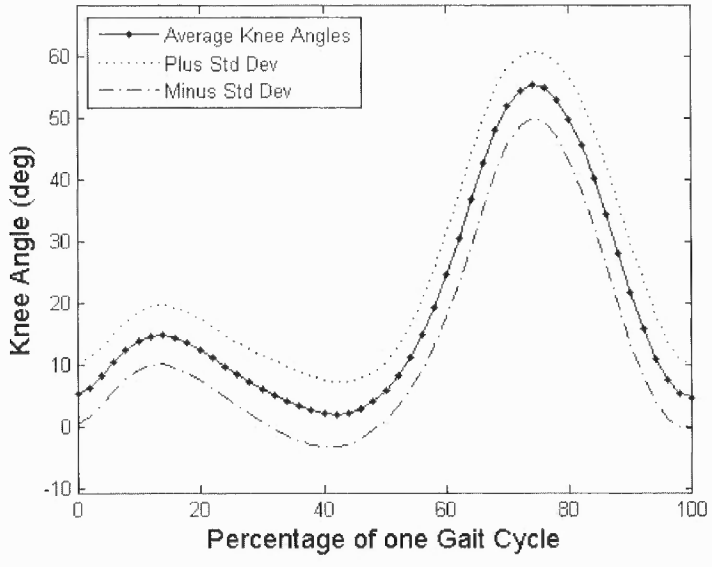

Figure 2.3 Knee flexion and extension angles in one gait cycle.

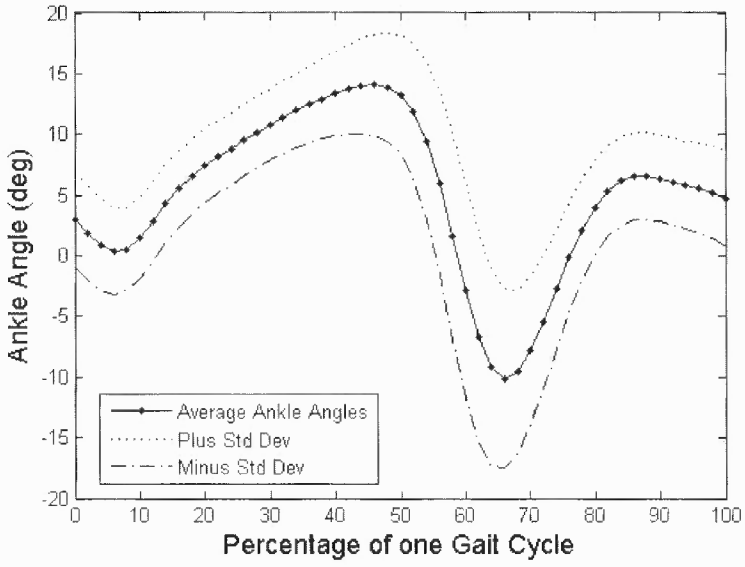

Figure 2.4 Ankle dorsi and plantar flexion angles in one gait cycle.

The upper and lower limits around the average pattern values resulted from adding and subtracting the standard deviation values to the average patterns, respectively.

While human gait form continuous cycles, it is natural to see variations among gait cycles and the reported data are the result of statistical process. This is noted from the above figures, where for each joint angle profile, the start and end values are not the same. This will cause a small discontinuity in the foot trajectory that is to be plotted. To overcome this, the last value in every figure was chosen to be equal to the start value, and thus there are 51 data points or 50 distinguished data points because point number one and 51 are equal.

2.3 Gait Kinematics

In order to use the hip and knee angles to derive the trajectory of ankle in the sagittal plane, one must have kinematic models of hip and knee joints in this plane. Since the hip is a ball-and-socket joint uniting the femur (thighbone) and the pelvis in human anatomy, it is modeled as a hinge joint in the sagittal plane. A simple hinge joint provides also a good approximation of the knee kinematics in the sagittal plane. In this study, the knee is also modeled as a hinge joint. One can treat the upper and lower legs as a two-link planar robot manipulator connected to torso via the hip and knee joint, and the foot can be treated as an end-effector.

Kinematics is the science of motion without regard to the forces which causes it. A very basic problem in the study of a mechanical robot manipulation is the forward kinematics. This is the static geometrical problem of computing the position of the robot if rotation of joints occurred. Transformation matrices [11] are used to compute such positions. The upper leg or the thigh will be treated as a link and will be called link one, while the lower leg will be treated as a link and called link two. When the hip, knee, and ankle joints rotate, the ankle will travel through a trajectory. This trajectory is to be found out using the forward kinematics. First, a universe coordinate system to which our descriptions will refer need to be defined. This coordinate system, shown in Figure 2.5, is called "base frame", which can be identified by X_{base} and Y_{base} axes in the figure. The hip, knee, and ankle joints are also shown in this figure. The frames, shown in the same figure, are attached to each joint according to the convention used in [11]. Frame {0}, which is identified by X_0 and Y_0 on the figure, is attached to the hip joint and does not rotate with this joint. Its coordinates, relative to the base frame, are given by

(X_{0base}, Y_{0base}). Frame {1} is attached to the hip joint and rotates with this joint. Frame {1} aligns with frame {0} when the hip joint or "hfe" is 0°. Frame {2} is attached to the knee joint and rotates with this joint. Frame {2} aligns with frame {1} when the knee joint or "kfe" is 0°. Frame {3} is attached to the ankle joint and rotates with this joint. Frame {3} aligns with frame {2} when the ankle joint or "apd" is 0°.

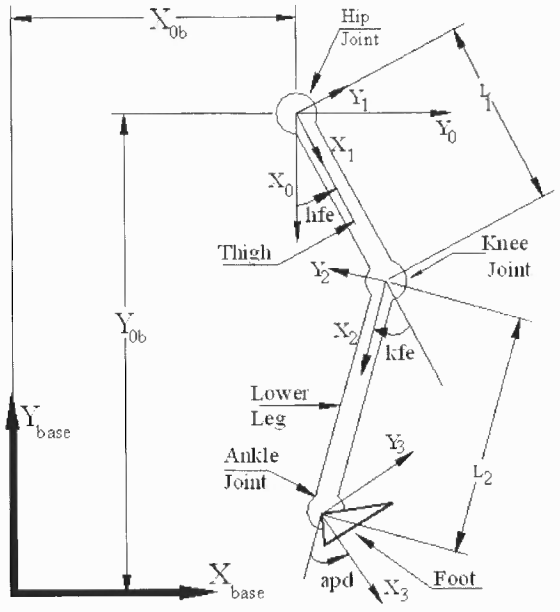

Figure 2.5 Link frame assignments.

Some parameters that describe each link and the way that the two links are connected will be presented next. These parameters are called "The Denavit-Hartenberg" (D-H) parameters, and are shown in Table 2.1.

Table 2.1 Denavit-Hartenberg Parameters for the Two Links in Figure 2.5

i	α_{i-1} (deg)	a_{i-1}	d_i	θ_i (deg)
1	0	0	0	hfe
2	180	L1	0	kfe
3	180	L2	0	apd

where

α_{i-1} : Twist angle of link $i-1$, (degrees)

a_{i-1} : Length of link $i-1$, (meters)

d_i : Offset of link i, (meters)

θ_i : Angle of joint i, (degree)

To find the transformation matrix between frame $i-1$ and frame i, ${}^{i-1}\mathrm{T}_i$, the corresponding Denavit-Hartenberg parameters are substituted in the general formula for the transformation matrix which is given by Equation 2.1 below [11]:

$$ {}^{i-1}\mathrm{T}_i = \begin{bmatrix} C\theta_i & -S\theta_i & 0 & a_{i-1} \\ S\theta_i \times C\alpha_{i-1} & C\theta_i \times C\alpha_{i-1} & -S\alpha_{i-1} & -d_i \times S\alpha_{i-1} \\ S\theta_i \times S\alpha_{i-1} & C\theta_i \times S\alpha_{i-1} & C\alpha_{i-1} & d_i \times C\alpha_{i-1} \\ 0 & 0 & 0 & 1 \end{bmatrix} \tag{2.1} $$

where $C\theta$ is shorthand for $Cos\,\theta$, $S\theta$ for $Sin\,\theta$ and so on.

Substituting the Denavit-Hartenberg parameters in Equation 2.1 yields the following transformation matrix:

$$ {}^{0}\mathrm{T}_{3}=\begin{bmatrix} C_{(hfe-kfe+apd)} & -S_{(hfe-kfe+apd)} & 0 & L_2C_{(hfe-kfe)}+L_1C_{hfe} \\ S_{(hfe-kfe+apd)} & C_{(hfe-kfe+apd)} & 0 & L_2S_{(hfe-kfe)}+L_1S_{hfe} \\ 0 & 0 & 1 & 0 \\ 0 & 0 & 0 & 1 \end{bmatrix} \tag{2.2} $$

The transformation matrix ${}^{0}\mathrm{T}_{3}$ describes the position and the orientation of frame {3} (or the foot) relative to frame {0} when the hip, knee and ankle joints rotate.

Now, a transformation matrix is needed that describes the position and orientation of frame {0} relative to the base frame.

To construct the transformation matrix ${}^{base}\mathrm{T}_{0}$, the position of the origin of frame {0} relative to the base frame is still needed. It can be easily seen that the origin of frame {0} is located at ($X_{0b}, Y_{0b}, 0$). Thus, ${}^{base}\mathrm{T}_{0}$ becomes:

$$ {}^{base}\mathrm{T}_{0}=\begin{bmatrix} 0 & 1 & 0 & X_{0b} \\ -1 & 0 & 0 & Y_{0b} \\ 0 & 0 & 1 & 0 \\ 0 & 0 & 0 & 1 \end{bmatrix} \tag{2.3} $$

The transformation matrix relating frame {3} and the base frame is needed. Thus, Equation 2.3 is multiplied by Equation 2.2 to get ${}^{base}\mathrm{T}_{3}$ as shown by Equation 2.4:

$$ {}^{base}\mathrm{T}_{3}=\begin{bmatrix} S_{(hfe-kfe+apd)} & C_{(hfe-kfe+apd)} & 0 & X_{0b}+L_1S_{hfe}+L_2S_{(hfe-kfe)} \\ -C_{(hfe-kfe+apd)} & S_{(hfe-kfe+apd)} & 0 & Y_{0b}-[L_1C_{hfe}+L_2C_{(hfe-kfe)}] \\ 0 & 0 & 1 & 0 \\ 0 & 0 & 0 & 1 \end{bmatrix} \tag{2.4} $$

2.4 Ankle Trajectory of a Human Foot

When the hip, knee, and ankle joints rotate during normal gait, the ankle of the foot will travel through a trajectory. Equation 2.4 can be used to produce the ankle trajectory with respect to the fixed hip.

A program written in MATLAB editor (M-file) is used to generate this trajectory. It basically finds the forward kinematics, thus, it was called for_kin.m. It uses the angle data "hfe" and "kfe" in Appendix A as its input. It will generate three trajectories corresponding to three different heights which are: 1.37, 1.75 and 2.13 meters (m). These three trajectories are shown in Figure 2.6. As shown, the size of each trajectory differs depending on the height used. The origin of the figure represents the origin of the base frame. One can simply choose another value of the height and find the corresponding trajectory.

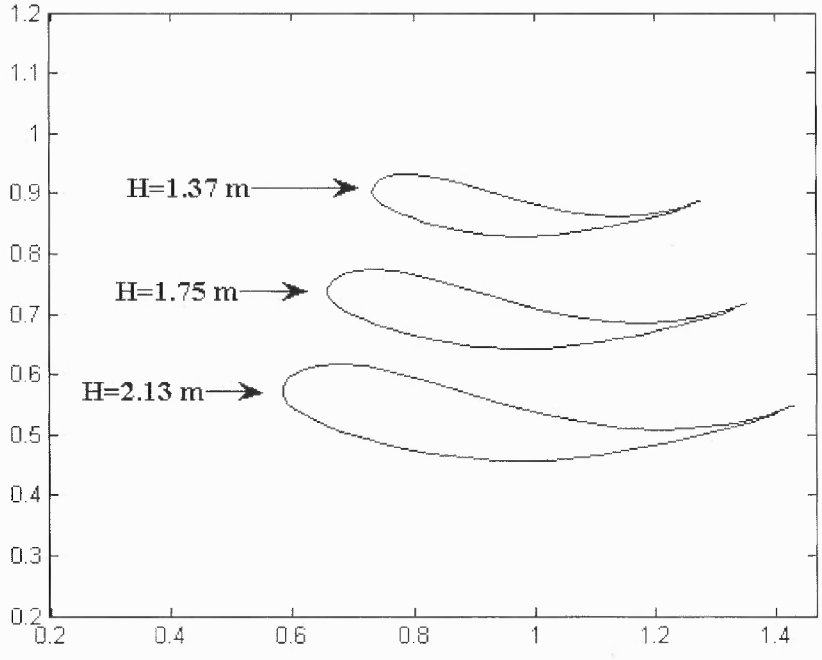

Figure 2.6 Three trajectories of the foot corresponding to three heights: 1.37, 1.75 and 2.13 m.

Since each of the hip and knee joints profiles consists of 51 values (50 distinguished values), the resulted desired ankle curve also consists of 51 points (50 distinguished points).

A relation between the body height and the body segment lengths is shown in Figure 2.7, which can be found in [12]. The upper leg's length or the thigh's length is equal to 0.245 of the body's height H, and the lower leg's length is 0.246 of H.

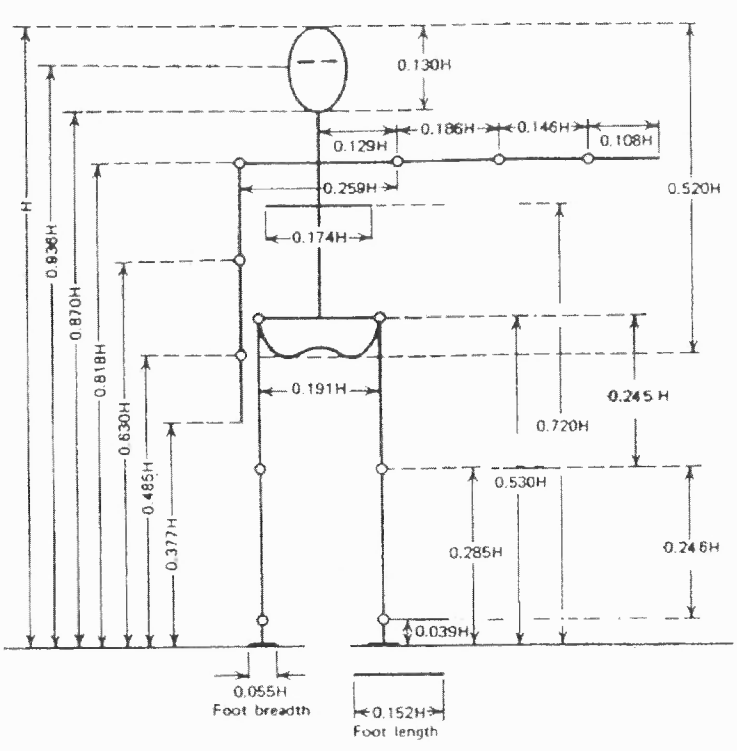

Figure 2.7 Body segment lengths expressed as a fraction of body height H [12].

These lengths ratios are used in the m-file "for_kin.m". The position part of the transformation matrix in Equation 2.4 contains the X, Y and Z coordinates of the ankle joint (frame {3}) relative to the base frame. This motion is planar, and so the Z coordinate is zero.

An ankle trajectory relative to the hip, which is generated when a person walks, was obtained. In the next sections, a four-bar mechanism is designed to generate this desired trajectory.

2.5 Synthesis of the Four-Bar Mechanism

One of the methods to design a four-bar mechanism which will generate a desired trajectory, is trying to match this desired trajectory with an atlas of coupler curves in which a displacement trajectory of a network of points on a coupler of a four-bar linkage are accurately reproduced for a wide variety of link ratios [13]. In this atlas, the charts are reproduced with the driving crank length link in all cases the same. Changing the actual link lengths but maintaining the same link length ratios does not alter the motion characteristics of the linkage. It merely introduces a scale change [13]. Thus if a linkage is designed twice the size of that shown the trajectory of a given point will be twice as large but unchanged in shape [13]. This feature means that once a trajectory is found by choosing a suitable links ratio, the scale can be changed according to the height of the person to produce the trajectories shown in Figure 2.6.

All the charts in this atlas are from Crank-Rocker type linkage. In this type of linkage, the input link (crank) is capable of rotating through a complete revolution while the output link (rocker) will oscillate between two positions. An example of a trajectory chart is shown in Figure 2.8. This is a schematic drawing that shows four motion trajectories, shown in dashed line, for four coupler points on the coupler link, for a certain link ratios.

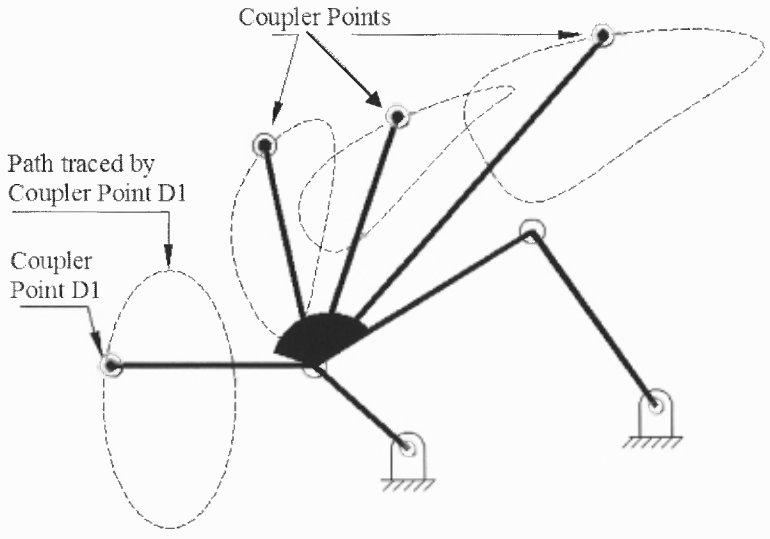

Figure 2.8 Schematic drawing that shows four motion trajectories, shown in dashed line, for four coupler points.

As shown in Figure 2.8, each coupler point will produce a different motion trajectory in shape and size. The atlas has many charts with different link ratios and different locations of the coupler points. This gives a wide range of motion trajectories. Choosing another set of link ratios, for Figure 2.8, will give different motion trajectories for the same coupler points.

There is a wide range of motion trajectories for different coupler points with different link ratios. Visual inspection to the charts can help in selecting from many different trajectories which are close in shape to the desired trajectory. Once a choice has been made for a certain trajectory, the corresponding link ratios can be used a starting point for fine tuning in order to produce better match in the shape of the trajectory.

To perform this comparison, the coupler curve (motion trajectory) of a given coupler point in a given four-bar mechanism must be drawn. There are six parameters needed to draw the displacement trajectory or coupler curve of a coupler point. These are:

frame length, coupler length, rocker length, coupler point radius (length), frame angle and the angle from the coupler line to the coupler point. A four-bar mechanism with these parameters is shown in Figure 2.9.

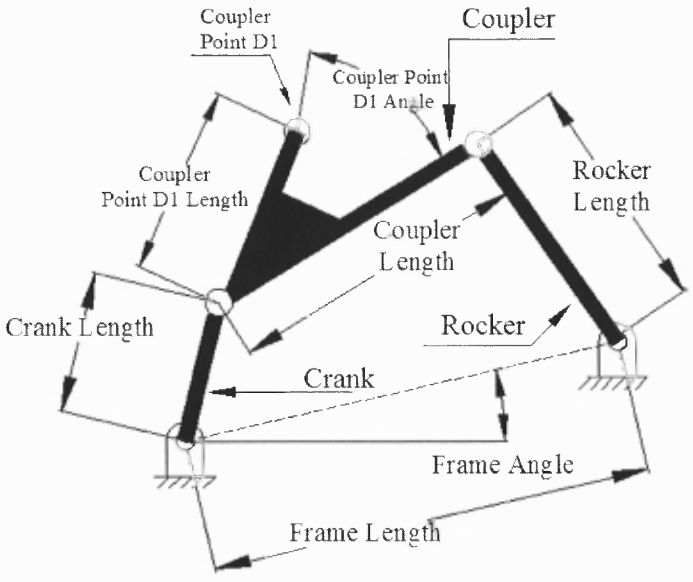

Figure 2.9 A four-bar mechanism.

A MATLAB m-file taken from [14] is used to plot coupler curves. This m-file, called "fourbar_analysis", is used to analyze a crank-rocker mechanism for position, velocity, and torque, and coupler curves [14]. Since our interest is only in the position of the crank-rocker mechanism and the coupler curve at the moment, the codes of the program dealing with velocity and torques of the mechanism are omitted and only the code relevant to the position and the coupler curve are kept. The code in the "for_kin.m" m-file is plugged into the modified "fourbar_analysis" m-file.

The nomenclature used in the "fourbar_analysis" m-file is shown in Figure 2.10, where r_1 is the frame length, Q_1 is the frame angle, r_2 is the crank length, r_3 is the coupler length, r_4 is the rocker length, cr_1 is the coupler point length or radius, and $Beta_1$ is the angle from the coupler line to coupler point.

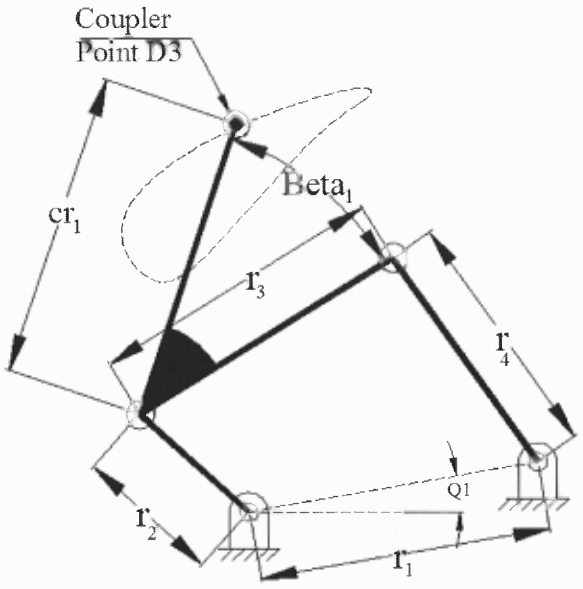

Figure 2.10 Nomenclature used in the "fourbar_analysis" m-file.

Many trajectory curves, in the atlas, are close in shape to the trajectories shown in Figure 2.6. However, many of these curves are different in their sizes and orientations from the desired trajectory. To solve the size difference, the link ratios must be scaled so that the size of the trajectory will be scaled. A scale parameter is plugged into the "fourbar_analysis" m-file to adjust the scale of the link ratios. One of the best trajectories found is shown in Figure 2.11, and a zoom-in view is shown in Figure 2.12. The solid curve is the coupler curve resulting from the selected link ratios, while the dotted curve represents the desired trajectory.

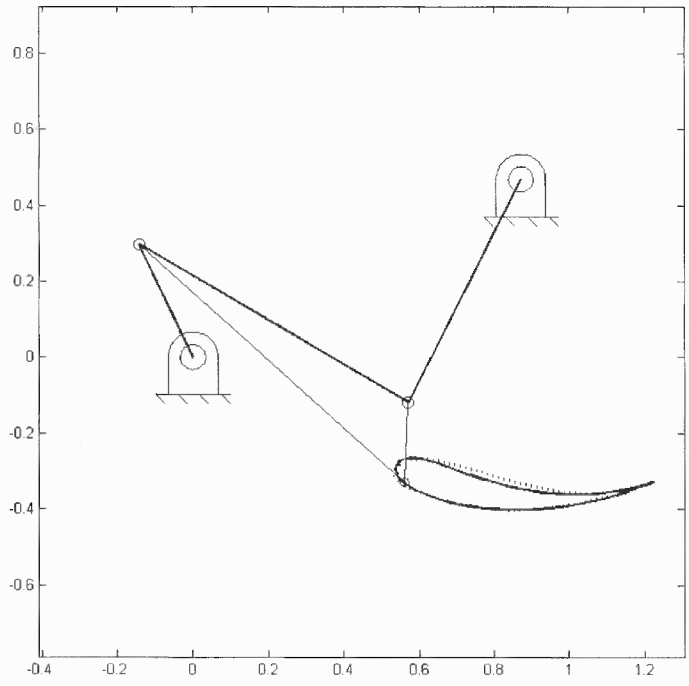

Figure 2.11 The desired trajectory compared with the trajectory generated by a four-bar mechanism for a person's height of H = 1.75 m.

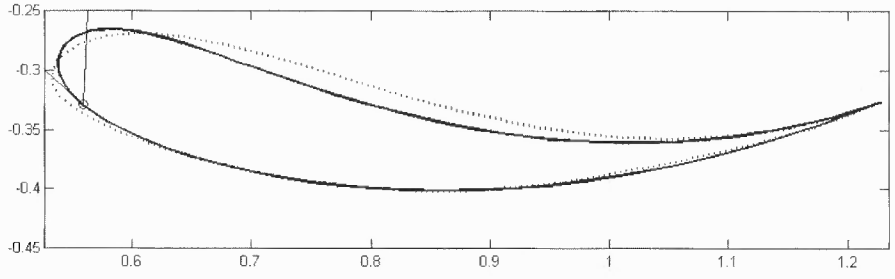

Figure 2.12 Zoom in view of Figure 2.11, where H = 1.75 m.

While the ankle trajectory i.e., the coupler curve generated by the mechanism resembles the shape and size of the desired ankle trajectory produced with the gait data, there are deviations in the trajectories. Therefore, there is a need to evaluate the results in terms of the flexion/extension at the hip and knee joints. Inverse kinematics (IK) should be performed to obtain these angles for the *generated ankle trajectory (coupler curve)* and compare it with the average gait data values shown in Figures 2.2 and 2.3.

For this purpose, the four-bar mechanism must be properly placed relative to the hip joint in the base frame so that both curves are aligned for the computation of inverse kinematics. For better match of points on the two curves, the generated points in the *coupler curve* should be far more than the number of data points in the curve obtained with the gait data (desired ankle trajectory) as shown in Figure 2.13, where the coupler curve was generated with 360 points. The box shown in the upper sub-plot is magnified and shown in the bottom sub-plot to observe the generated points on the coupler curve.

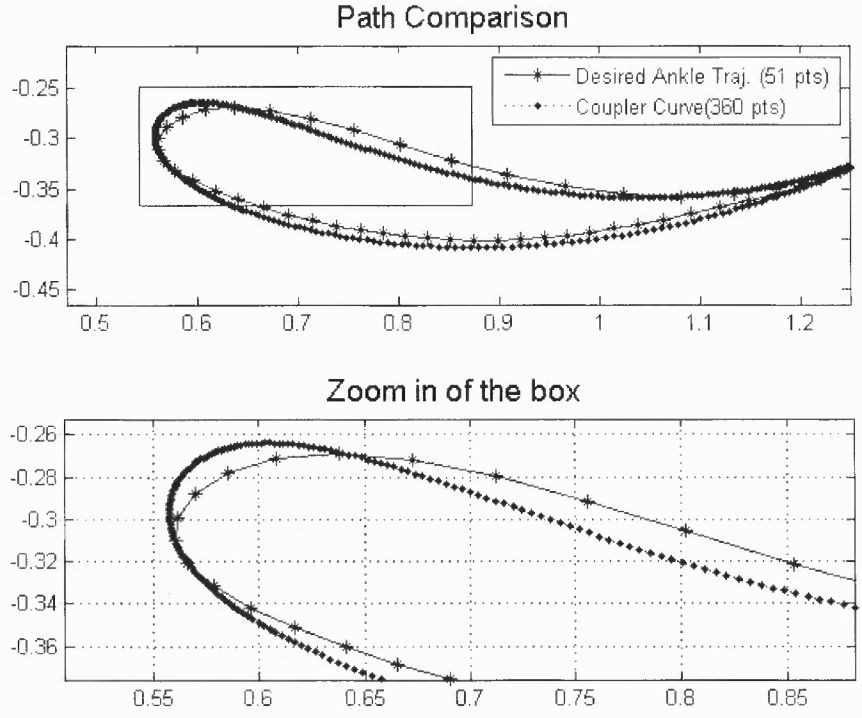

Figure 2.13 Comparison for the coupler curve with the desired ankle trajectory.

A matching routine is then performed where the coordinates of the points on the two curves are compared and the closest pairs are matched. The result of the matching is shown in Figure 2.14. In the next section, Inverse kinematics is used to obtain the resulted hip and knee angle joints.

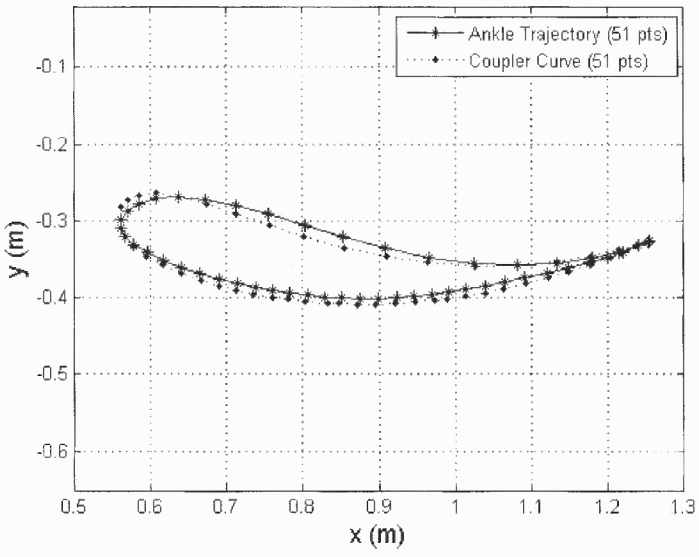

Figure 2.14 Result of matching the two curves in Figure 2.13.

2.6 Inverse Kinematic

The flexion/extension angles at the hip and knee joints resulting from moving the ankle along the generated coupler curve need to be obtained for evaluating the mechanism. Figure 2.15 is a simplified version of Figure 2.5 for obtaining these angles through the solution of the inverse kinematics.

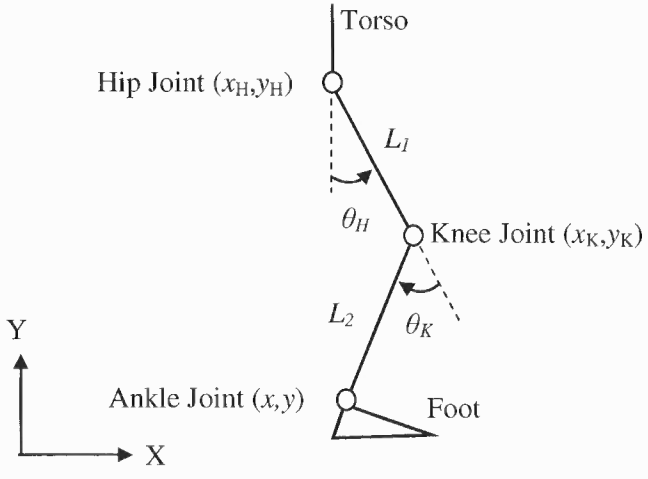

Figure 2.15 Schematics of gait kinematics.

The position of the ankle joint relative to the coordinate frame shown in Figure 2.15 was given from forward kinematics by the position part in Equation 2.4 and is shown here below with Equation 2.5:

$$\begin{aligned} x_i &= x_H + L_1 \sin\theta_{H,i} + L_2 \sin(\theta_{H,i} - \theta_{K,i}) \\ y_i &= y_H - L_1 \cos\theta_{H,i} - L_2 \cos(\theta_{H,i} - \theta_{K,i}) \end{aligned} \quad ,(i = 1,\cdots,51) \tag{2.5}$$

(x_i, y_i) represents the coordinates of the ith point in the 51 ankle positions on the coupler curve as shown in Figure 2.14. Equation 2.5 could be written as follows:

$$\begin{aligned} (x_i - x_H) &= L_1 \sin\theta_{H,i} + L_2 \sin(\theta_{H,i} - \theta_{K,i}) \\ (y_i - y_H) &= -L_1 \cos\theta_{H,i} - L_2 \cos(\theta_{H,i} - \theta_{K,i}) \end{aligned} \quad ,(i = 1,\cdots,51) \tag{2.6}$$

Squaring each line of Equation 2.6 and adding the resulted equations together yields:

$$\cos(\theta_{K,i}) = \frac{(x_i - x_H)^2 + (y_i - y_H)^2 - {L_1}^2 - {L_2}^2}{2\,L_1 L_2} \quad ,(i = 1,\cdots,51) \tag{2.7}$$

An expression for $\sin(\theta_{K,i})$ could be written as:

$$\sin(\theta_{K,i}) = +\sqrt{1 - \cos^2(\theta_{K,i})} \quad ,(i = 1,\cdots,51) \tag{2.8}$$

where it is chosen to have the positive solution in Equation 2.8 as it is known that $0° \le \theta_{K,i} \le 90°$. Then $\theta_{K,i}$ can be found as follows:

$$(\theta_{K,i}) = ATAN2(\sin(\theta_{K,i}), \cos(\theta_{K,i})) \quad ,(i = 1,\cdots,51) \tag{2.9}$$

Having found $\theta_{K,i}$, $\theta_{H,i}$ must be found. First, Equation 2.6 is expanded to get:

$$\begin{aligned} (x_i - x_H) &= L_1 \sin\theta_{H,i} + L_2\left[\sin(\theta_{H,i})\cos(\theta_{K,i}) - \cos(\theta_{H,i})\sin(\theta_{K,i})\right] \\ (y_i - y_H) &= -L_1 \cos\theta_{H,i} - L_2\left[\cos(\theta_{H,i})\cos(\theta_{K,i}) + \sin(\theta_{H,i})\sin(\theta_{K,i})\right] \end{aligned} \quad ,(i = 1,\cdots,51) \tag{2.10}$$

Combining the common terms in each line in Equation 2.10, yields:

$$\begin{aligned}(x_i - x_H) &= \left(L_1 + L_2\cos(\theta_{K,i})\right)\sin\theta_{H,i} - \left(L_2\sin(\theta_{K,i})\right)\cos(\theta_{H,i}) \\ (y_i - y_H) &= -\left(L_1 + L_2(\cos(\theta_{K,i}))\right)\cos\theta_{H,i} - \left(L_2\sin(\theta_{K,i})\right)\sin(\theta_{H,i})\end{aligned} \quad ,(i = 1,\cdots,51) \qquad (2.11)$$

Equation 2.11 can be solved for $\cos(\theta_{H,i})$ and $\sin(\theta_{H,i})$ as:

$$\begin{aligned}\cos(\theta_{H,i}) &= \frac{-(x_i - x_H)L_2\sin(\theta_{K,i}) - (y_i - y_H)\left[L_1 + L_2\cos(\theta_{K,i})\right]}{L_1^2 + L_2^2 + 2L_1L_2\cos(\theta_{K,i})} \\ \sin(\theta_{H,i}) &= \frac{(x_i - x_H)\left[L_1 + L_2\cos(\theta_{K,i})\right] - (y_i - y_H)L_2\sin(\theta_{K,i})}{L_1^2 + L_2^2 + 2L_1L_2\cos(\theta_{K,i})}\end{aligned} \quad ,(i = 1,\cdots,51) \qquad (2.12)$$

$$(\theta_{H,i} - \gamma) = ATAN2\left[\left(\frac{x_i - x_H}{r}\right),\left(\frac{y_i - y_H}{-r}\right)\right] \quad ,(i = 1,\cdots,51) \qquad (2.13)$$

The above inverse kinematics solution was programmed in MATLAB and the joint angles corresponding to the trajectory in Figure 2.13 are shown in Figure 2.16.

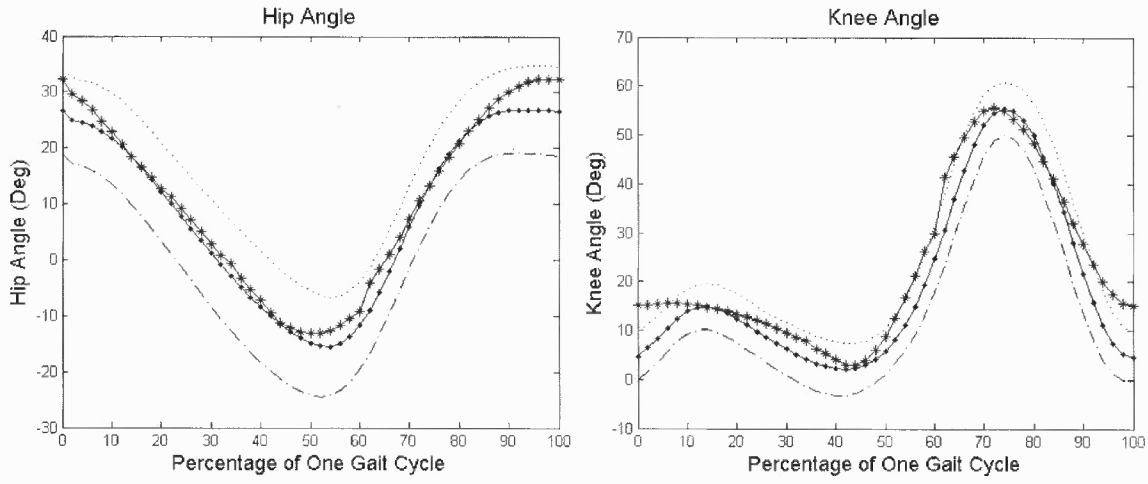

Figure 2.16 Hip and knee joint angles resulting from the coupler curve in Figure 2.14.

While the values of the hip joint angles in the figure are within the limits for most of the gait cycle, some are far from the average values especially these values in the start and end of the gait cycle. Not only is that, but the values of the knee joint angles around the start and end of the gait cycle are outside the limits.

This difference is expected since the set of link parameters is obtained from the atlas based on visual inspection. This set of values serves as the initial set and refinement is needed in order to improve the resulted hip and knee joint angles.

2.7 Refining the Four-Bar Parameters

The coupler curve shape and geometry depends on eight parameters. Seven of these are shown in Figure 2.17. These are the four link lengths (a, b, c, d), the frame angle (ψ), length (e) and angle (γ) for the coupler point P. The eighth parameter is the scale factor, k, for the link lengths. One approach of refining the four-bar link parameters is as follows. There is point P_i on the coupler curve which is closest to a point $Q_i(x_i, y_i)$ of the given ankle trajectory where $(i = 1, \cdots, 51)$. An objective function J is established, which represents the sum of the distances between these paired points. Then, different combinations of these eight parameters are generated to have different sets, and the corresponding J function value for each set is found.

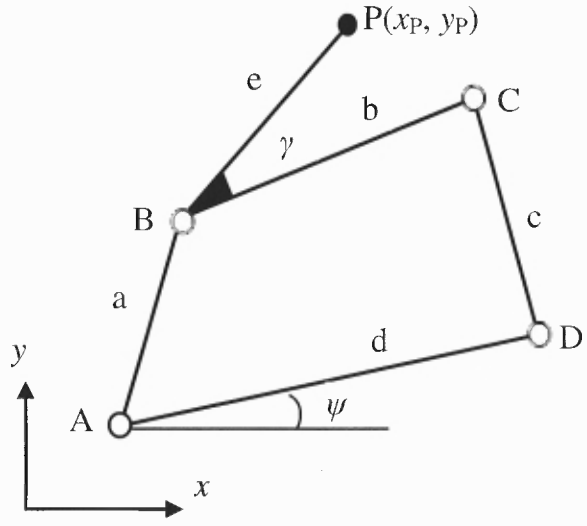

Figure 2.17 Design parameters of the four-bar mechanism.

As a certain parameter value is chosen, the step value of this change is an important factor; having smaller step value will give us extra combinations in our search to find a closer coupler curve. However, this smaller step value will need longer evaluation time when programmed through any programming language.

These different combinations were implemented in an m-file in MATLAB to find the corresponding value of function J. Table 2.2 shows some of the results.

Table 2.2 Some Results of Different Combinations

a	b	c	d	e	ψ	γ	k	J
0.99	2.36	2.09	2.9	2.75	30.03	-11	3.02	**0.1723**
1.01	2.38	2.06	2.9	2.75	29.05	-11	3.03	**0.1898**
0.99	2.38	2.07	2.9	2.78	29.05	-11	3.03	**0.1925**
1.01	2.35	2.02	2.9	2.76	29.05	-12	3.05	**0.2823**

Figure 2.18 shows the resulted hip, knee joint angles and the coupler curve for the first row.

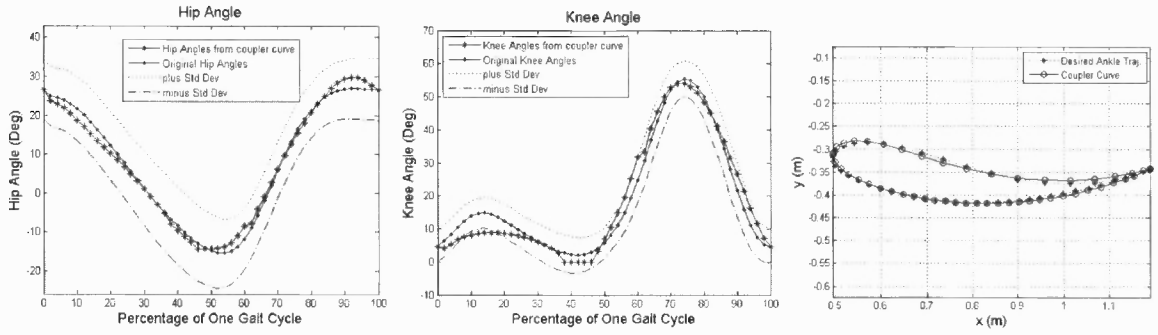

Figure 2.18 Results from the first row in Table 2.2.

Although the J value for this set of parameters is one of the lowest values calculated, the knee joint profile gave some values that were outside the range. Moreover, some values (around 40% of the gait cycle) of the knee profile could not be evaluated with the inverse kinematics as the coupler curve at these locations is slightly below the desired ankle trajectory and there is no solution for them. Yet, the hip joint angles gave results that are within the desired limits. Figure 2.19 shows the results from the hip and knee joint angles only for the remaining rows in Table 2.2.

Row 2:

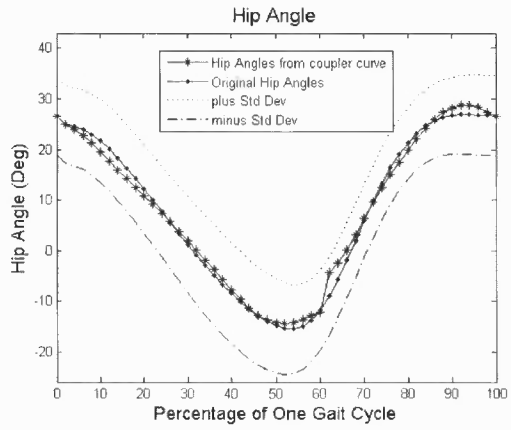

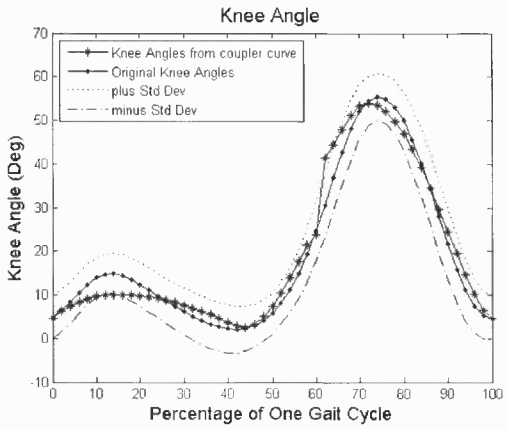

Row 3:

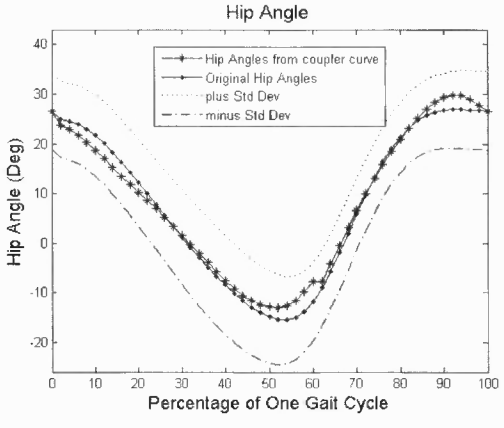

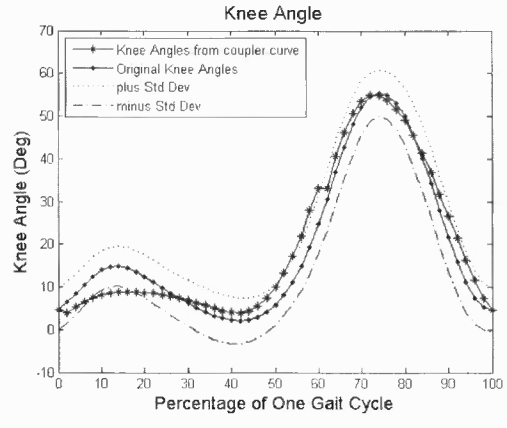

Row 4:

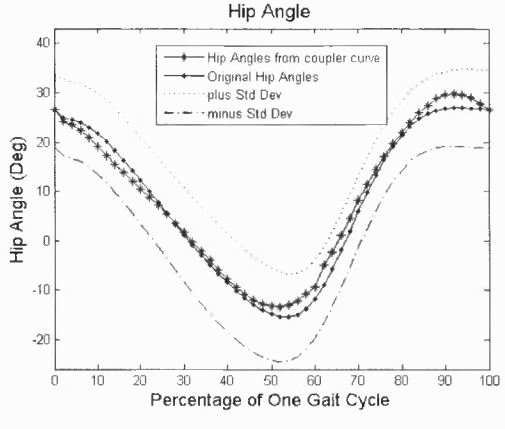

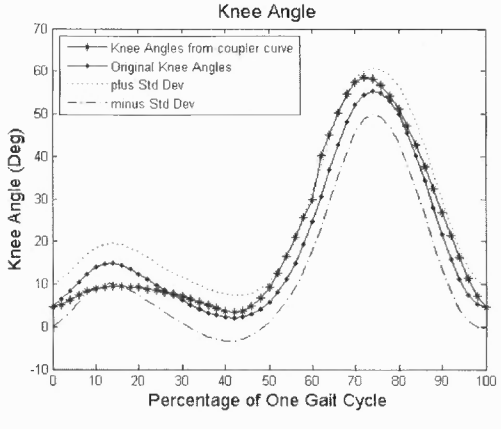

Figure 2.19 Results from rows two, three, and four in Table 2.2.

The joint profiles from the second and third rows are not smooth around 62% of the gait cycle; this is because the matching of the coupler curve in that area was not smooth. This is shown inside the ellipse in Figure 2.20 below for the coupler curve

generated with the second row parameters. Another choice of the link parameters is needed to smooth that area.

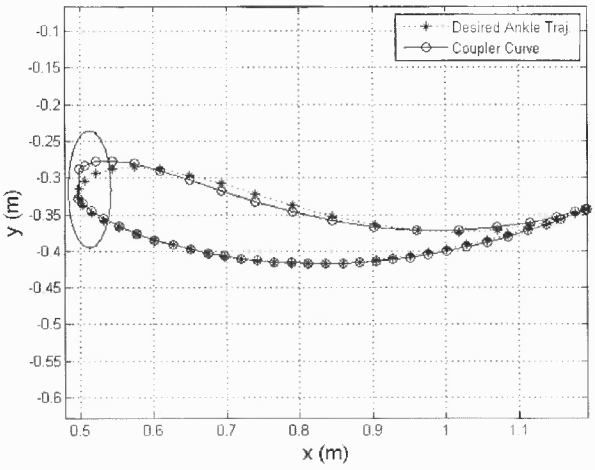

Figure 2.20 Coupler curve generated with the parameters in second row in Table 2.2.

It is obvious that not all small values of J will give us good results; some might have inverse problems, others might give unsmooth results. The joint profiles obtained from the fourth row parameters are better, although their J 's value is much larger than the other rows. Yet, some values in the knee joint profile are slightly outside the limits around 15% and 62% of the gait cycle.

This approach of refining the link parameters is time-consuming, and having a small J function value is not the only factor that will determine if good set of link parameters is obtained. Other factors include having: inverse kinematics problems, results outside the desired limits, unsmooth hip or knee joint profiles. All these factors require having a different approach, which is explained next.

This second approach, explained in details [15], implements a nonlinear least-square optimization to minimize the mean-square distance between the 50 prescribed points on the desired ankle trajectory and the coupler curve.

A point $P(x_P, y_P)$, shown in Figure 2.17, on the coupler curve can be expressed as

$$\begin{cases} x_P = x_A + a\cos\theta + e\cos(\varphi+\gamma) \\ y_P = y_A + a\sin\theta + e\sin(\varphi+\gamma) \end{cases} \tag{2.14}$$

Where the relationship between angles φ and θ can be expressed as:

$$2ab\cos(\varphi-\theta) - 2bd\cos\varphi - 2ad\cos\theta + a^2 + b^2 + d^2 - c^2 = 0 \tag{2.15}$$

On the coupler curve there is point P_i which is closest to a point $Q_i(x_i, y_i)$ of the given ankle trajectory. The sum of the distance between these paired points can be used to establish an objective function to be minimized [15]:

$$F(\mathbf{z}) = \sum_{i=1}^{m} \frac{w_i}{W}\left[\left(x_{P,i}(\mathbf{z}) - x_i\right)^2 + \left(y_{P,i}(\mathbf{z}) - y_i\right)^2\right], \quad W = \sum_{i=1}^{m} w_i \tag{2.16}$$

Where $\mathbf{z}$ is a vector of the design variables and w_i serves as a weighting factor for each pair of points. The value of m is 50 for our application. One essential step in the optimization is to locate 50 points on a coupler curve that are closest to the respective 50 points on the ankle trajectory. Each of these points must satisfy the normality condition [16] which minimizes the distance between points P_i and Q_i over crank angle θ:

$$g(\theta) = \left[x_P(\theta) - x_i\right]\frac{\partial x_P(\theta)}{\partial\theta} + \left[y_P(\theta) - y_i\right]\frac{\partial y_P(\theta)}{\partial\theta} = 0, \quad i = 1,\cdots,50 \tag{2.17}$$

From Equations 2.14 and 2.15, the following equation is obtained:

$$\begin{cases} \dfrac{\partial x_P(\theta)}{\partial\theta} = -a\sin\theta - e\sin(\varphi+\gamma)\dfrac{\partial\varphi}{d\theta} \\ \dfrac{\partial y_P(\theta)}{\partial\theta} = a\cos\theta + e\cos(\varphi+\gamma)\dfrac{\partial\varphi}{d\theta} \end{cases} \tag{2.18}$$

And

$$\varphi' = \frac{\partial \varphi}{\partial \theta} = \frac{ab\sin(\varphi-\theta)+ad\sin\theta}{ab\sin(\varphi-\theta)-bd\sin\varphi}. \tag{2.19}$$

By choosing one of points on the ankle trajectory as an exact point on the coupler curve, the design variables are eight and they are the Cartesian coordinates of the four hinge joints in Figure 2.17 are chosen as design variables, which form an 8-dimensional vector $\mathbf{z} = [x_A, y_A, x_B, y_B, x_C, y_C, x_D, y_D]^T$.

The minimization is implemented using the optimization toolbox in MATLAB, where the objective function in Equation 2.16 is re-written in a form suitable to use in MATLAB as follows:

$$F(\mathbf{z}) = \sum_{k=1}^{m} f_k^2(\mathbf{z}) \tag{2.20}$$

where

$$f_k(\mathbf{z}) = \begin{cases} \sqrt{w_k / W}\left(x_{P,k}(\mathbf{z}) - x_k\right), & (k = 1,\cdots,m) \\ \sqrt{w_{k-m} / W}\left(y_{P,k-m}(\mathbf{z}) - y_{k-m}\right), & (k = m+1,\cdots,2m) \end{cases} \tag{2.21}$$

A $2m\times 8$ Jacobian matrix $\mathbf{J}(\mathbf{z})$ is needed and can be obtained by differentiating it with respect to $\mathbf{z}$:

$$\mathbf{J}(\mathbf{z}) = \frac{\partial \mathbf{f}}{\partial \mathbf{z}} \tag{2.22}$$

An initial guess of linkage parameters is needed for the optimization, and this is obtained from the earlier sections. The desired ankle trajectory and the resulted coupler curve, which were shown in Figure 2.14, are aligned at their tips. The precision point in the optimization is therefore the tip point. This is the configuration used to form the initial

guess of **z**. To find a point P_i on the coupler curve generated with a particular **z** to match with a given point Q_i on the ankle trajectory, θ_i must be solved with Equation 2.17 and the result is substituted in Equation 2.14 [15]. An orderly search along the discrete coupler curve is conducted to locate the point that is the closest to Q_i. The points on the ankle trajectory are divided into two portions. The lower portion contains 30 intervals between points one and 31, corresponding to standing phase. The upper one contains 20 intervals between points 31 and 51, corresponding to swing phase. The points of the coupler curve are also divided into two portions for the matching process.

The five shape-defining link parameters (angle γ and four length ratios *b/a*, *c/a*, *d/a* and *e/a*) are extracted from the solution **z** obtained through the optimization. Figure 2.21 shows the path generated with this set of link parameters. The value of the objective function, F, in Figure 2.21 is 0.118 m; a value smaller than any of the results in Table 2.2. The hip and knee joint angles corresponding to the coupler points in Figure 2.21 are obtained with inverse kinematics and are shown in Figure 2.22.

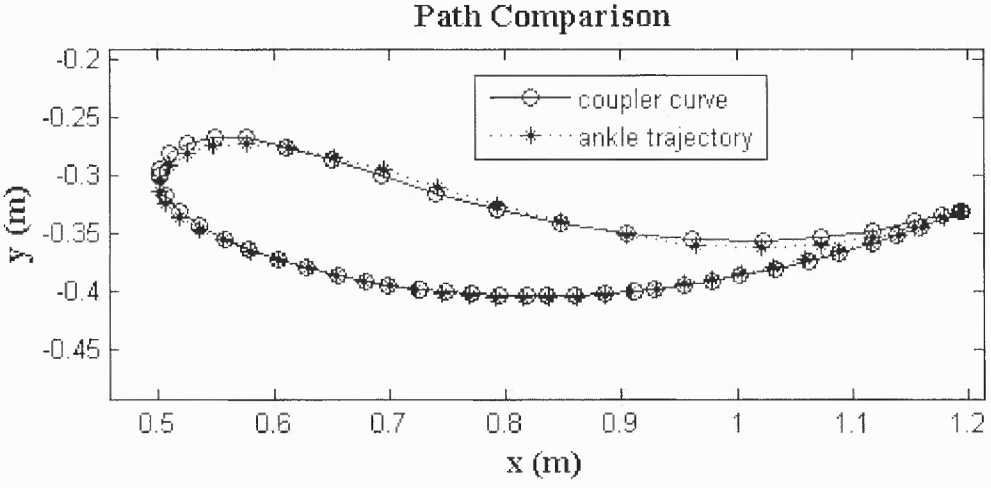

Figure 2.21 Desired ankle trajectory compared to the coupler curve generated with the resulted set of linkage parameters.

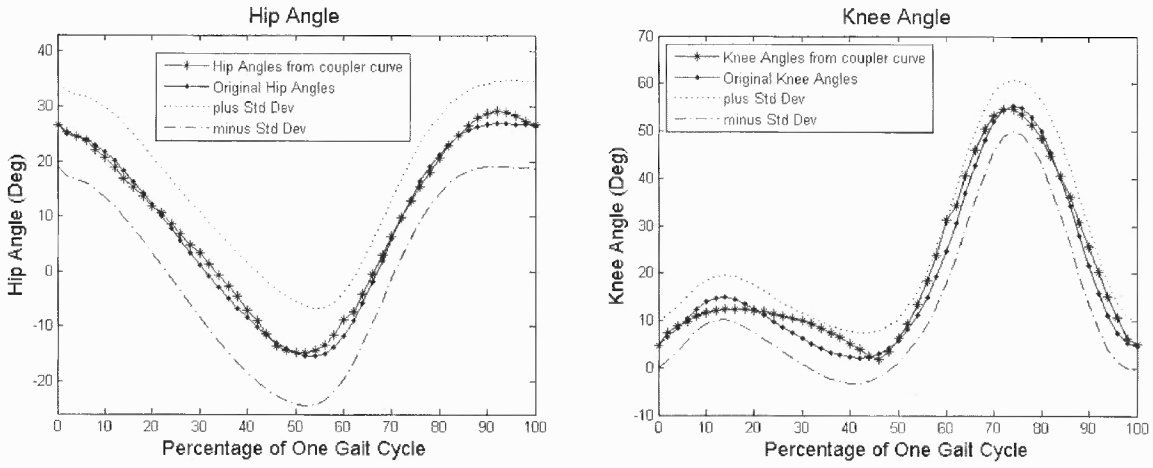

Figure 2.22 Hip and knee joint angles corresponding to the path generated in Figure 2.21 by the designed linkage.

The hip and knee joint angles profiles are within the desired limits, and for most part of the gait cycle, they are close to the average patterns. It is obvious that the four-bar mechanism limits the range of motion (ROM) in the joints (see Section 1.3).

Figure 2.23 shows the conceptual design of the four-bar mechanism, based on the obtained set of parameters, where the crank, coupler, frame and rocker links are shown. Also shown is a foot paddle which will guide the patient's foot through the *resulted coupler curve* which is also shown in the figure.

The conceptual development of the gait generation mechanism (or gait rehabilitation system) also featured a human model with average anthropometric dimensions that allowed better visualization and understanding of the actual machine operation [17]. The human model is kinematically coupled to the machine and the whole assembly presents a complex mechanism that closely simulates gait training session [17]. The human model and the total gait generation mechanism are shown in Figure 2.24.

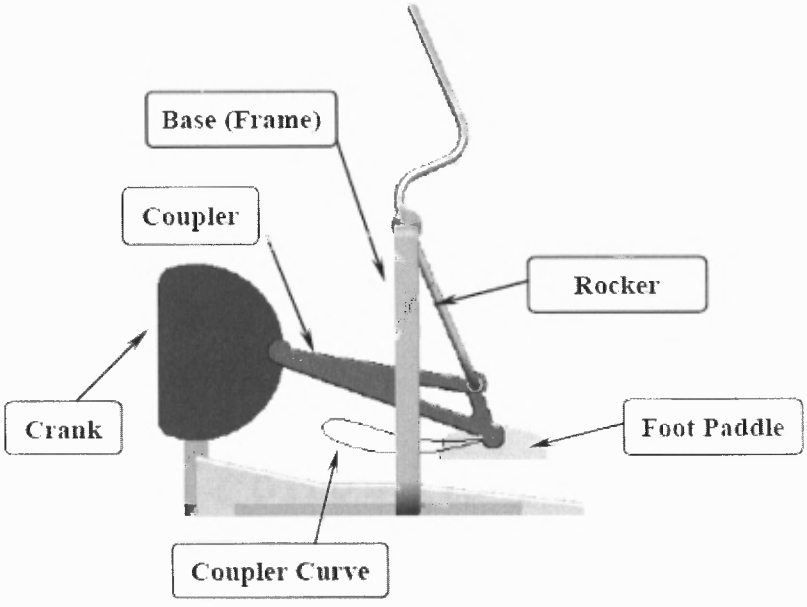

Figure 2.23 Conceptual design of the mechanism for a person of stature 1.75 m [17].

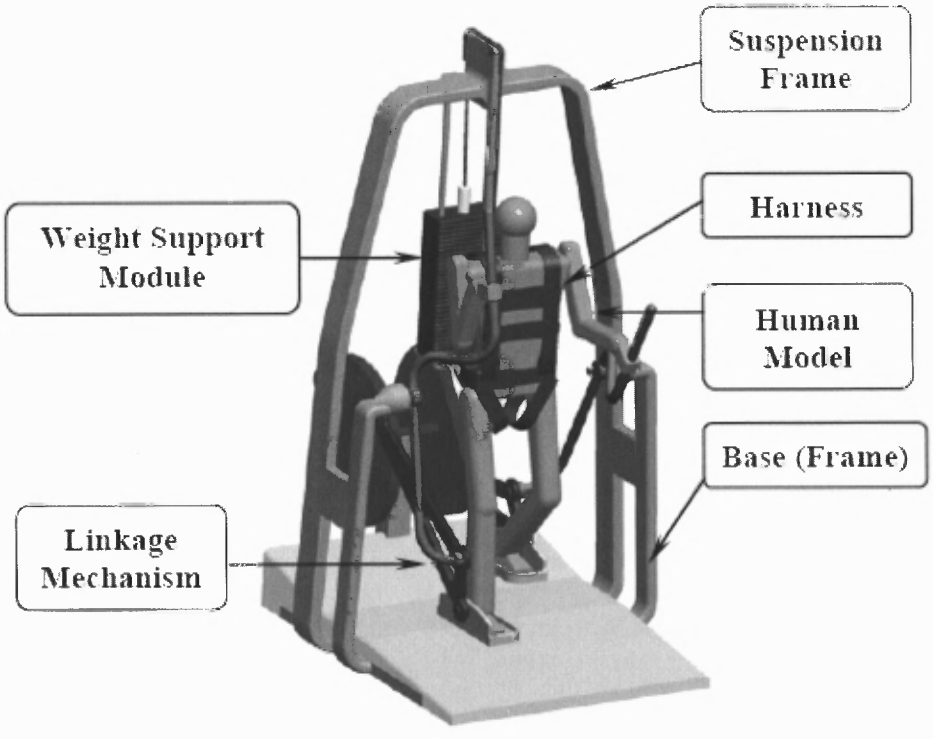

Figure 2.24 Gait generation mechanism with a human model [17].

The harness is used to hold the patient during the training session. The patient's weight is supported by the weight support system shown. The four-bar linkage mechanism delivers the desired ankle trajectory but the timing of the motion must be controlled. Since the original gait data were all normalized to a full gait cycle of 50 equal time-intervals, the linkage should guide the ankle through the 50 coupler points on the trajectory at the same time intervals. However, the crank angles corresponding to these 50 coupler points do not have the same increment. Thus the crank must rotate at a specific variable speed to achieve the desired timing of the ankle movement. Controlling the timing of the motion of the gait generation mechanism is the topic of the next chapter.

CHAPTER 3

MOTION CONTROL OF THE GAIT GENERATION MECHANSIM

3.1 Introduction

In the previous chapter, dimension synthesis for the gait generation mechanism has been performed to generate the desired ankle trajectory and then the four-bar link parameters were refined. In this chapter, we will focus on the control of this mechanism so that its motion can be properly timed according to the normative gait data. The motion profile of the input crank of the mechanism will be defined. Methods for achieving the desired motion are then discussed. In particular, the design of a mechanical timing mechanism with some motion transmission elements will be presented.

3.2 Timing Issue in Gait Generation

The mechanism presented in the previous chapter has been envisioned for achieving various objectives. It can be used as a research tool in a clinical setting where therapists can study the effects of specially designed training programs by adjusting the amount of assistance and/or resistance at certain phases of the gait.

When used as training in a home or community setting, it can be customized to have the assistance to leg movement from the unaffected leg and/or hand. The system should therefore be capable to be operated under either active or passive modes, which are defined in the sense of user effort. In the active mode, the user initiates the motion of the mechanism using the affected leg, with or without assistance from other limbs. No external actuator is used in this mode, although resistance to the user's movement may be

provided. In the passive mode, the mechanism is controlled by actuator(s) to manipulate the affected leg(s) in the desired speed.

To better understand the timing issue in the gait generation, the **desired ankle's locations** on the desired ankle trajectory must first be identified. Since the points on the gait data are collected and normalized at the fixed rate, the time elapsed between any two consecutive points on the trajectories represents 2% of the gait cycle. Thus the ankle should be guided to move through these points also at the interval of 2% of the gait cycle. There are 31 points of the points located in the lower portion of the curve, which corresponds to the stance phase which constitutes approximately 60% of the gait cycle. Figure 3.1 shows the desired timing of the ankle's locations on the desired ankle trajectory for within one gait cycle.

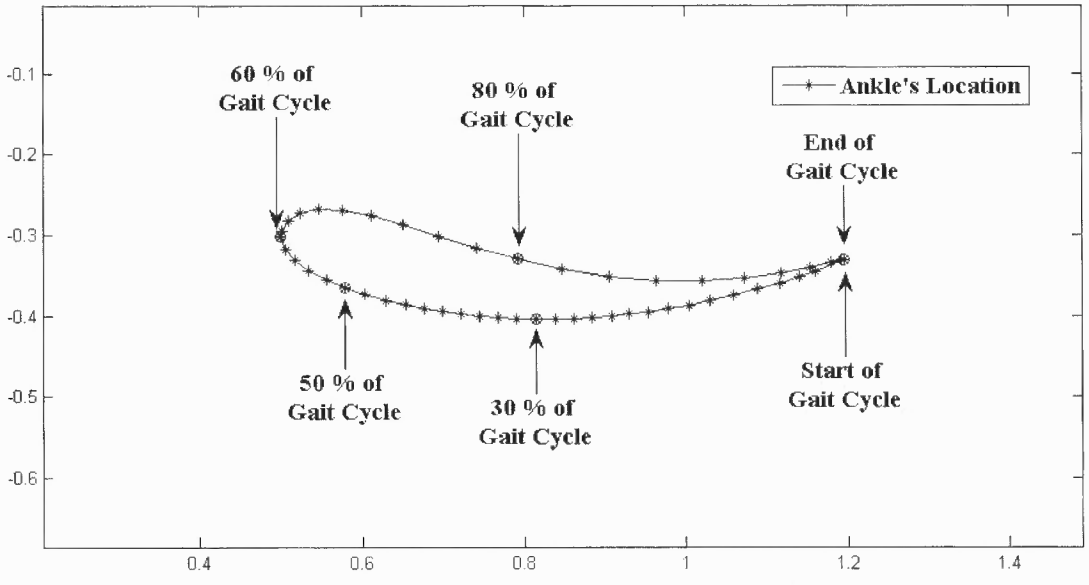

Figure 3.1 Desired timings of the ankle's locations in one gait cycle projected on the desired ankle trajectory (units are in meter).

However, the ankle position on the trajectory will not follow the desired timing if the input crank of the gait generation mechanism is moving at constant-speed. Figure 3.2 illustrates this incorrect timing with the input crank at constant speed.

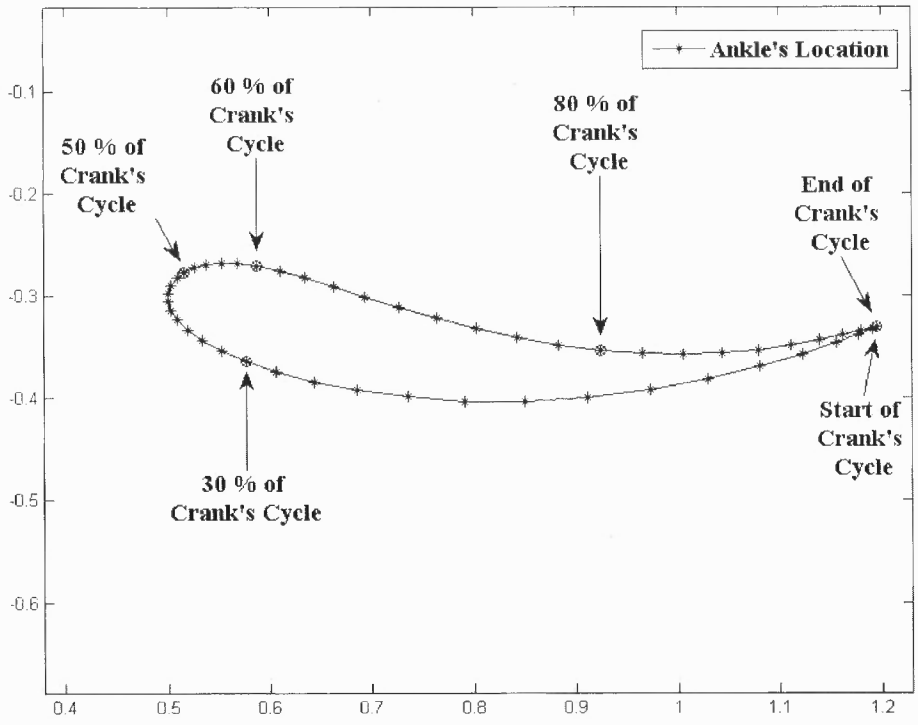

Figure 3.2 Timing of the ankle's locations when moving the input crank at constant speed in a crank's cycle (units are in meter).

It is clear that rotating the crank at constant speed will not give us the desired gait timing shown in Figure 3.1. Figure 3.3 shows the hip and knee joint angles corresponding to the timing in Figure 3.2. Thus the input crank should not be rotating at a constant speed when the motion of the mechanism is in the passive control mode.

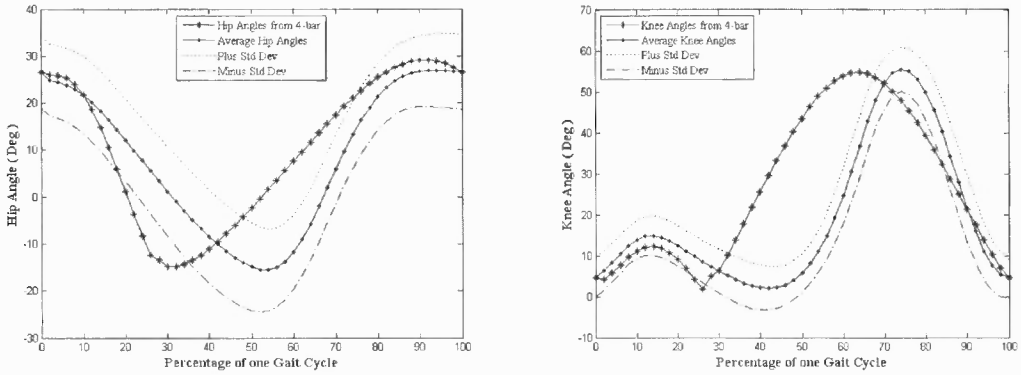

Figure 3.3 Resulted hip and knee joint angles when moving the input crank at a constant speed.

In order for the gait generation mechanism to achieve the correct timing, a motion of the input crank must be properly controlled and a continuous motion profile must be defined for the input crank so that the ankle can be guided to produce a normal physiological gait pattern. Note that the percentage of gait cycle, instead of the actual time, has been used for timing reference. This treatment enables us to define the timing of the crank rotation independent of the duration of the gait cycle, which is adjustable during gait training.

3.3 Motion Profile for the Crank of the Gait Generation Mechanism

For the purpose of defining the motion profile for the crank of the gait generation mechanism, the rotation of the crank can be viewed as the output of a timing mechanism. Because the motion of the gait generation mechanism is continuous in cycles, the input to the timing mechanism is also in the form of rotations. Thus, the motion profile for the crank of the gait generation mechanism will be defined as the input/output relation of the timing mechanism.

The first step is to identify on the generated coupler curve the points that are corresponding to the 50 points marked on the desired ankle trajectory. Let the coordinates of the points on the ankle trajectory be (x_i, y_i), $i = 1, \cdots, 50$, and the coordinates of a point on the generated coupler curve be $\big(x(\theta), y(\theta)\big)$. A search is then conducted on the generated coupler curve to locate those points, $\big(x(\theta_i), y(\theta_i)\big)$, that are the closest in distance while maintain the proper order to the individual points (x_i, y_i) on the ankle trajectory. While the generated coupler curve is continuous in nature, the search is conducted on a discrete coupler curve with sufficiently small increment of the crank angle.

Let θ_{ref} be the crank angle or crank position corresponding to the first point in the gait cycle. The resulted θ_{out} of this match process is shown in Figure 3.4 and is expressed as: $\theta_{out}(i) = f[\theta_{in}(i)] = \theta_i - \theta_{ref}$, $(i = 1, \cdots, 51)$, where θ_i is the crank position corresponding to the coupler curve points that resulted from the search above.

θ_{in} is the angular position of the gait points and can be expressed as $\theta_{in}(i) = (i-1) \times 7.2^\circ \quad (i = 1, \ldots, 51)$.

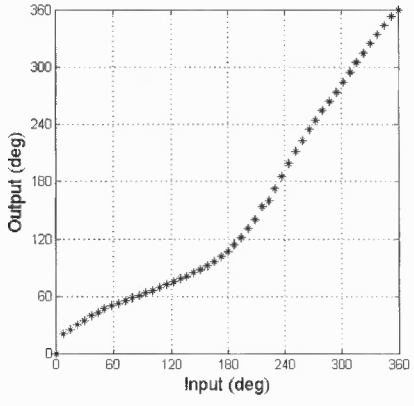

Figure 3.4 Crank displacement for gait timing from θ_{ref}.

The input/output relation of the timing mechanism is represented by a discrete set of 51 points, where the input angle θ_{in} is a linear function of time. A **continuous version of this timing function** is needed for controlling the crank of the linkage mechanism, this is to be derived in the next section.

3.4 Curve Fitting of the Timing Curve

The discrete timing curve in Figure 3.4 must be converted to a continuous function for real time control of the crank movement in the gait generation mechanism. Thus, curve fitting is used for this purpose. In curve fitting of a certain data, there are mainly two general approaches that are distinguished from each other on the basis of the amount of error associated with the data [18-20].

The first approach involves data that are experimentally obtained which might contain some experimental errors. The approach here is to avoid incorporating these errors in the approximating function but rather to find an approximation which *reflects the general trend* of the given function without reproducing local fluctuations. This approximation need not agree with the data at any point [19]. The *least-squares regression* is designed to achieve this first approach [19, 21].

The second approach involves data that are known to be *very precise*. The basic approach is to fit a curve or a series of curves that pass *directly through* each of the points. Such data usually originates from tables. The estimation of values between well-known discrete points is called *interpolation* [18].

The discrete 51 points of the input/output relation are not *very precise*. They were obtained from a geometric fit between the coupler curve and the desired ankle trajectory curve. Although this geometric fit gives close points on the coupler curve, they are not exactly located on the desired ankle trajectory curve. Even if one is able to locate them exactly on the desired ankle trajectory curve, this curve originates from the normative gait data that are presented in the form of *mean values* that have *standard deviation values*. Thus, the word *very precise* or *exact* here can not be applied to our discrete 51 points. Instead of using *interpolation* to fit these points exactly which may cause distortion to the resulted curve and not gain a smooth curve, the principle of least squares regression is the most widely used solution for the first approach [22], thus *least-squares regression* is used find an approximation that reflects the general trend of these discrete 51 points and give a smooth curve.

The least-squares regression finds a curve that minimizes the discrepancy between a certain data and this curve [18]. This is done by minimizing the squares of the residuals, or errors between the true values of the data points: $\zeta_j\,(j=1,\cdots,51)$, and the approximated values found by the regression model. The simplest example of a least-square approximation is fitting a *straight line* through a certain data, and this is called *Linear Regression*. The first step in any regression analysis should be to plot and visually inspect the data to ascertain whether a linear model applies [18].

In cases where data are obvious to be curvilinear, *polynomial regression* technique is appropriate [18]. In other cases, *transformations* can be used to express the data in a form that is compatible with linear regression. Basically, mathematical manipulations are used to transform a non-linear model to a linear one and linear

regression is applied [18]. Examples of these non linear models include using exponential equation, or a simple power equation, or a saturation-growth–rate equation [18]. All of these non-linear models are introduced to fit different data according to its behavior. Inspecting Figure 3.4 in the previous section, it can be easily seen that the data *does not form a linear behavior*, but form a curvilinear behavior. Thus, a simple line using the linear regression will not be appropriate. Although exponential or simple power models could be used, *polynomial regression* is chosen. The use of polynomial regression will allow us to *add* more terms to the approximation polynomial function to get a better fit *even after* deriving the general form of the *normal equations.* The *normal equations* are these equations that when solved, will give the required coefficients in the approximate polynomial function that yields the least squares of the errors.

One point that should be added is the use of weighted least squares in some data. Certain points through out the data are considered to be "stronger" or "better", and thus more weight is assigned to these stronger points. Such cases can happen in surveying and in astronomy [23]. In our data, all the points are equally important and no point is preferred over the others. In conclusion, the least-squares technique with polynomial regression and equal weight is used.

The general expression of the polynomial function can be given by Equation 3.1 below:

$$y = \sum_{i=0}^{n} (a_i \times x^i) \tag{3.1}$$

where:

y : is the dependent variable that represents fitted value or approximated amount of crank rotation.

i : is the index of the coefficients of the polynomial function.

n : is the degree of the polynomial function, to be decided.

a_i : is the "i^{th}" coefficient of the polynomial function.

x : is the angular position of the gait points (in degrees).

Variable x is actually time or percentage of gait cycle expressed in terms of rotary displacement of the gait points given by $\theta_{in}(i) = (i-1)\times 7.2° \quad (i = 1,\ldots,51)$.

The resulted polynomial function needs to be continuous to at least the first order since the motion and the velocity profiles of the input/output relationship will be going through several continuous cycles. Constraints to guarantee these conditions should be imposed. Using these constraints, some of the polynomial coefficients can be found in terms of these constraints. The input/output function starts at 0° and ends at 360°, which will be the start for a new cycle. To have a continuous motion, the polynomial function value at the start and end points should be 0° and 360°, respectively. The velocity should be continuous at the start and end of the cycle and this means that the first derivative of the polynomial function or the slope at these two locations should be equal to each other. However, the slope's *value* is not controlled.

Equation 3.1 has $n+1$ unknown coefficients; $a_0,\ldots,a_n$. Since, there are three constraints, this will enable us to find three coefficients, and thus the number of unknown coefficients drops to $n-2$.

The three constraints are given as:

$$y(x_0) = 0° \tag{3.2}$$

$$y(x_N) = y_N = 360° \tag{3.3}$$

$$\frac{dy}{dx}(x_0) = y'(x_0) = \frac{dy}{dx}(x_N) = y'(x_N) \tag{3.4}$$

where:

x_0 : The angular position of the gait point at the start of the gait cycle.

x_N : The angular position of the gait point at the end of the gait cycle.

For convenience of derivation, the polynomial function, Equation 3.1, can be written in the following form:

$$y = \sum_{i=0}^{n} \left(a_i \times \left(\frac{x - x_0}{x_N - x_0} \right)^i \right) \tag{3.5}$$

Since there are three constraints, they can be used to express *three of the coefficients* in terms of the remaining coefficients. Writing the polynomial function in the form of Equation 3.5 will make it easier to obtain such expressions. For example, substituting x_0 for x in the previous equation will make all the terms equal to zero, except the first term associated with a_0. Similarly, substituting x_N for x will make all the fractions equal to one, which provides a simple relation for the coefficients.

The sum of the squared difference between the true value of the discrete point and the approximated value can be used to establish an objective function to be minimized. When taking the first derivative of this function with respect to every coefficient we have, we get a set of equations, called *normal equations,* which will be solved to find the

unknown coefficients in the polynomial function. This objective function, F, is given by the below equation.

$$F = \sum_{j=1}^{N} (y_j - \zeta_j)^2 \tag{3.6}$$

where

j : Index of the discrete points.

N : Number of total points.

y_j: Approximated value of crank rotation, given by Equation 3.5, of the point with index j in the discrete points.

ζ_j: True value of the point with index j in the discrete points.

A set of polynomials' coefficients that minimizes this function is to be found. First, the partial derivative of this function is taken with respect to each of polynomials' coefficients and the resulted normal equations are set to zero, i.e. by making $\partial F / \partial a_k = 0$, where "$k$" denotes the index of the corresponding coefficient that we are taking the partial derivative of "F" with respect to. A set of equations will be obtained that could be solved for the polynomials' coefficients.

The first derivative of Equation 3.5 with respect to x is:

$$y'(x) = \sum_{i=1}^{n} \left(\left(\frac{a_i \times i}{x_N - x_0} \right) \times \left(\frac{x - x_0}{x_N - x_0} \right)^{i-1} \right) \tag{3.7}$$

Note that the summation in Equation 3.7 starts with $i = 1$ instead of $i = 0$ as in Equation 3.5.

Substituting the first constraint $y(x_0) = 0$ in Equation 3.5 yields:

$$a_0 = 0 \tag{3.8}$$

Using the second constraint, $y(x_N) = y_N = 360°$ in Equation 3.5 yields:

$$y_n = \sum_{i=0}^{n}(a_i) = a_n + \sum_{i=1}^{n-1}(a_i) + a_0 = a_n + \sum_{i=1}^{n-1}(a_i) + 0 \tag{3.9}$$

From Equation 3.9, the coefficient a_n can be written in terms of the other coefficients:

$$a_n = y_n - \sum_{i=1}^{n-1}(a_i) \tag{3.10}$$

Equation 3.10 guarantees that both the first and second constraints are satisfied. To use the third constraint, the relations for both $y'(x_0)$ and $y'(x_N)$ must be determined first. Substituting x_0 in Equation 3.7 yields:

$$y'(x_0) = a_n \times n \times \left(\frac{x_0 - x_0}{x_N - x_0}\right)^{n-1} \times \left(\frac{1}{x_N - x_0}\right) + a_{n-1} \times (n-1) \times \left(\frac{x_0 - x_0}{x_N - x_0}\right)^{n-2} \times \left(\frac{1}{x_N - x_0}\right) + \ldots$$

$$+ a_1 \times \left(\frac{x_0 - x_0}{x_N - x_0}\right)^{0} \times \left(\frac{1}{x_N - x_0}\right) \tag{3.11}$$

Noting that the all the terms will be zero expect the last term yields:

$$y'(x_0) = \frac{a_1}{(x_N - x_0)} \tag{3.12}$$

Substituting x_N in Equation 3.7 yields:

$$y'(x_N) = \sum_{i=1}^{n}\left(\frac{a_i \times i}{x_N - x_0}\right) \tag{3.13}$$

Or,

$$y'(x_N) = \left(\frac{1}{x_N - x_0}\right) \times \sum_{i=1}^{n} (a_i \times i) \tag{3.14}$$

Equating Equations 3.14 and 3.12 to satisfy the third constraint yields:

$$\left(\frac{1}{x_N - x_0}\right) \times \sum_{i=1}^{n} (a_i \times i) = \left(\frac{a_1}{x_N - x_0}\right) \tag{3.15}$$

which leads to:

$$\sum_{i=2}^{n} (a_i \times i) = n \times a_n + \sum_{i=2}^{n-1} (a_i \times i) = 0 \tag{3.16}$$

Or,

$$a_n = \sum_{i=2}^{n-1} \left(\frac{a_i \times i}{-n}\right) \tag{3.17}$$

Equations 3.17 and 3.10 are now equated.

$$a_n = \sum_{i=2}^{n-1} \left(\frac{a_i \times i}{-n}\right) = y_n - \sum_{i=1}^{n-1} (a_i) \tag{3.18}$$

Either a_1 or a_{n-1} could be extracted from the summation term in the right side. To unite the starting and ending indices in both summation terms in Equation 3.18, a_1 is extracted:

$$a_n = \sum_{i=2}^{n-1} \left(\frac{a_i \times i}{-n}\right) = y_n - \sum_{i=2}^{n-1} (a_i) - a_1 \tag{3.19}$$

Rearranging Equation 3.19 yields:

$$a_1 = y_n - \sum_{i=2}^{n-1} (a_i) + \sum_{i=2}^{n-1} \left(\frac{a_i \times i}{n}\right) \tag{3.20}$$

The above Equation for coefficient a_1 guarantees that the three constraints given by Equations 3.2, 3.3, and 3.4 will be satisfied. Joining the two summations in Equation 3.20 together yields:

$$a_1 = y_n + \sum_{i=2}^{n-1}\left(\frac{a_i \times i}{n} - a_i\right) \tag{3.21}$$

Uniting the denominators for both terms inside the summation term yields:

$$a_1 = y_n + \sum_{i=2}^{n-1}\left(\frac{a_i \times (i-n)}{n}\right) \tag{3.22}$$

Equation 3.22 should be used in the general expression for the polynomial function in Equation 3.5, since it accounts for the three constraints we need to satisfy. The summation term in Equation 3.22 starts from two and ends with $(n-1)$.

Having three constraints has enabled us to find expressions for three coefficients; Equation 3.8 for a_0, Equations 3.10 and 3.17 for a_n , and Equation 3.22 for a_1. These coefficients' Equations will be used in Equation 3.5, the general expression for the polynomial function.

Although there are two equations for a_n, the starting index of the summation terms for all the coefficient equations must be united when using them in the general expression for the polynomial function.

The summation term in Equation 3.22 starts from two and so the summation term in coefficient $a_n's$ equation needs to start from two as well, and thus Equation 3.17 is chosen.

After substituting the expressions of a_0, a_1, and a_n into Equation 3.5, the general expression for the polynomial function, this general expression is substituted in the objective function's Equation, 3.6, and the partial derivative of this function is taken with respect to each of polynomials' coefficients and the resulted equations are set to zero, i.e. by making $\partial F / \partial a_k = 0$, where "$k$" denotes the index of the corresponding coefficient that the partial derivative of "F" is taken with respect to. These resulted equations could be solved for the remaining coefficients: $a_2, \cdots, a_{n-1}$. The detailed derivations are given in appendix B, and can be expressed in the following form:

$$\mathbf{x} = \mathbf{B}^{-1}\mathbf{d} \tag{3.23}$$

where

$$\mathbf{B} = \begin{pmatrix} B_{22} & \cdots & B_{2(n-1)} \\ \vdots & \ddots & \vdots \\ B_{(n-1)2} & \cdots & B_{(n-1)(n-1)} \end{pmatrix}, \quad \mathbf{d} = \begin{pmatrix} D_2 \\ \vdots \\ D_{n-1} \end{pmatrix}, \quad \mathbf{x} = \begin{pmatrix} a_2 \\ \vdots \\ a_{n-1} \end{pmatrix}.$$

where $B_{ki} = \sum_{j=2}^{N-1} \left(b_{ij} \times b_{kj} \right)$ and $D_k = \sum_{j=2}^{N-1} \left(\left(\zeta_j - c_j \right) \times b_{kj} \right)$ can be calculated with

$$b_{ij} = \left[\left(\frac{-i}{n} \right) \times \left(\frac{x_j - x_0}{x_N - x_0} \right)^n + \left(\frac{x_j - x_0}{x_N - x_0} \right)^i + \left(\frac{i-n}{n} \right) \times \left(\frac{x_j - x_0}{x_N - x_0} \right) \right]$$

and

$$c_j = \left(y_N \times \left(\frac{x_j - x_0}{x_N - x_0} \right) \right).$$

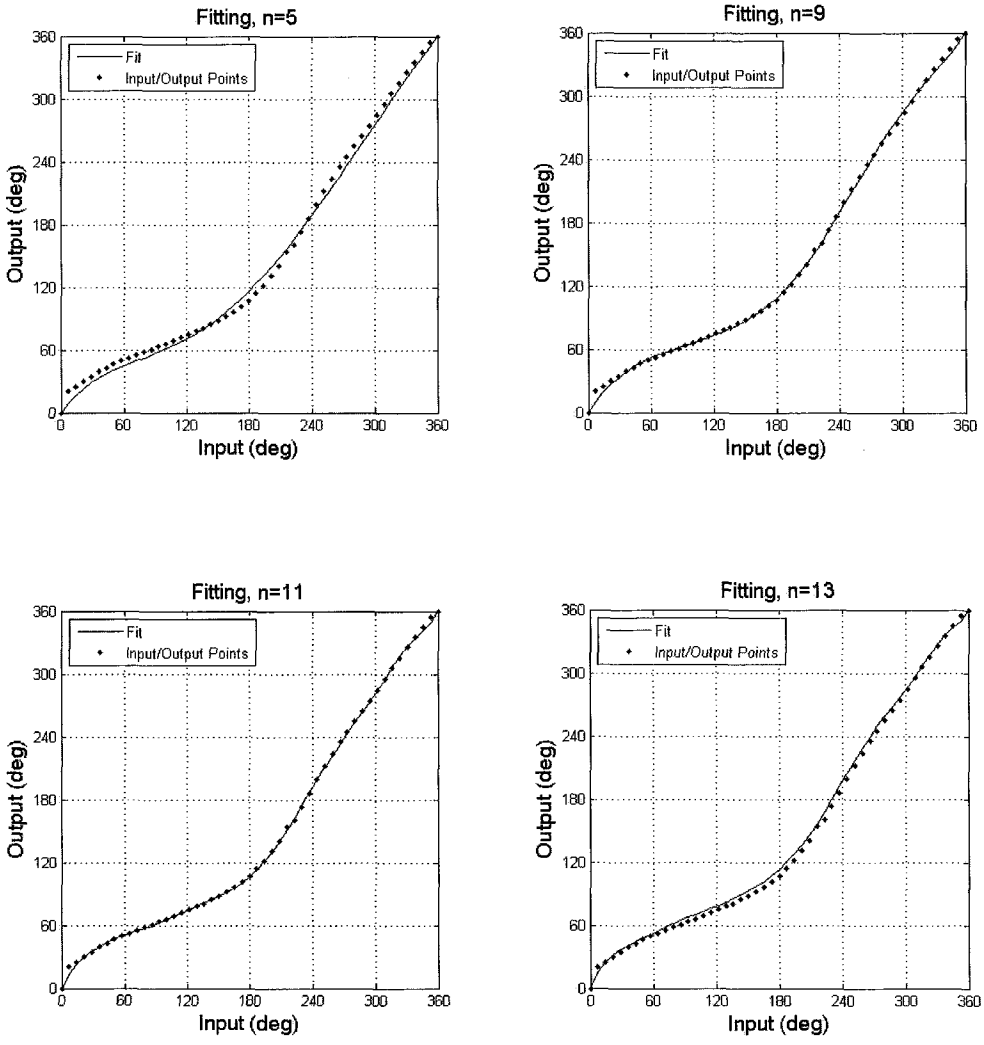

Figure 3.5 Different polynomial function fits for $n = 5, 9, 11,$ *and* 13.

The lowest value of the objective function is *176.69,* which was obtained when $n = 11$. It should be noted that the shape of the coupler curve will not be affected at all by the degree of polynomial function chosen for timing the crank rotation. We only control *where* the crank (and thus the foot on the coupler curve) will be at a certain time. This effect can be noticed on the points on the *coupler curve,* shown in Figure 3.6, for different polynomial's degrees. These points represent the foot's locations using the four-bar mechanism and they are compared to the desired foot's (ankle's) locations.

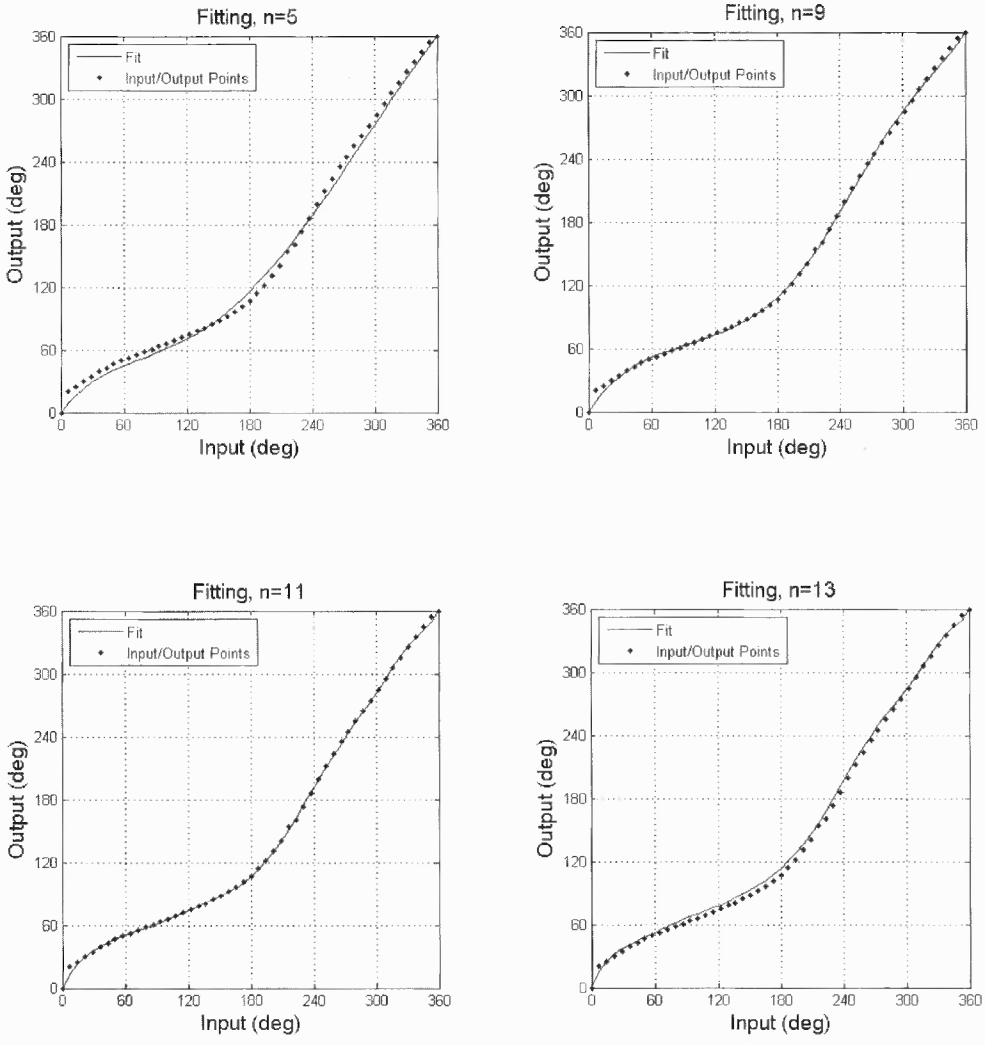

Figure 3.5 Different polynomial function fits for $n = 5, 9, 11,$ *and* 13.

The lowest value of the objective function is *176.69,* which was obtained when $n = 11$. It should be noted that the shape of the coupler curve will not be affected at all by the degree of polynomial function chosen for timing the crank rotation. We only control *where* the crank (and thus the foot on the coupler curve) will be at a certain time. This effect can be noticed on the points on the *coupler curve*, shown in Figure 3.6, for different polynomial's degrees. These points represent the foot's locations using the four-bar mechanism and they are compared to the desired foot's (ankle's) locations.

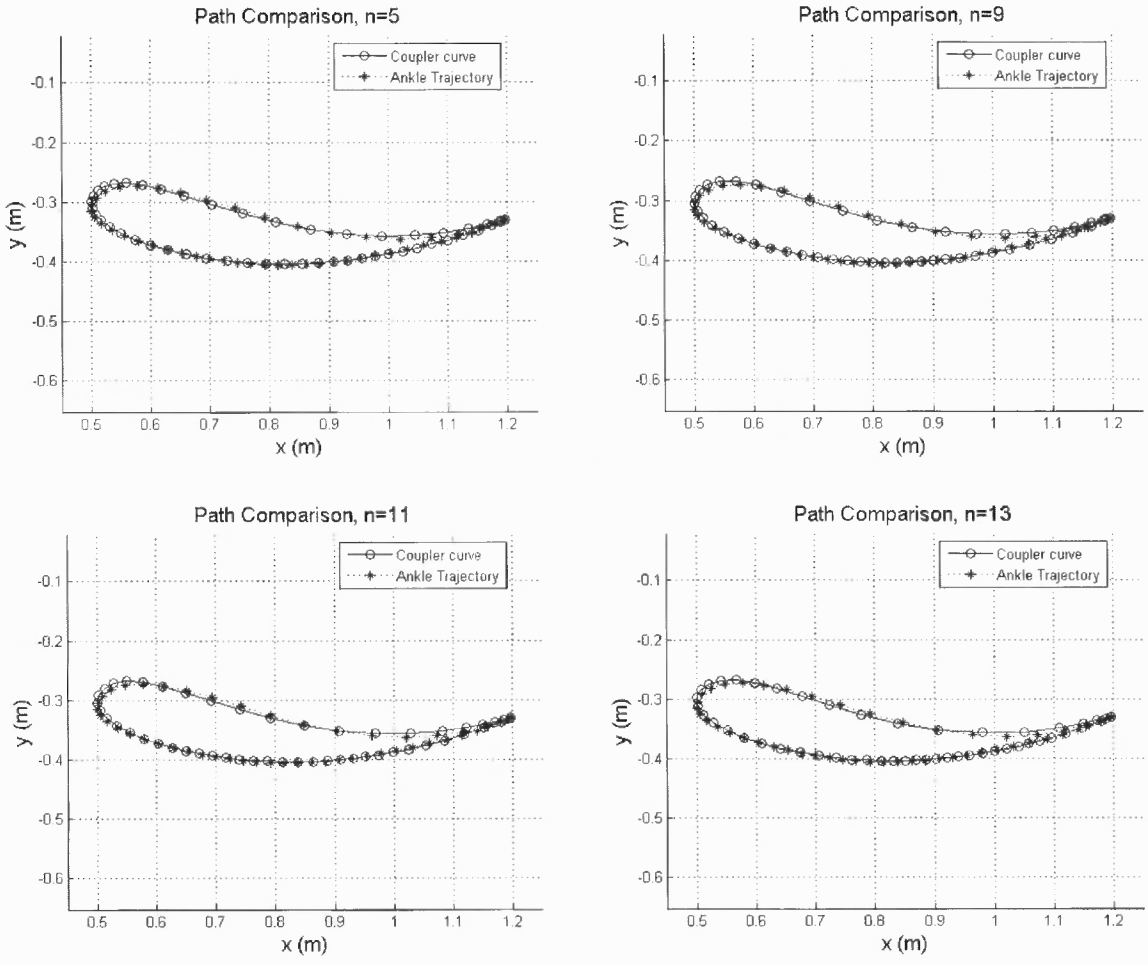

Figure 3.6 Effect of different polynomial's degree ($n = 5, 9, 11,$ *and* 13) at the foot's locations on coupler curve.

Inverse kinematics for the results in Figure 3.6 is used to find the corresponding hip and knee profiles, and compare them with average values for the normative data, or the *true values*. The comparison is shown in Figure 3.7.

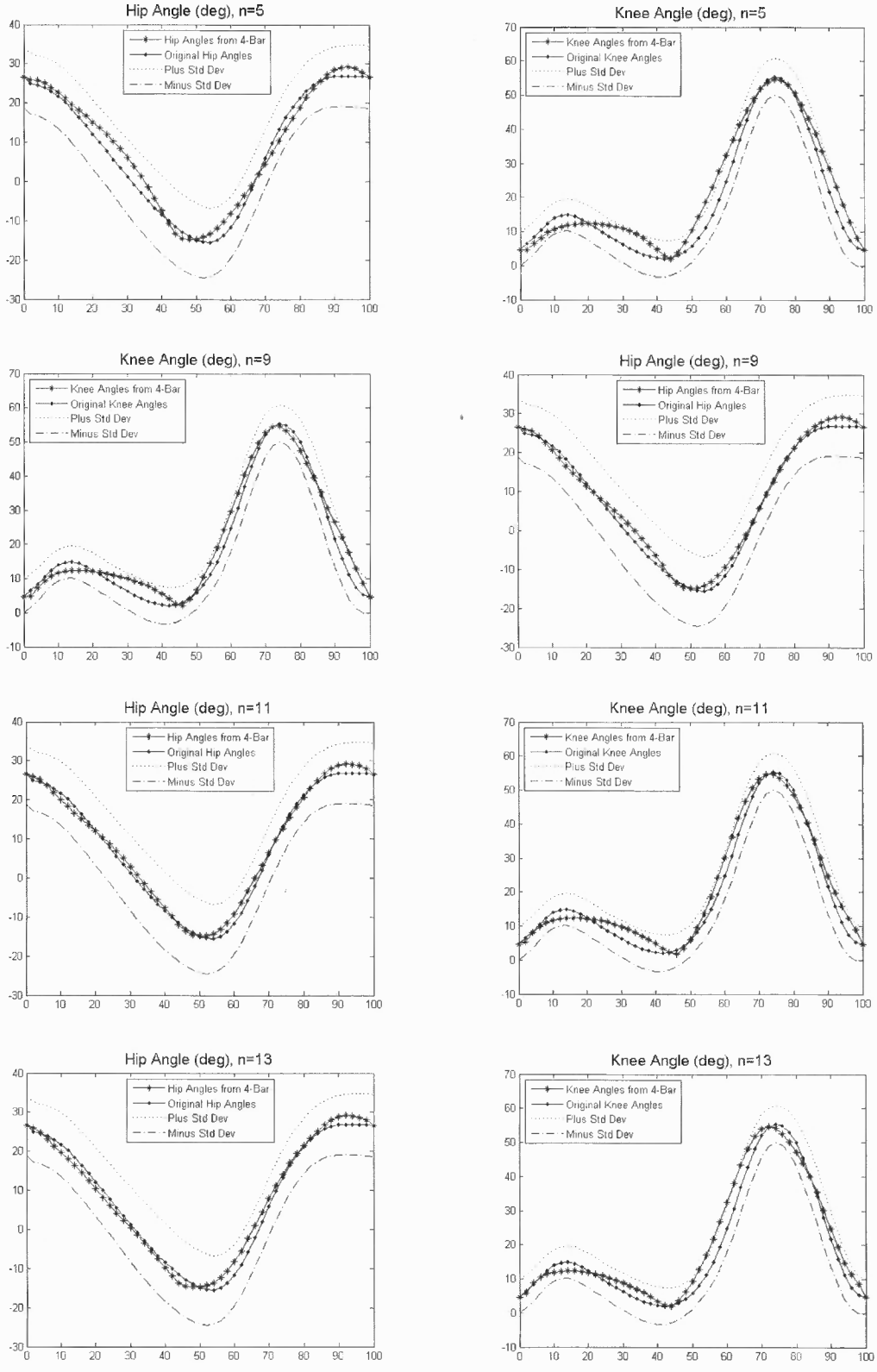

Figure 3.7 Hip and knee profiles for $n = 5,\ 9,\ 11,$ *and* 13 .

If one wants to find the sum of the squared difference between true values of the joints angles and the values resulting from a certain polynomial degrees, then it could be found using the following equation:

$$F_\theta = \sum_{l=1}^{M} (\theta_l - \beta_l)^2 \tag{3.24}$$

where:

l: Index of the discrete point.

θ_l: Hip/Knee angle value that results from the Inverse kinematics of the fitting with index "l" in the discrete points.

β_l: True value of the hip/knee angle with index "l" in the discrete points.

M : Number of total points.

For polynomial degrees ranging from 5 to 14, the value of the function F_θ at each of these polynomials for both the hip and knee profiles is found. The results are summarized in Tables 3.2 and 3.3.

Table 3.2 Hip Values of Function F_θ Values for Different Polynomial Degrees

n	5	6	7	8	9	10	11	12	13	14
F	321.6	169.4	123.8	114.9	113.8	93.6	93.3	519.2	977.4	27,872.6

Table 3.3 Knee Values of Function F_θ values for Different Polynomial Degrees

n	5	6	7	8	9	10	11	12	13	14
F	875	497.1	480.7	486.7	478.2	390	388	531.4	836.8	14,376.8

It can be seen that the polynomial function of degree "11" gave the smallest value of the function in Equation 3.24 for the hip and knee profiles, a result that agrees with that found in Table 3.1.

It should be noted that the velocity profile unit is deg/deg as can be verified by Equation 3.7. If we want to find the above velocity profile dy/dx with respect to time, i.e. we want to find dy/dt, then we need to multiply dy/dx with the *constant* angular velocity of crank ω (dx/dt) as shown below:

$$\frac{dy}{dx}\times\omega=\frac{dy}{dx}\times\frac{dx}{dt}=\frac{dy}{dt} \tag{3.25}$$

The continuous motion profile found through curve fitting is to be used to control the rotation of the cranks. A direct approach is to use a servomotor system to drive the crank of the gait generation mechanism. Since there are two cranks in this gait generation mechanism, **two separate servomotor systems are needed** to drive the two cranks independent of each other. While the right and left legs have the same movement patterns, their phases are shifted and the two servomotors systems must have *coordinate* motion control. Elements of a servomotor system are shown below in Figure 3.8:

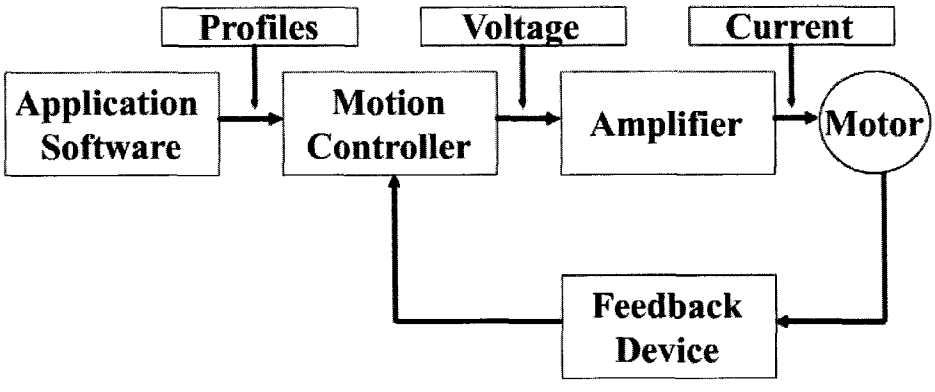

Figure 3.8: A schematic representation of elements for a servomotor [24].

Motion profile is programmed and stored in an *application software.* The *motion controller* acts as brain of the servomotor system by taking the motion profile and creating the trajectories for the motor to follow and then outputting electric pulses or analog signals to an *amplifier.* The *amplifier* generates the current required to drive or turn a *motor.* A position *feedback device* is needed to sense the motor position and report the result to the controller which, if necessary, will adjust its output to the amplifier to drive the motor to the desired position [24, 25]. Many commercial motion control systems can be used to coordinate the control of the two cranks according to the continuous timing function obtained earlier.

Since we intend to have the gait generation systems used by patients at home as a ***daily use application***, a simpler way, if can be found, to coordinate and time the motion of the two cranks will be desirable. Any chance of failure of control electronics in the gait generation system will put the patients in danger. Our use of closed trajectory to coordinate the hip and knee angles has greatly reduced the danger of failure in each individual linkage mechanism. But failure in the coordination of the two legs is still not to be tolerated. Two separate servomotor systems also add cost to the entire system. This led us to the development of mechanically based timing and coordination mechanism.

3.5 Mechanical Timing Mechanism

The input crank displacement has to follow the solid curve shown in Figure 3.9 below, with the input angle changes linearly with time. If the input crank is rotating at constant speed, then the crank's displacement will follow dotted-style line shown in the figure and the movement of the ankle along the trajectory will not be properly timed.

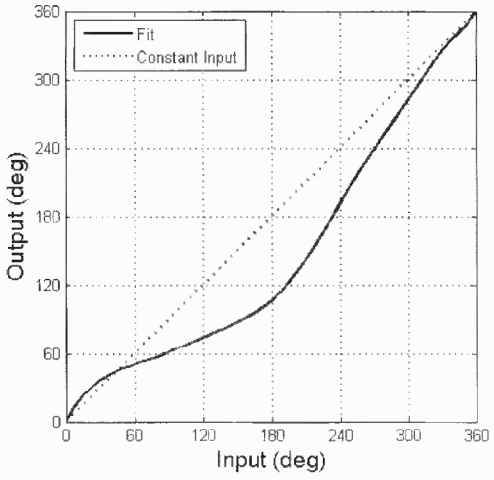

Figure 3.9 Two crank displacement curves, each is generated from a different input.

Let us image the crank of the gait generation mechanism as the output of another "fictitious" mechanism, while the input link of this mechanism is able to make full rotation at constant speed. If a "fictitious" mechanism can be found such that its input-output relationship follows our desired timing curve, then the control of the gait generation system can be greatly simplified. Any motor with simple speed control can be used to drive the input link of this "fictitious" mechanism and the rotation of the crank will be properly timed. Furthermore the same motor can be used to drive both the left and right gait generation linkages through two such "fictitious" mechanisms and there is no need to coordinate the left and right sides. This motivated us to investigate the feasibility to turn the "fictitious" mechanism into reality.

A comparison between the solid curve and the dotted straight line shows that the solid curve leads or lags the straight line during each cycle. While a drag linkage mechanism is often used to produce a non-uniform output from a uniform input rotation, it is not considered for the generation of the desired timing function. A cam-follower mechanism appears to be a more feasible way to deliver the desired lag and lead in the

follower (the crank), while the cam rotates at a constant speed. The concept of such a mechanism is shown in the next sub-section. To allow the rotation of the cam, motion must be transmitted to it through some transmission elements. The cam and the motion transmission elements compose our proposed *mechanical timing mechanism.* This mechanical timing mechanism has several advantages over the servomotor system. First, dependence on electronics will be minimized because there will be only mechanical elements that will be *controlling the motion* of the gait generation mechanism. Any failure in mechanical elements will be due to wear with time or misuse of the gait generation mechanism during training and not due to any electronics failure. Just as many elliptical trainers at home that depend on pure mechanical elements to run, our gait generation mechanism will be similar after adding the timing mechanism. Of course, just as any other mechanical system, maintenance, like lubrication, will always be needed.

Another advantage is the ability to have *only one input* for the gait generation mechanism and not *two independent inputs* as the case with the two servomotor systems. This single input will be the input to the mechanical timing mechanism. Although there will be *one single input*, this will be delivered to *both cranks* in the gait generation mechanism, unlike the case with the servomotors option. This input could be a *simple motor running at a constant speed* or an input resulting from turning a *wheel by the patient.* The phase shift in the two legs will still be achieved using the mechanical timing mechanism. A cost study of this mechanism still needs to be done.

The use of two servomotor systems to control the gait generation mechanism could still be implemented as a *research tool*, where medical researchers could research and decide, for example, if certain coordinated movements are better than others. This

option should be decided by the medical researchers in the best interest of patients. As for patients at home, a *daily use solution* consists of *the gait generation mechanism controlled by a mechanical timing mechanism* is recommended and it will be discussed in details in the next section.

3.5.1 Components of the Mechanical Timing Mechanism

As shown in Figure 3.10, the carrier link serves as the base of the cam-follower mechanism and connects the two pivots O and C. The crank link of the gait generation mechanism serves as the follower of the cam mechanism and thus the pin joint of the roller follower is on the crank. When the carrier link rotates about the pivot O, which is also the pivot of the crank, at a constant speed, it will drag the crank to move together due to the spring that maintains force-closure between the cam and its follower.

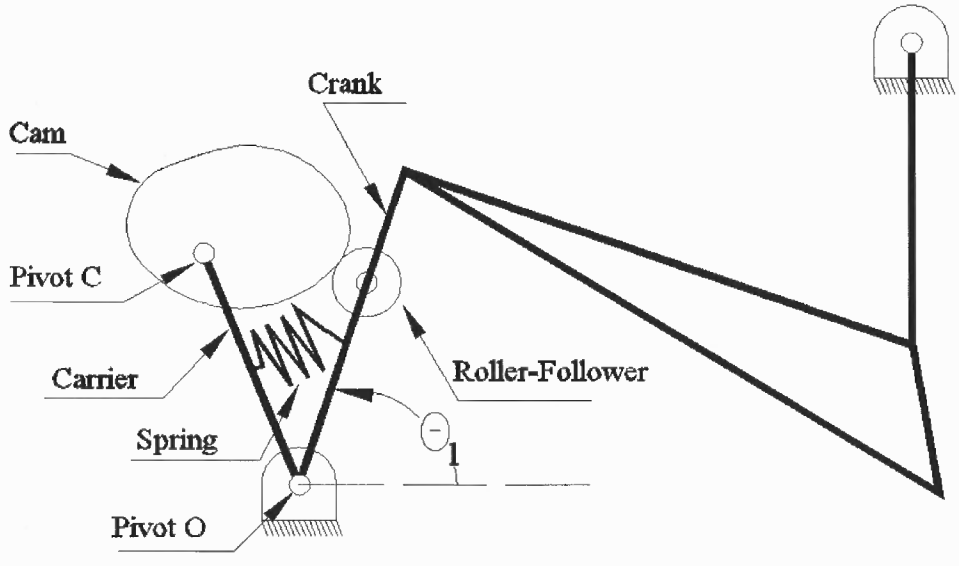

Figure 3.10 Schematic representation of the mechanical timing mechanism along with the four-bar mechanism.

If the cam does not rotate relative to the carrier link, then the crank will rotate at the same constant speed as the carrier link. To provide the desired lead and lag motion between the crank and the carrier link, the cam must be able to rotate relative to the carrier link at a proper speed and its profile is to be determined.

Motion transmission elements such as belts and pulleys systems or planetary gears could be used, but the required pulleys diameters ratios or teeth ratios for these motion transmission elements must be found.

As a summary, a simple schematic representation for the proposed mechanical timing mechanism is shown inside a dashed box shown in Figure 3.10 below. θ_1 represents the *crank angle* where it is measured from the horizontal axis.

When the crank link is driven by the mechanical timing mechanism, it will have two inputs that vary its motion and thus control and determine its motion and position. The **first input** comes from *the dragging* caused by the carrier link. The **second input** comes from *the push and drag* caused by the cam when rotating about pivot "C". Our main objective is having a timing mechanism that will make the crank link of the four-bar mechanism follow the continuous motion profile derived earlier, and thus obtain the goal of controlling the motion of the crank link and the total gait generation mechanism.

3.5.2 Design of the Motion Transmission Elements

In this section, the *gear ratios required* for a planetary gear or pulley trains that will transmit the motion from the main input to the cam are to be found. Let's assign a global coordinate system at pivot "O" that measures the angular displacement of our components. One of the requirements of this motion control is that the carrier link has to

rotate in a counter-clockwise direction so that the crank link rotates in a counter-clockwise (CCW) direction too. This angular requirement can be written in the following form:

$$\omega_{carrier} = +1 \tag{3.26}$$

The positive sign indicates a counter-clockwise direction of rotation. A negative sign would indicate a clockwise direction of rotation. Another requirement is that the cam should complete one rotation relative to the carrier about its own pivot "C" when the carrier at the same time is completing one rotation about the axis of pivot "O". There are two options for the direction of the cam's relative rotation; counter-clockwise (CCW) and clockwise (CW) directions; both options will be explored.

The angular velocity of the cam with respect to the global coordinate system can be written in the following form:

$$\omega_{cam} = \omega_{cam/carrier} + \omega_{carrier} \tag{3.27}$$

where

ω_{cam} : Angular velocity of the cam with respect to the global coordinate system.

$\omega_{cam/carrier}$: Angular velocity of the cam with respect to the carrier link.

$\omega_{carrier}$: Angular velocity of the carrier link with respect to the global coordinate system.

Since the carrier link will always make one CCW rotation (as required), i.e. $\omega_{carrier} = +1$ and $\omega_{cam/carrier}$ can be either +1 or -1, ω_{cam} can be found as:

$$\omega_{cam} = \begin{cases} 2, \text{if } \omega_{cam/carrier} = +1 \\ 0, \text{if } \omega_{cam/carrier} = -1 \end{cases} \tag{3.28}$$

The above results indicate that the cam should rotate twice as fast as the carrier or maintain a *stationary* orientation with respect to the global coordinate system.

The synthesis of the cam profile will determine which direction the cam must in; either $\omega_{cam/carrier} = +1$ (CCW direction) or $\omega_{cam/carrier} = -1$ (CW direction). The required gear ratios for both options will now be derived. Since the joint of the cam is moving in a circle generated by the carrier, the motion of the cam is similar to a planet gear in a planetary gear train, or epicyclic gear train [26].One arrangement of planetary gear train is shown in the below figure, where there are three gears in this train. A global coordinate system is assigned at pivot "O".

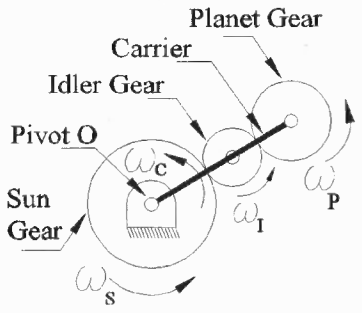

Figure 3.11 Planetary gear train with three gears.

The symbols in the figure are defined as follows: ω_P, ω_S , ω_I and ω_C are respectively the angular velocities of the planet gear, the sun gear, the idle gear and the carrier, all relative to the global coordinate system. In our timing mechanism, the cam will be attached to the planet gear such it rotates with it simultaneously. If needed, the idler gear is used to reverse the direction of rotation of the next gear in the gear train. If the number of idler gears used between the sun and planet gear is odd, then the direction of rotation of the planet gear with respect to the carrier link will be opposite to that of the

sun gear about the carrier link. If an even number is used, then there is no change in the direction of rotation between the sun and planet gears.

Another arrangement of a planetary gear train is shown in the below figure, where only two gears exist in the gear train.

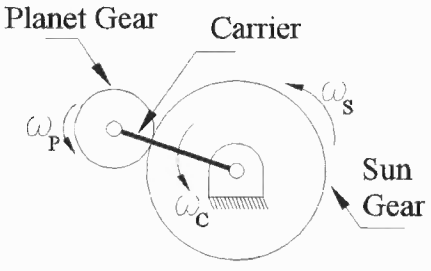

Figure 3.12 Planetary gear train with two gears.

The fundamental relation for the angular velocities of the gears in a planetary gear train (independent of the gears number in between) is given by [26]:

$$\frac{\omega_{PC}}{\omega_{SC}} = \frac{\omega_P - \omega_C}{\omega_S - \omega_C} = \pm \frac{N_S}{N_P} \tag{3.29}$$

where

ω_{PC} : The angular velocity of the planet gear in the train relative to the carrier link.

ω_{SC} : The angular velocity of the sun gear in the train relative to the carrier link. And N_S and N_P are the number of teeth of the sun and planet gears, respectively. The positive sign indicates that the sun and planet gears rotate in the same direction relative to the carrier link, while the negative sign indicates that the sun and planet gears rotate in an opposite directions relative to the carrier link. The sign depends on whether the number of idle gears used in the train is even or odd.

If a pair of pulleys, instead of gears, is used, then:

$$\frac{\omega_{PC}}{\omega_{SC}} = \frac{\omega_P - \omega_C}{\omega_S - \omega_C} = \frac{R_S}{R_P} \tag{3.30}$$

The carrier's angular velocity, ω_C, is known. The sun gear is fixed to limit the degree of freedom of the gear train, so $\omega_C = 1$ and $\omega_S = 0$.

For each of the two options of the cam's direction of rotation (CCW and CW), the required gears ratio (N_S / N_P) must be found using Equation 3.29 as shown in Table 3.4 below.

Table 3.4 Gears Ratios for CCW and CW Directions of the Cam's Rotation

ω_P (ω_{cam})	ω_C	ω_S	$\frac{N_S}{N_P}\left(\frac{\omega_{PC}}{\omega_{SC}}\right)$
0	+1	0	+1
+2	+1	0	-1

When ω_P (ω_{cam}) is 0, then (N_S / N_P) will be +1, which means that $(\omega_{PC} / \omega_{SC})$ is +1 as will. This means that the planet gear in the train, and thus the cam, should be rotating *in the same direction relative to the carrier link as that of the sun gear rotating relative to the carrier link.* Since the sun gear is fixed, and the carrier is rotating in a CCW direction relative to this fixed gear, this fixed gear is rotating in a *CW direction relative to the carrier link.* The *planet gear* then has to rotate in a *CW direction relative to the carrier link*; to meet the condition $(\omega_{PC} / \omega_{SC})$ equal to +1. The suitable gear train arrangement must be chosen from Figures 3.11 and 3.12 that will provide these required directions of rotations.

When ω_P (ω_{cam}) is +2, then (N_S / N_P) will be -1, which means that $(\omega_{PC} / \omega_{SC})$ is -1 as will. The planet gear (and thus the cam) must be rotating in an opposite direction to that of the sun gear relative to the carrier link and the number of idle gears between the sun gear and the planet gear should be **odd**. This requirement can be achieved by the arrangement in Figure 3.12 or any other arrangement that has odd number of idle gears.

The choice of the direction of the cam rotation will determine which planetary gear arrangement should be used in the mechanical timing mechanism. If a pair of pulleys is to be used, then the direction of rotation of the planet gear will be the same as of that of sun gear with respect to the carrier link. Thus, there is only one option in this case: the cam must rotate in CCW direction with respect to the carrier link.

We now proceed to the design of the cam profile which requires first finding the follower (crank) angular displacement profile.

3.5.3 Follower (Crank) Angular Displacement Profile

Before proceeding to find the required cam profile, the required follower (crank) angular displacement profile must be found. Figure 3.13 below will help in finding this profile, from which we will be able to design the cam profile.

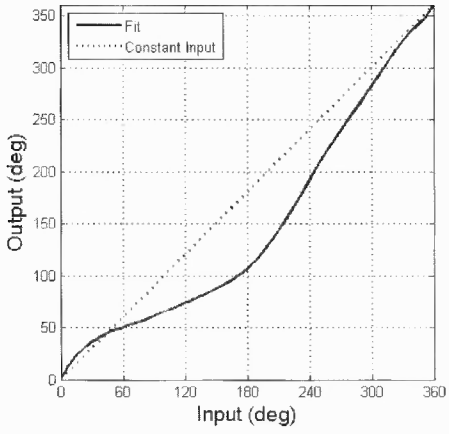

Figure 3.13 Profiles needed to find the follower angular displacement profile.

The amount of compensation or the follower angular displacement profile can be found by subtracting the continuous function from the constant input. The constant input will be of the form Cx, where "C" is a constant and "x" was defined earlier as the angular position of the gait points. The continuous function will be of the form $Y(x)$. Thus, the follower displacement profile ($\psi(x)$) can be given by:

$$\psi(x) = C\,x - Y(x) \tag{3.31}$$

The resulted follower angular displacement profile is shown below in Figure 3.14.

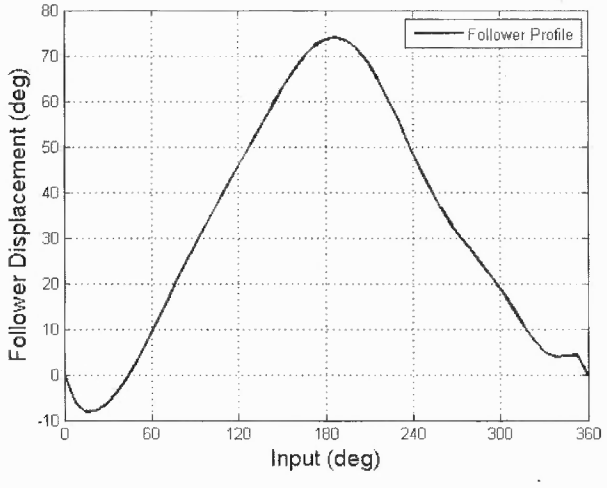

Figure 3.14 The follower angular displacement profile (compensation profile required for the follower).

If Equation 3.31 is differentiated with respect to x, the *follower velocity profile* is obtained, $(d\psi(x)/dx)$, which is given by Equation 3.32 below:

$$\frac{d\psi(x)}{dx} = C - \frac{d(Y(x))}{dx} \tag{3.32}$$

The slope of the continuous function, $\frac{d(Y(x))}{dx}$, was constrained earlier to have equal values at the start and end points. Since the *follower velocity profile is found from the slope of the continuous function subtracted from a constant "C"*, the end points of the *follower velocity profile* will also be equal, which also could be seen from the slopes at the start and end points in Figure 3.14.

The displacement profile in Figure 3.14 shows negative values at the starting position. This presents a problem for our synthesis of the cam, since we must have positive displacement relative to the base circle. To overcome this problem, the reference position of the displacement profile must be shifted as shown in Figure 3.15-b below.

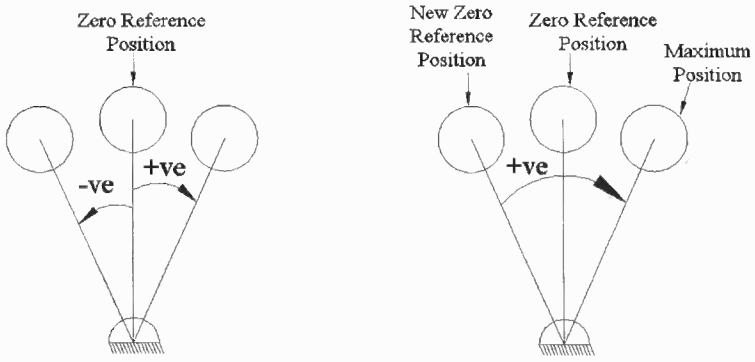

Figure 3.15 **(a)** Oscillation with negative values. **(b)** Oscillation without negative values.

The values of the follower displacement profile in Figure 3.14 range from about -8° to 75°. The follower will be oscillating between these two positions just as in Figure 3.15(a). After *vertically* ***shifting*** the follower displacement profile by adding the absolute minimum value of this profile; in this case: +8°, the follower will be oscillating between 0° and a maximum position as in Figure 3.15(b). The resulted *shifted* follower displacement profile is shown below in Figure 3.16, where it now oscillates between 0° and 83°.

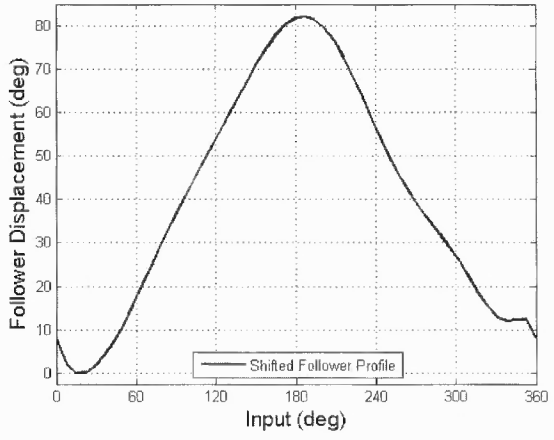

Figure 3.16 Shifted follower displacement profile.

With this shifted follower displacement profile, the follower will still have its same physical movements. However, this shifting in the follower displacement profile also requires a change in the starting position of the crank when using the mechanical timing mechanism. θ_{ref} was defined as the crank's starting position corresponding to the first point in the gait cycle. Before shifting, the required compensation for this position is 0° as can be found from Figure 3.14. However, after shifting the follower displacement profile, the corresponding compensation is 8° not 0°, see Figure 3.16. The crank position that will have the *new* 0° compensation will be called $\theta_{ref\ 2}$. The part of the cam that

gives this 0° displacement of the follower is the base circle. The crank should be placed at the $\theta_{ref\ 2}$ position and attached to the cam at the base circle. If the follower, the crank, is installed to another part of the cam, the follower (the crank) will not get the required compensations throughout its rotation.

Although the values of the follower displacement profile in Figure 3.16 are now all positive, the lowest point of the profile start is at $x = 8°$ and not at $x = 0°$. Since the cam will be used in repeated cycles, we can choose to start the cycle at the lowest point of the displacement profile. This is equivalent to moving the portion before the lowest point to the end. The rearranged profile is shown below in Figure 3.17.

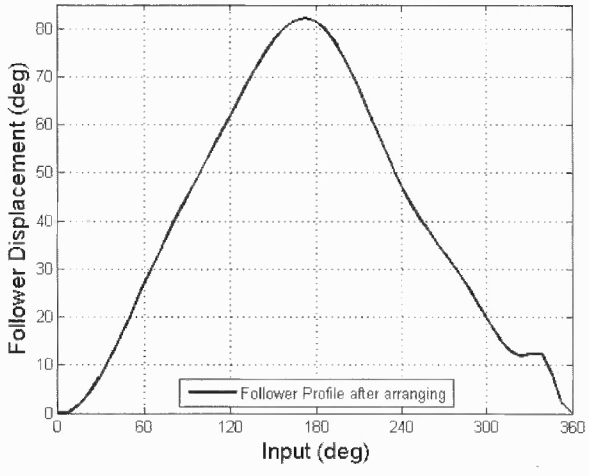

Figure 3.17 Follower displacement profile after arranging.

However, this rearrangement, while not affects the displacement continuity, will not guarantee the continuity of the *follower velocity profile.* A discontinuity at the start and end of the cycles will result in an infinite acceleration. This issue must be dealt with during the cam design.

A bump in the fall phase of the follower displacement profile is noticed. This means that *during the fall segment*, the cam profile will change its concave surface to a convex surface and then to a concave surface. Depending on the roller-follower size, undercutting might occur [26] and there might be a need to limit the roller-follower size.

To overcome the problem of discontinuity in the *follower velocity profile*, and the problem of the bump in the displacement profile, another way is proposed to define the follower displacement profile, instead of using the one derived from Equation 3.31. The essence of the idea is to smooth out the effect of discontinuity and the bump through curve-fitting based on the original discrete timing mapping data.

Since the discrete timing curve (see Figure 3.4) is represented by a set of 51 points, the *discrete follower displacement profile* will also be consisting of 51 points as shown below in Figure 3.18.

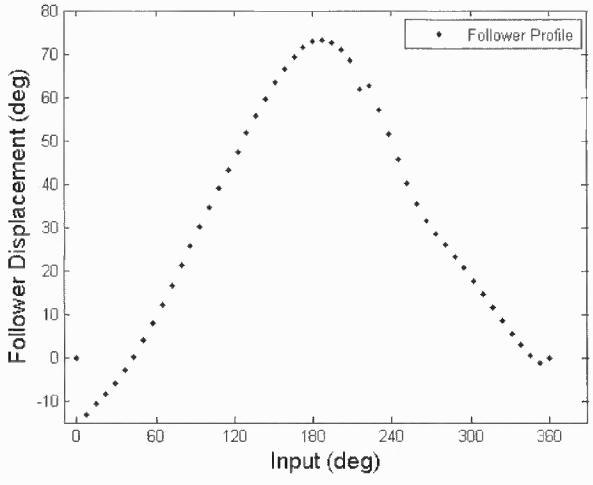

Figure 3.18 The discrete follower displacement profile.

Since no fitting has been performed to the discrete timing curve, the values of the *discrete follower profile* will be slightly different than the *continuous follower profile* in Figure 3.14.

After the necessary vertical shifting and the rearrangement performed earlier on the continuous displacement profile, the resulted profile is shown in Figure 3.19 below.

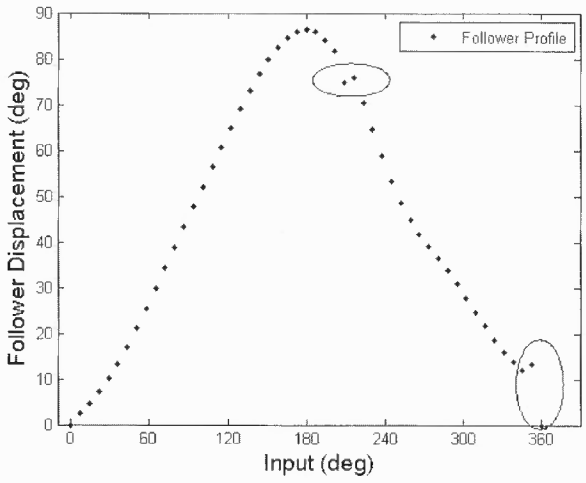

Figure 3.19 Discrete follower displacement profile after shifting and rearranging.

Two bumps are noticed in Figure 3.19. One bump, located at the end of the fall segment, is expected since it is the same one we had previously in the continuous follower profile. The other bump, located near the top of the profile, is resulted directly from the discrete input-output relation but it does not show in the continuous displacement profile because it has been smoothed out in the fitted curve.

The same *least-squares regression* with polynomial function and equal weights, introduced in Section 3.4, is now used to obtain the continuous displacement profile based on the discrete data shown in Figure 3.19. The slopes of the follower profile at the start and end points will be constrained to be equal. Thus, the follower velocity profile will be continuous and the acceleration profile will be finite.

The polynomial function that will be used to fit the points in Figure 3.19 can be written in the following form:

$$P(x_c) = \sum_{i=0}^{n} \left(a_i \times \left(\frac{x_c - x_{c0}}{x_{cN} - x_{c0}} \right)^i \right) \tag{3.33}$$

The variables n, i, a_i, were defined in Section 3.4. x_c is the cam angle (in degrees), x_{c0} is the cam angle at the start point, and x_{cN} is the cam angle at the end point. In this fitting, four constraints are applied. The first two constraints guarantee the continuity of the resulted follower displacement profile and assign a value, P_0, for the start and end points. In the same way, the last two constraints guarantee the continuity of the resulted velocity profile and assign a slope value at the start and end points. It should be mentioned that in the earlier derivation in Section 3.4, the constraints of the slope of the function at the start and end points were to be equal only and we did not assign it any value. In this derivation, there is a need to assign a value, P_0', for the slope at the start and end points. The justification for this need will be shown with illustrative figures after deriving the general expression of the polynomial function. No constraints are added to make the acceleration profile continuous because this will complicate the derivation. Although the derivative of the acceleration, the jerk profile, will be infinite at the discontinuity locations of the acceleration profile, this will cause vibration if we intend to move the mechanism in a high speed; in our gait generation mechanism the speed will be low.

The four constraints to be applied are:

$$P(x_{c\,0}) = P_0 = 0° \tag{3.34}$$

$$P(x_{cN}) = P(x_{c0}) \tag{3.35}$$

$$\frac{dP}{dx_c}(x_{c0}) = P_0^{'} \tag{3.36}$$

$$\frac{dP}{dx_c}(x_{cN}) = \frac{dP}{dx_c}(x_{c0}) \tag{3.37}$$

where

P_0 : The polynomial function value at x_{c0} .

$P^{'}_0$: The slope of the polynomial function at x_{c0} .0

As has been done before, the sum of the squared difference between the true value of the discrete point and the approximated value can be used to establish an objective function to be minimized. This objective function, F_2 , is given by Equation 3.38 below:

$$F_2 = \sum_{j=1}^{N} (P_j - \alpha_j)^2 \tag{3.38}$$

where

j : Index of the discrete displacement point.

N : Number of total discrete displacement points.

P_j : Approximated value of the discrete displacement point with index j , given by Equation 3.33.

α_j : True value of the discrete displacement point with index j .

Since there are four constraints, they can be used to express *four of the coefficients* in terms of the remaining coefficients. The same procedure used in Section 3.4 for solving for the coefficients is used here. Details of this procedure can be found in appendix C.

Again, the derivation is independent of the polynomial's degree, i.e. it was not limited to any degree. Thus, different degrees of a polynomial function must be compared and then a particular value to fit the discrete follower displacement profile must be chosen. In addition to the degree, n , it is important to note that the results of the fitting is also affected by the selected value of P_0', *the slope at the start and end points*. To be able to choose the most suitable slope value, we need first to take a look at the behavior of the data at the start and end of the cycle. At the start location, the data tends to be increasing, while at the end location it tends to be decreasing. Increasing values result from positive slopes, while decreased values result from negative slopes. The assigned slope value must account for these two behaviors as much as possible. This happens only if we choose a **zero slope value**. Assigning a non-zero slope value will introduce the problem of having **negative displacement values**. The crossing into the negative side is independent of the polynomial's degree, *n*. The figure below shows the resulting fit, using the results obtained in appendix C, for $n=5$ when P_0' is a *negative value,* where P_0' is chosen to be -0.5.

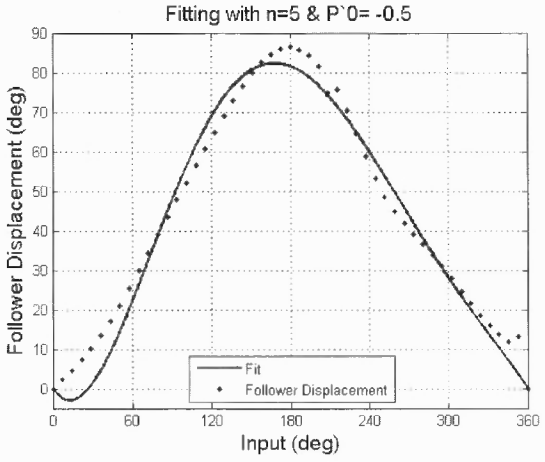

Figure 3.20 Fit function for $n = 5$ and $P_0^{'}$ is -0.5.

The corresponding velocity and acceleration profiles are shown in the below figure.

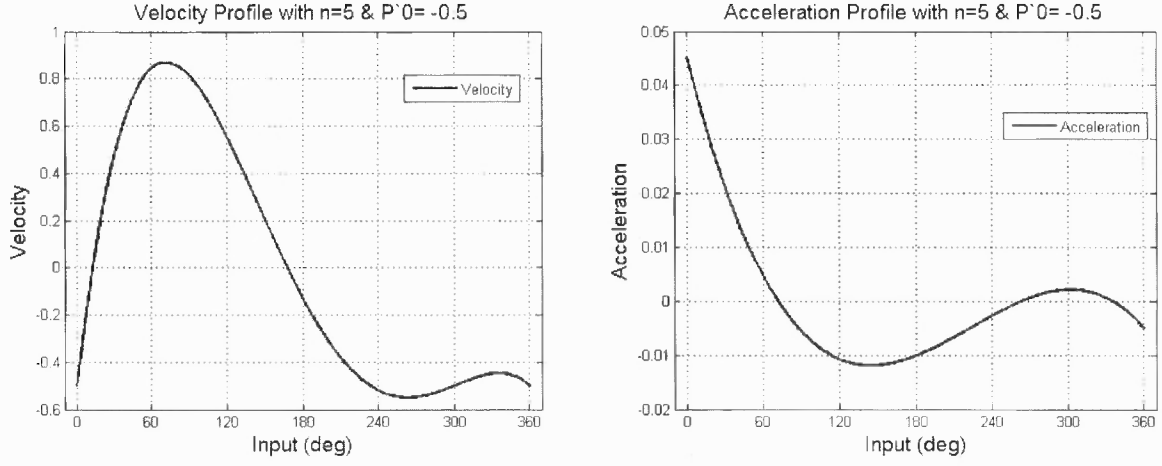

Figure 3.21 Velocity profile and acceleration profile for $n = 5$ and $P_0^{'}$ is -0.5.

The velocity profile is continuous and both of its ends have a value of -0.5. Since the velocity profile is continuous, the acceleration profile is finite throughout the cycle. The displacement fit function crosses the negative side at the start of the cycle, or

at the start of the rise segment. This is independent of the polynomial's degree, as can be seen in the below figure, where the resulting fit for $n = 9$ and $n = 11$ is shown.

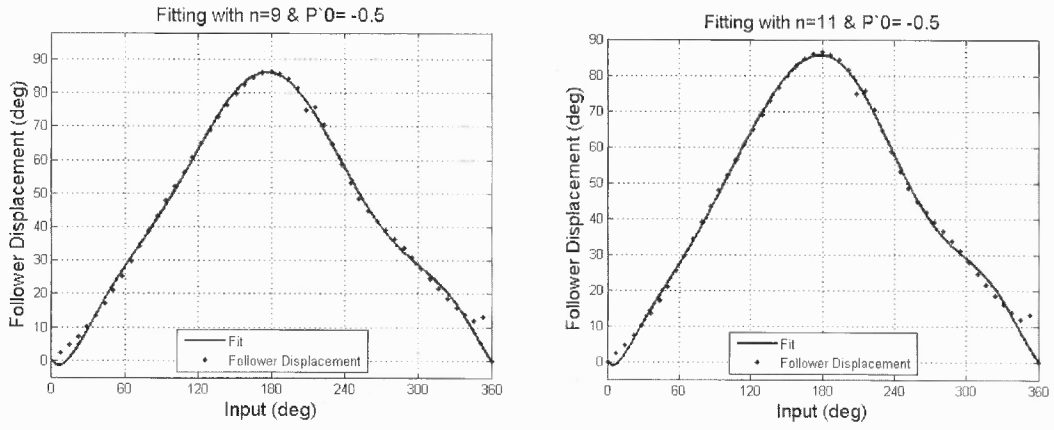

Figure 3.22 Fit functions for $n = 9$ and 11 when $P_0^{'}$ = - 0.5.

Both plots show that the displacement function crosses the negative side. Assigning a positive value for $P_0^{'}$ will cause the displacement function to cross the negative side at the end of the cycle, as shown in Figure 3.23 where $P_0^{'}$ is 0.3 and $n = 5$.

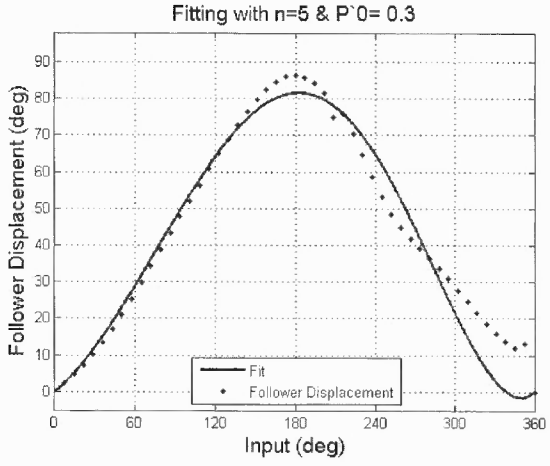

Figure 3.23 Fit function for $n = 5$ and $P_0^{'}$ is 0.3.

This is also independent of the polynomial's degree, as shown in Figure 3.24 where $n = 9$ and 11.

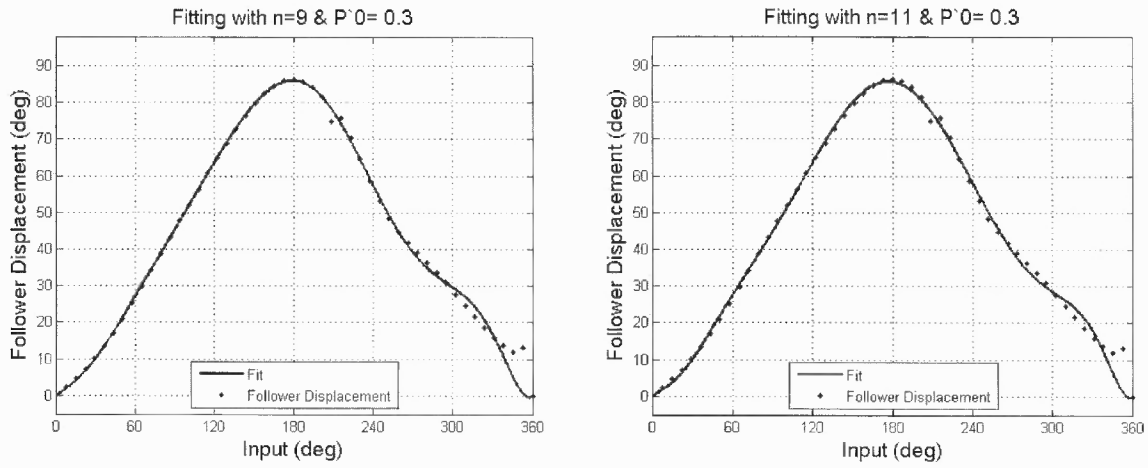

Figure 3.24 Fit functions for $n = 9$ and 11 when $P_0^{'} = 0.3$.

Figures 3.25 and 3.26 show different polynomial degrees of displacement functions where all have $P_0^{'} = 0$. It is clear that in all cases, the displacement functions stay in the positive side.

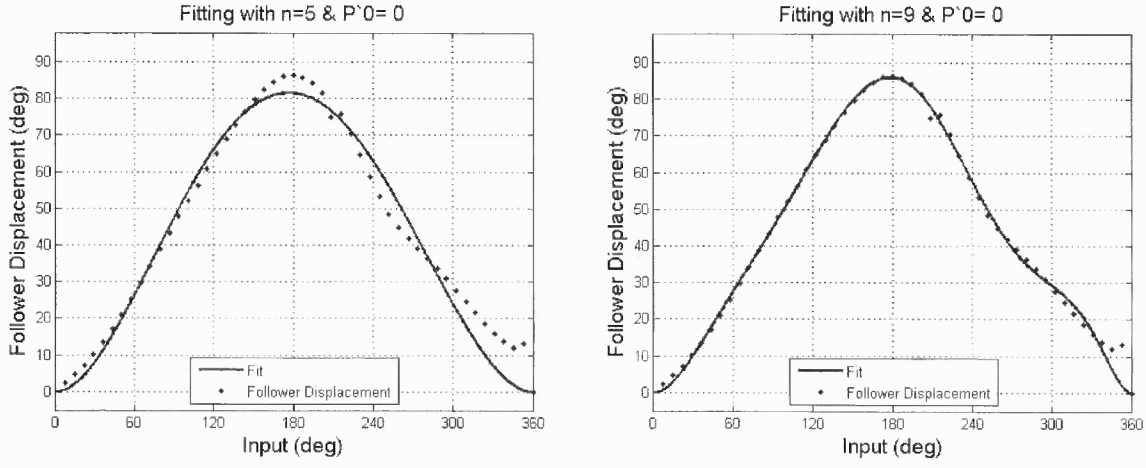

Figure 3.25 Fit functions for $n = 5$ and 9 when $P_0^{'} = 0$.

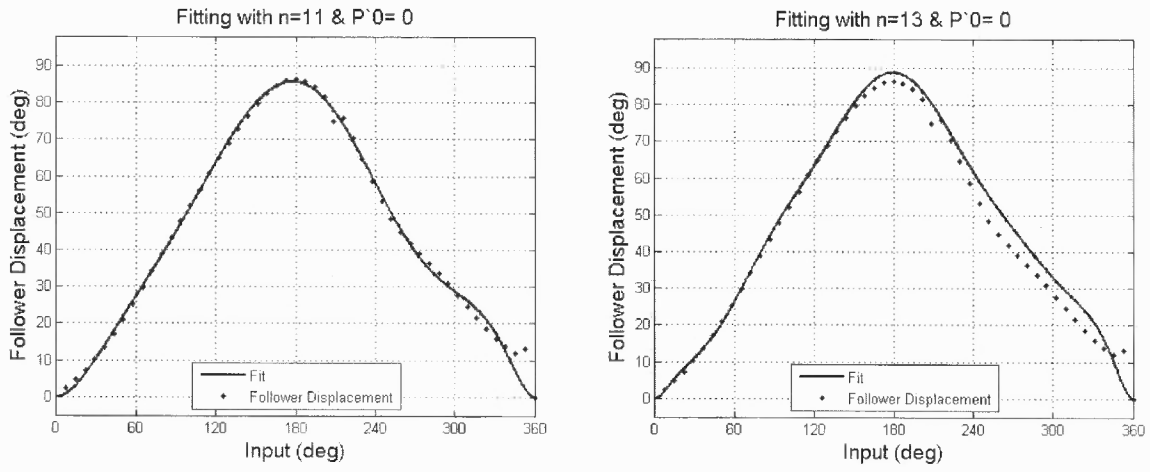

Figure 3.26 Fit functions for $n = 11$ and 13 when $P_0^{'} = 0$.

The velocity profiles for the fit functions in Figures 3.25 and 3.26 are shown in Figures 3.27 and 3.28, respectively. As shown, both ends of any velocity profile are zeros.

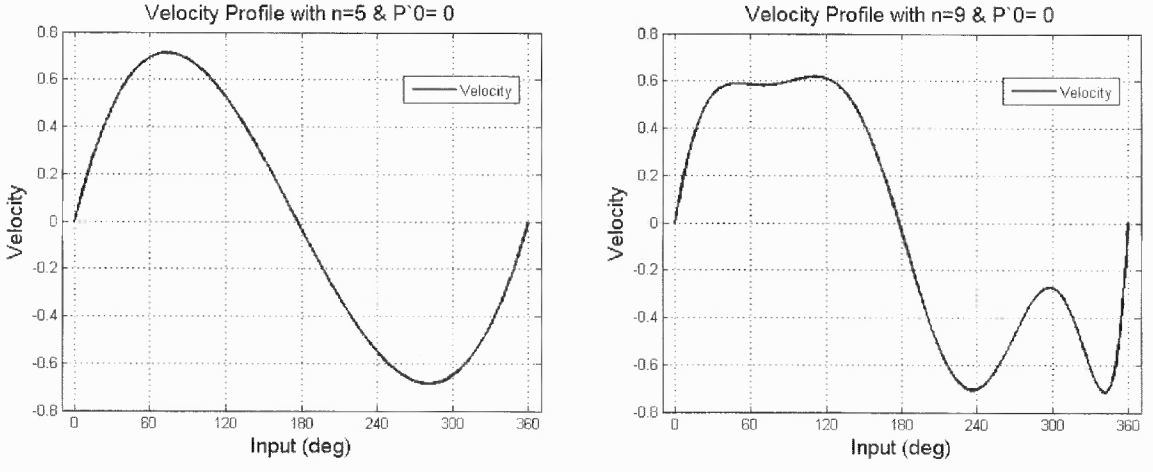

Figure 3.27 Velocity profiles for $n = 5$ and 9 when $P_0^{'} = 0$.

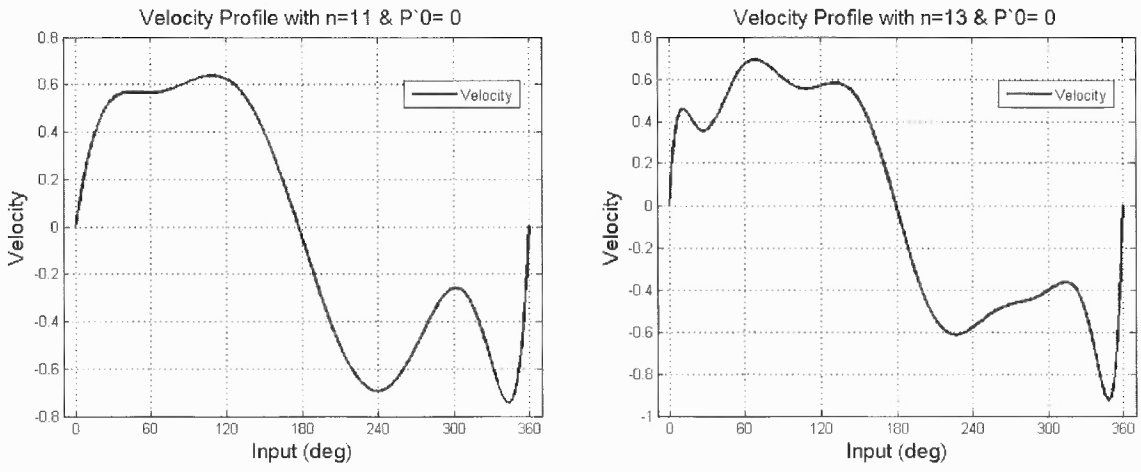

Figure 3.28 Velocity profiles for $n = 11$ and 13 when $P_0^{'} = 0$.

The third constraint, given by Equation 3.36 provides the feasibility for controlling the slope at both ends of the displacement function.

Having determined the value of $P_0^{'}$, *the slope at the start and end points*, we now proceed to select the degree for the polynomial fit function. We will choose the degree that gives the lower value of the objective function, F_2, given in Equation 3.38. For degrees $n = 5$ to $n = 14$, the corresponding F_2 values are found. The results are shown in Table 3.5, where the lowest value of F_2 happens when $n = 11$.

Table 3.5 Values of F_2 for Different Polynomial Degrees

n	5	6	7	8	9	10	11	12	13	14
F_2	1088.5	1088.5	973.6	273.5	205.9	200.8	199.8	567.4	569.5	50,333

It can be seen that increasing the degree to $n = 13$ or 14 does not improve the fit as indicated by the F_2 value for these two cases in Table 3.5, and as indicated too by Figure 3.29 below.

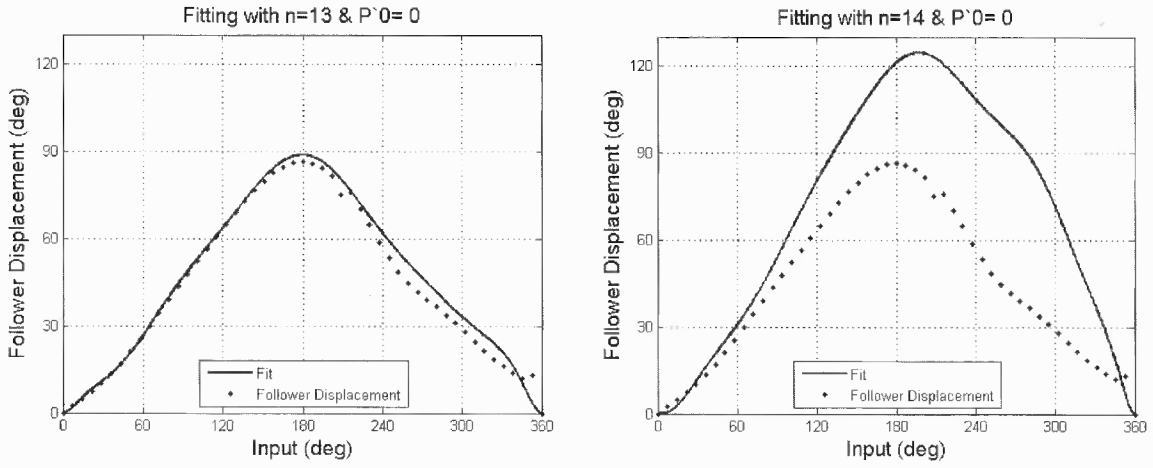

Figure 3.29 Fit functions for $n = 13$ and 14 .

Based on Table 3.5 values, n is chosen to be 11. The corresponding fit function, velocity and acceleration profiles are shown in Figure 3.30. A zoom-in plot of a rectangle in fit function profile is shown next to the fit function profile.

The fit function values range from 0° to around 86°. The velocity profiles starts and ends with a zero value as constrained, and the acceleration profile is finite. The two bumps that existed were originally in the discrete follower displacement profile are smoothed out after fitting. However, the second bump shown inside the rectangle in the fit function profile was fitted by almost 11° below the true value at that location as shown in zoom-in plot; the value was decreased from 13.2° to 2.3°. This means that the required compensation needed by the cam *at that location only* will be smaller by almost 11°. That location happened to be the start of the gait cycle.

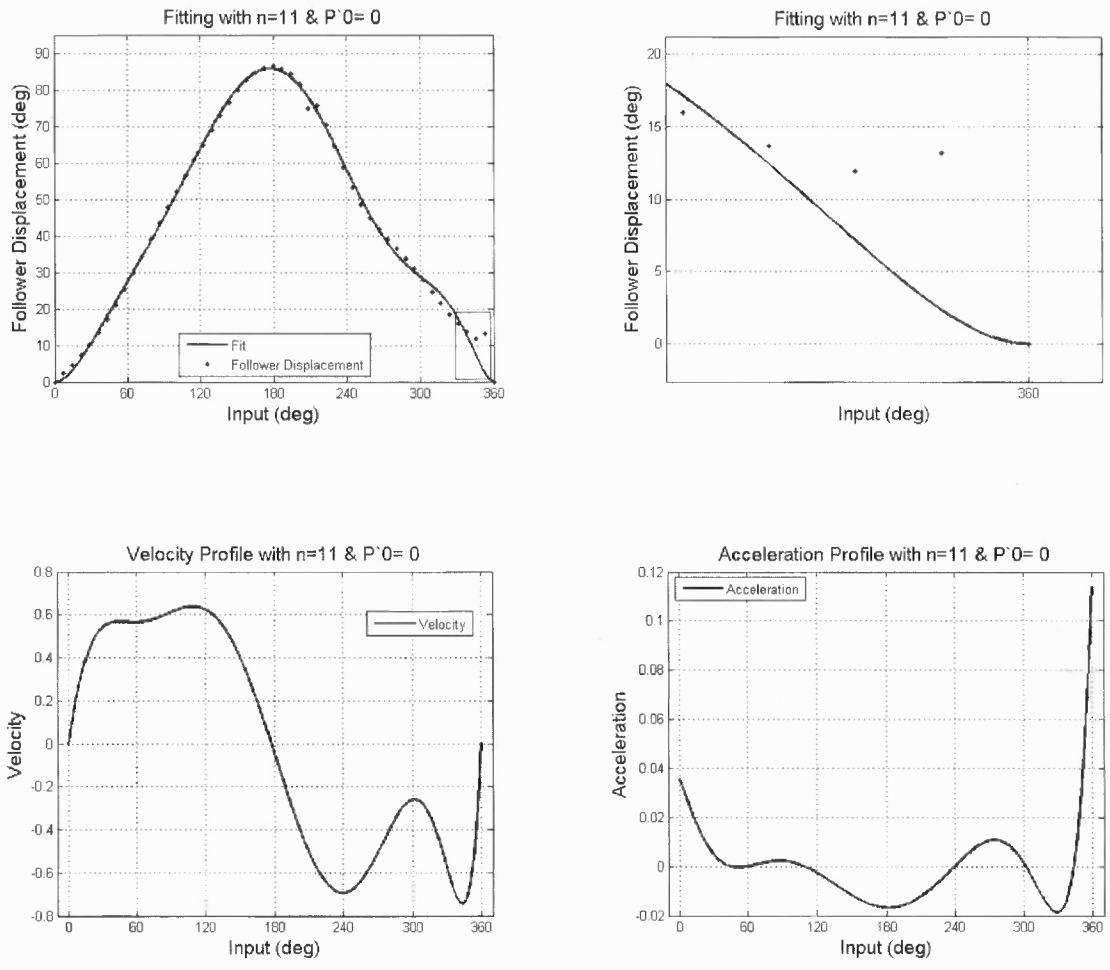

Figure 3.30 Fit function, velocity and acceleration profiles for $n = 11$.

It was mentioned before that the positive values of the follower profile indicate that the crank is exceeding the required position and the cam must push the follower back to the required position. Having 2.3° instead of 13.2° means that **the cam** will push the crank back by only 2.3°, and so the crank will ***exceed the required position (in this case the gait cycle starting position) by around 11°***. In other words, we will have **a new gait cycle starting location,** and this has to be taken into consideration when assembling the gait generation mechanism or any simulation of this mechanism. In fitting and smoothing any discrete points, trade-offs are to be expected.

3.5.4 Determination of the Cam Profile

Using the follower (crank) displacement profile obtained in the previous section, the cam surface can now be determined based on the equations and programming codes provided in [14]. In addition to the follower displacement profile, the basic parameters needed to determine the cam profile are: *follower length*, *roller-follower radius*, distance between the follower's pivot and cam's pivot (*pivots distance*), and *direction of the cam rotation.* The follower length is defined as the distance from the follower's pivot to the *center* of the roller-follower, as shown in Figure 3.31 below.

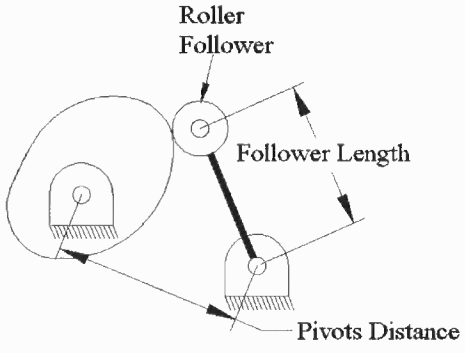

Figure 3.31 Parameters needed in finding the cam profile.

The selection of the *pivots distance* will directly affect the size of the cam; the larger the pivots distance is, the larger the size of the cam is. Having a bulky cam in our gait generation mechanism is not desirable, so the smallest possible size of the cam must be found. We discussed a procedure to minimize the size of disk cams with roller-followers under pressure angle constraint [27]. The development of that procedure is motivated by the type of applications where the displacement profiles are not the conventional motion programs, such as cycloidal, but fully specified curves. Thus it is particularly useful in this cam design. This procedure is explained in the next sub-section.

3.5.4.1 Size Minimization of Disk Cams with Roller-Followers under Pressure Angle Constraint

The maximum pressure angle and the cam curvature are constraints that should be taken into consideration in the cam synthesis. The maximum pressure angle allowed in oscillating followers is recommended to be around 45° [28]. The cam curvature profile should be examined to make sure no undercutting occurs. The paper also provides the flexibility for meeting the requirement on the cam curvature during the design process.

In the paper in [27], the problem is reduced to locate the cam center in a permissible region that is closest to the follower path. Choosing the cam center in this permissible region will guarantee that the maximum pressure angle in the system will not exceed a prescribed maximum value.

An example of this permissible region is shown in Figure 3.32 below [27], where this region was generated for a maximum pressure angle $(\alpha_{\max}) = 40°$.

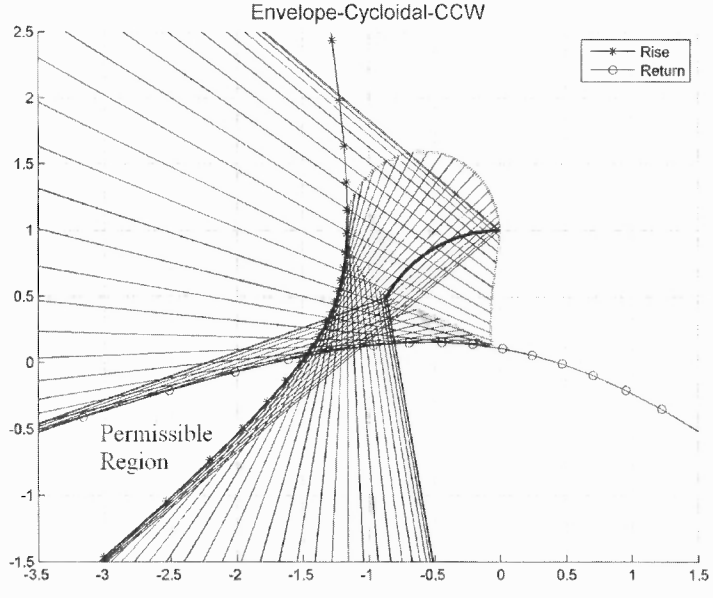

Figure 3.32 Computed envelopes of permissible region for a cam with oscillating roller-follower (maximum pressure angle $(\alpha_{\max}) = 40°$) [27].

The motion is a cycloidal motion for an oscillating follower and the cam is rotating counter-clock wise where a rise then return (fall) are occurring. The *follower pivot* is located at the origin point (0, 0). The solid circular arc inside the water-drop shaped curve is the path of the roller-follower center. The lines drawn are not really needed to find this permissible region. Choosing the cam center anywhere inside permissible region will guarantee that $\alpha_{\max}$ will not exceed 40°. To get the possible smallest size of the cam however, the cam center needs to be located at the intersection of the *rise and return envelopes* shown in the figure, which bounds the permissible region. The distance between the chosen cam center and the follower pivot represents the *pivots distance* required in the cam design. If the cam curvature profile has undercutting, the cam must be made larger by choosing the cam center farther away from the intersection point of the rise and return envelopes and within the permissible region. If the prescribed pressure angle is changed from $\alpha_{\max} = 40°$ to $\alpha_{\max} = 32°$ for the same example in Figure 3.32, the resulted permissible region is as shown in Figure 3.33. The region is not only narrower, but also farther away from the roller path, compared with that in Figure 3.32. This means a smaller maximum pressure angle value can be obtained, but the cost will be a larger cam.

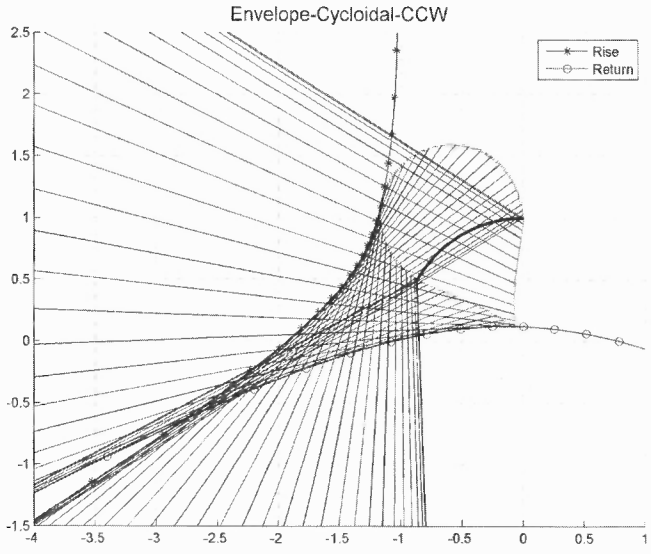

Figure 3.33 Computed envelopes of permissible region for a cam with oscillating roller-follower (maximum pressure angle $(\alpha_{\max})$ = 32°) [27].

However, there is a limit on how small the prescribed maximum pressure angle can be for cams with oscillating followers. The permissible region can only exist if the minimum value of the prescribed maximum pressure angle is more than half of the amplitude of the follower rotation [27]. The amplitude of our fit function in Figure 3.30 is around 86°. Thus, the minimum allowed prescribed maximum pressure angle should not be less than 43°. When using this paper, it is important to note that the actual size of a cam mechanism can be scaled in terms of the follower's length, since the envelopes computed are directly proportional to this length. The follower's length is actually the scaling factor which the *base circle radius (thus the cam size), the roller radius, and the pivots distance* will all be proportional to.

3.5.4.2 Size Minimization of the Disk Cam in the Timing Mechanism

Knowing that the follower's length is the scaling factor in the cam mechanism and since placing the roller-follower anywhere on the crank link will still give the crank the same required angular displacement, the follower's length and the crank's length need not be the same. Thus, the follower's length can be minimized, and consequently the size of the cam will be smaller. However, the follower's length should be minimized according to other design considerations; considerations like stress analysis, the roller radius and the radius of curvature to avoid undercutting for example. We chose the follower length to be less than the crank's length and the roller follower radius will be 20% of the follower's length. This choice is intended only to show how the overall mechanical timing mechanism works. But further study is needed to determine the optimal follower length and the roller's radius. The follower's length is needed in finding the required envelopes to determine the permissible region. As mentioned before, the minimum allowed prescribed maximum pressure angle should not be less than 43°. In this research, it was chosen to be 50°.

The corresponding permissible region for this pressure angle value is shown below in Figure 3.34 along with the follower and cam pivots locations, where the direction of rotation is CCW.

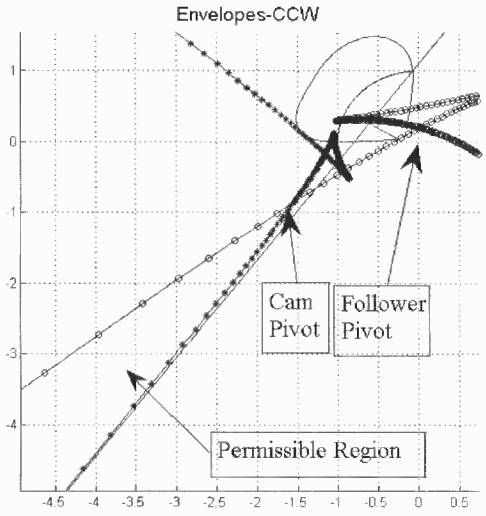

Figure 3.34 Computed envelopes of permissible region for cam of the timing mechanism (α_{max} = 50°, direction is CCW).

The cam pivot is chosen at the intersection of the envelopes in the figure to give the smallest possible pivots distance and thus the smallest possible cam when α_{max} = 50° and the direction of rotation is CCW. Since the pivots distance, the follower length, the roller radius, and the direction of rotation are all known, the cam profile is synthesized using the equations and codes in [14].

Figure 3.35 below shows the cam profile along with the follower profile, the cam curvature profile and the pressure angle profile. It is clear that the maximum pressure angle value does not exceed 50°.

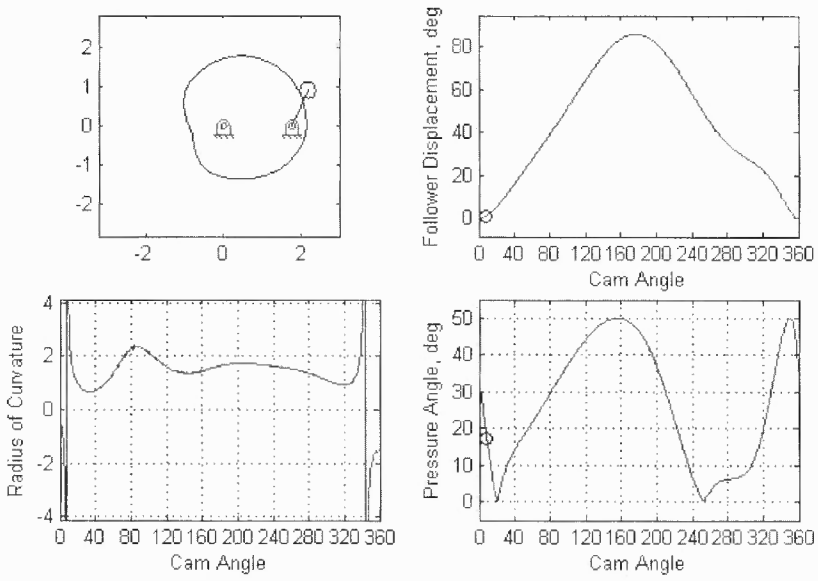

Figure 3.35 The resulted cam, follower displacement, cam curvature and pressure angle profiles for α_{max} = 50° and CCW direction.

For a unit follower length, the pivots distance is 1.7645 units length, and the base circle radius is 0.8151 unit length. If the direction of rotation is CW and α_{max} is still 50°, then the corresponding permissible region is shown below in Figure 3.36.

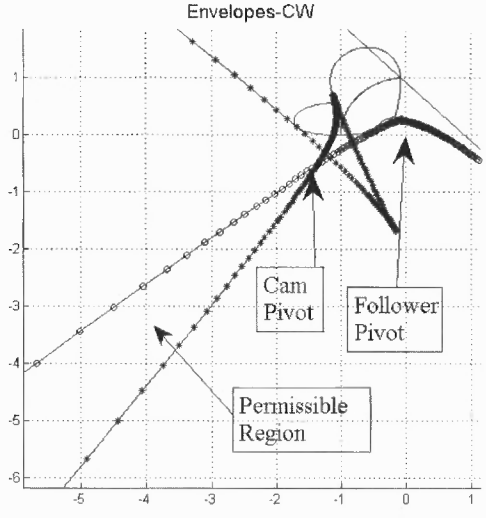

Figure 3.36 Computed envelopes of permissible region for cam of the timing mechanism (α_{max} = 50°, direction is CW).

For this case, the different parameters needed in designing the cam are the direction of rotation and the pivots distance. The follower length and the roller radius are the same. The resulted cam, follower, cam curvature, and the pressure angle profiles are shown in Figure 3.37 below. The maximum pressure angle value also does not exceed 50°. For a unit follower length, the pivots distance is 1.4608 units length and the base circle radius is 0.4401 unit length.

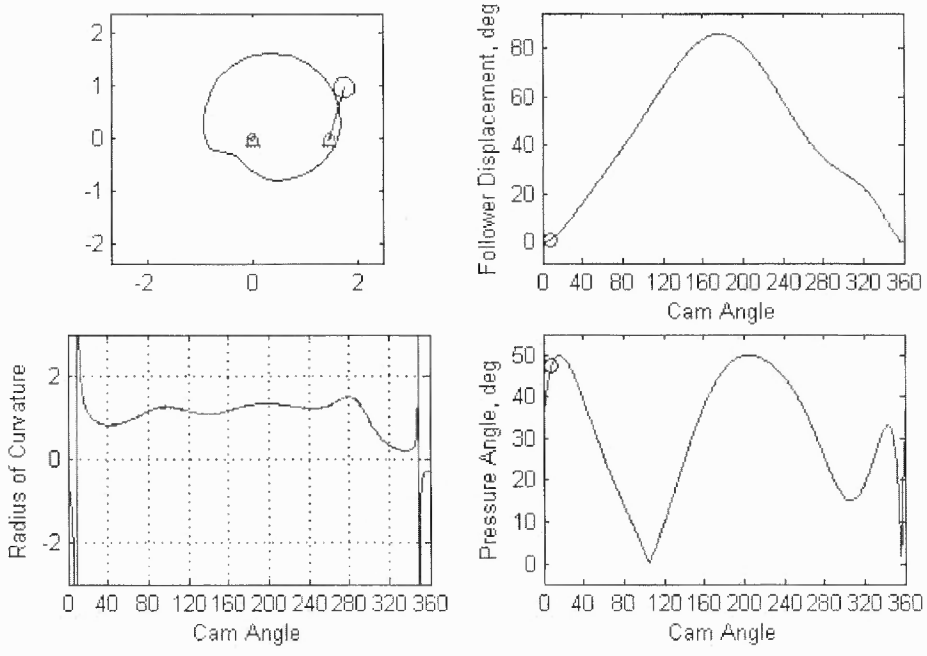

Figure 3.37 The resulted cam, follower displacement, cam curvature and pressure angle profiles for α_{max} = 50° and CW direction.

Comparing the base circle radii in the CCW and CW cases, it can be seen that the CW case gives a smaller base circle radius and thus a smaller cam size for the same follower length, the same roller-radius, and the same maximum pressure angle value, as shown in Figure 3.38 below.

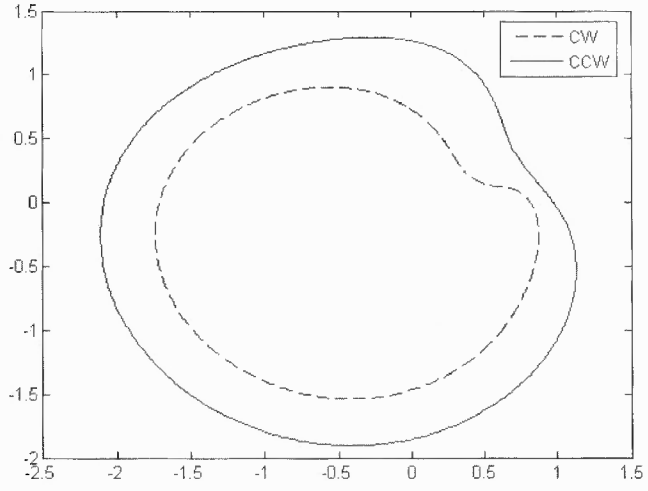

Figure 3.38 Comparing the cam sizes for both the CCW and CW direction of rotations.

For α_{max} ranging between 43° and 60°, the CW case will always give a smaller cam size, as shown in the table below, where the base circle radii for different α_{max} are found. To be able to compare the CCW and CW cases for a certain α_{max} value, the follower length and the roller radius is the same in both cases, and the cam center is chosen at the intersection of the two envelopes

Table 3.6 Comparing Base Circle Radii (in unit length) for CCW and CW Cases with Different α_{max}

α_{max}	43°	45°	50°	55°	60°
CCW	24.31	3.12	0.82	0.24	0.12
CW	13.72	1.99	0.44	0.14	0.08

The system could be designed to a pressure angle that is less than 50°, but we will end up getting a cam that is larger, as can be seen from the table. It is clear that with a higher maximum pressure angle value, a smaller cam is obtained.

It is clear also that the CW rotation produces a cam with smaller base circle than the CCW rotation for all cases in Table 3.6. A large size of the cam should be avoided as it might causes interference with the patient or other parts of the mechanism during the operation of the gait mechanism. To get a smaller cam size, the cam must rotate in a CW direction. To achieve this, the gear train arrangement in Figure 3.11 must be used. As mentioned in Section 3.5.3, the cam in this arrangement will maintain *stationary* orientation while the carrier link is moving. While certain parameters are used for obtaining Figure 3.38 and Table 3.6, *these parameters need to be properly selected according to other design considerations such as the stress.*

3.5.5 Simulation of the Mechanical Timing Mechanism in Pro/Engineer

A CAD model of the mechanical timing mechanism was built to simulate and test its motion control of the four bar mechanism. For a crank length of 0.3297 meters (m), a follower length is chosen to be 0.2 m and α_{max} to be 50°. The resulted roller follower radius is 0.04 m, the resulted cam base circle radius is 0.086 m, and the pivots distance is 0.291 m. Figure 3.39 below shows a side view side of the four-bar mechanism along with the mechanical timing mechanism designed to move the left leg only for now.

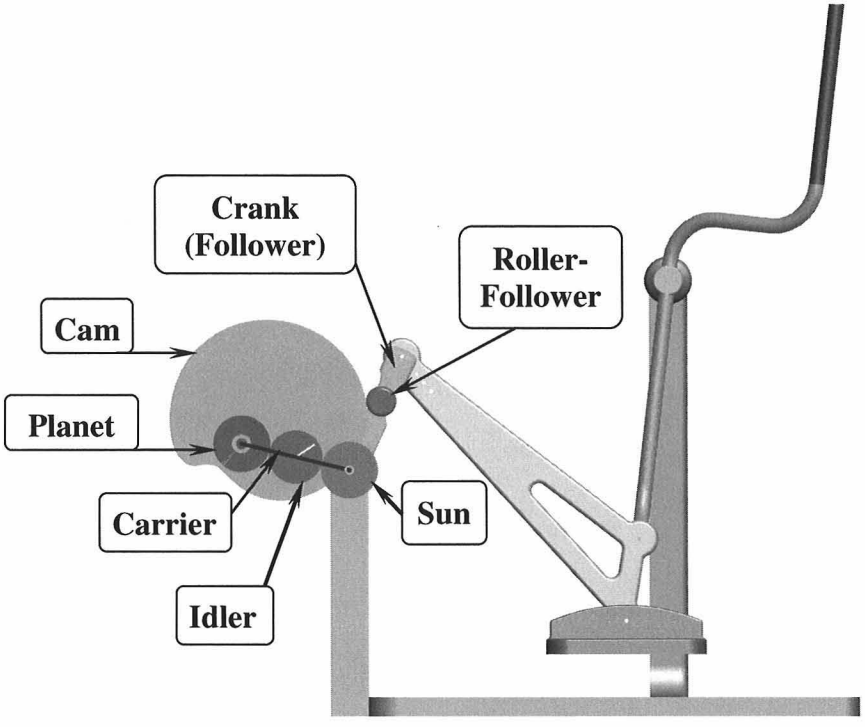

Figure 3.39 Side view of the mechanical timing mechanism added to the four-bar mechanism.

Figure 3.40 3D view of the mechanical timing mechanism added to the four-bar mechanism.

Each crank must have a separate mechanical timing mechanism to provide the necessary compensation throughout the operation of the mechanism, as shown in Figure 3.41 below. The suspension frame and weight support system is not shown here to make the figure less complicated.

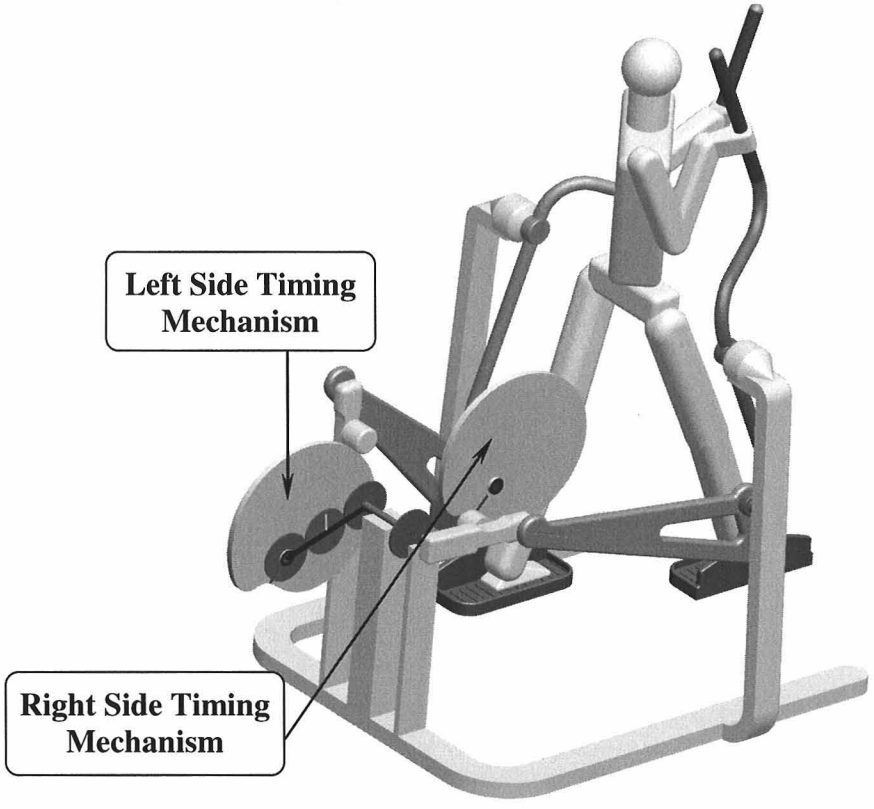

Figure 3.41 Separate timing mechanism for each side of the gait mechanism.

The two carriers in the two timing mechanisms share the same main input through a coupling shaft, as shown in Figure 3.42 below. This is an advantage since this will simplify controlling both sides with one single input.

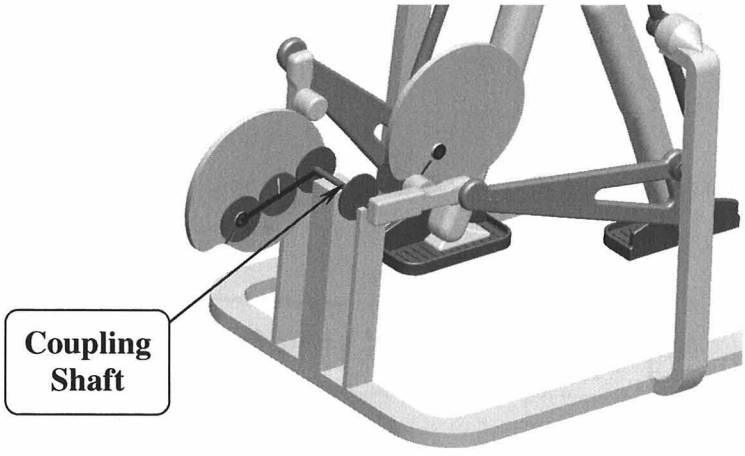

Figure 3.42 Main input shared by the two timing mechanisms.

The way each timing mechanism arranged is an important issue. It should be noted first that the right and left timing mechanism will be symmetrical about the middle plane of the gait generation mechanism. Both the crank and the coupler links are rotating in different but parallel planes. For both the left and right sides, the crank's *plane of motion* is closer to the middle plane than the coupler's plane of motion. There are two options to install the timing mechanism with respect to the *crank's plane of motion*; either in the closer side to the middle plane or the farther side. If it is installed on the farther side, there will be an interference problem between the *coupler link* and each of the roller and the main input shaft; the coupler will hit both the roller and the main input shaft during the coupler's rotation. Figure 3.43 below shows the interference of the roller and the coupler if this option is used. To make the figure less complicated, the timing mechanism is not shown. It is clear how the coupler interfere with the roller during its rotation. The crank will also interfere with the main input shaft that would extend to the carrier link. Thus, there can not be any installed component on *the farther side* of the crank's plane of motion as it will be hit by the coupler.

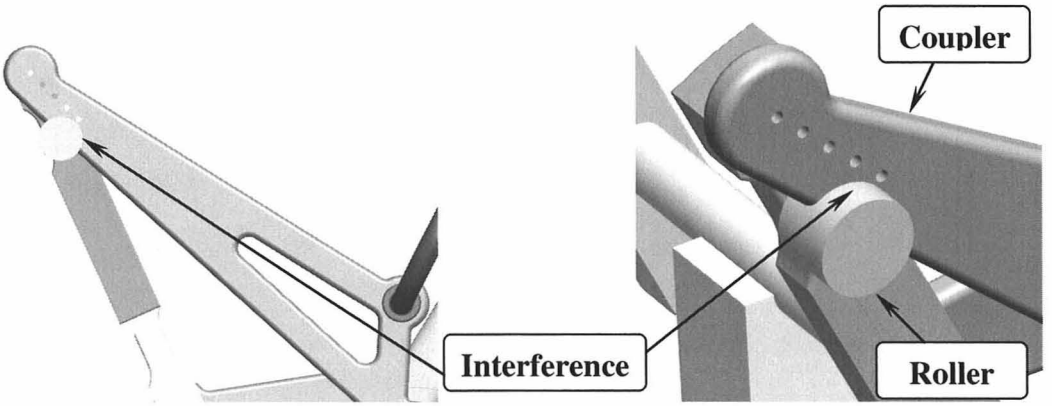

Figure 3.43 Side and 3D views of the interference between the roller and the coupler.

However, if the crank and the coupler planes of motions are switched, the timing mechanism could be installed on the farther side and no interference will happen between the coupler and the roller. However, there can't be one main input shaft in the middle of the gait mechanism as the coupler link will interfere with it. In this case, there must be *two separate main inputs* to avoid interference, and this is not desired as the whole gait generation mechanism is desired to be driven with *one main input*. As a conclusion for the current configuration where the crank's plane of motion is closer to the middle plane, the timing mechanism must be installed on the side of the crank that is closer to the middle plane.

An important issue to be addressed is how the components of the timing mechanism itself should be arranged to avoid interference. It is known that the cam is rotating with the carrier about the axis of the carrier which is the same axis of the main input shaft. From the CAD model built, it is found that during the cam's rotation and although the cam is rotating about the axis of the main input shaft, the cam *passes by the axis of the main input shaft* and this will cause interference between the cam and the main input shaft.

This means, the main input shaft can not be *in the way of the cam* as it will interfere with it as shown in Figure 3.44. This interference is caused by the cam size.

As mentioned earlier, the mechanism can be scaled by reducing the follower's length and consequently, the cam size will be reduced. However, the follower's length should be minimized according to other design considerations, such as the roller radius and the radius of curvature to avoid undercutting for example.

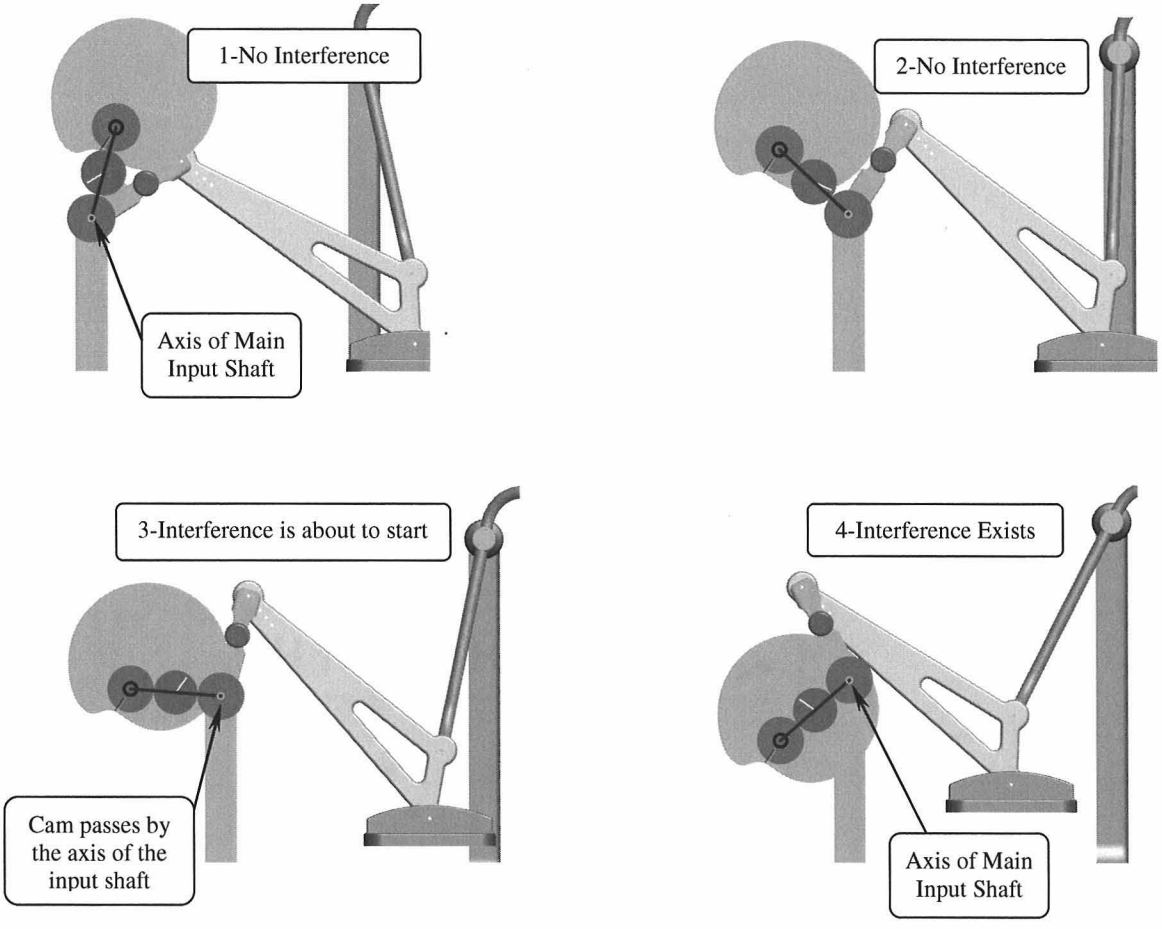

Figure 3.44 Different positions of the crank that show how the cam interferes with the axis of the input shaft in certain positions.

Since the cam size is not yet finalized and there is a possibility to not be able to make the cam smaller, a solution must be found that will work in any case. A *space* could be this solution. This is needed for the cam to rotate freely as shown in Figure 3.45.

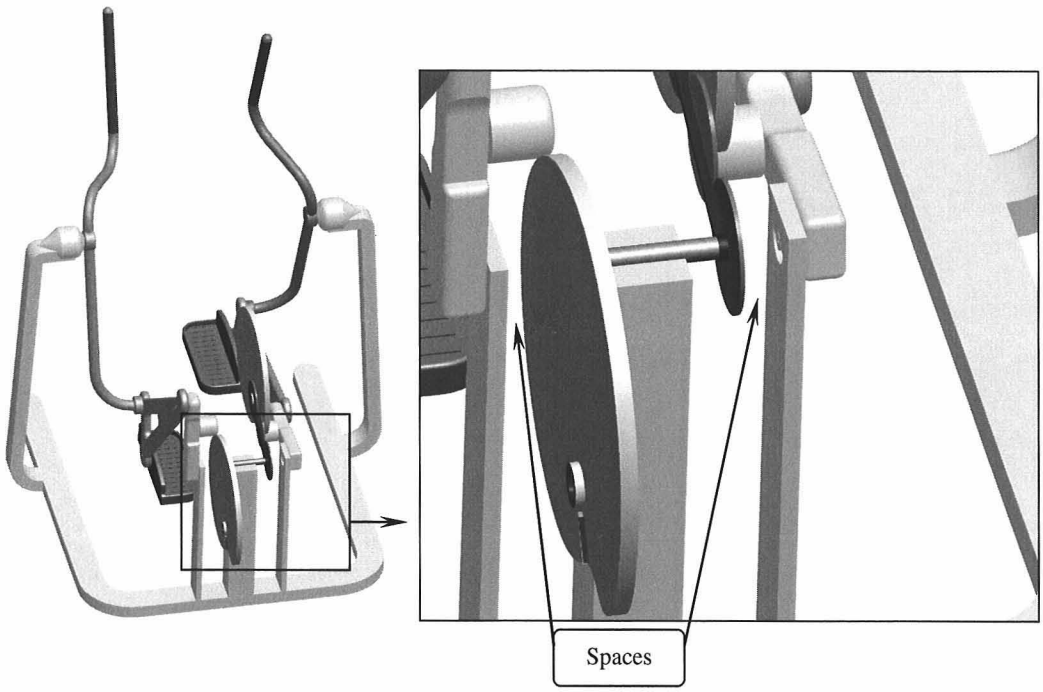

Figure 3.45 Back view of the mechanism showing spaces for both cams on both sides.

The main input shaft will be in between the timing mechanism. The order of the planes of motion for the timing mechanism components arranged starting from the middle plane, going farther from it should be as shown in Figure 3.46, where only the right side is shown.

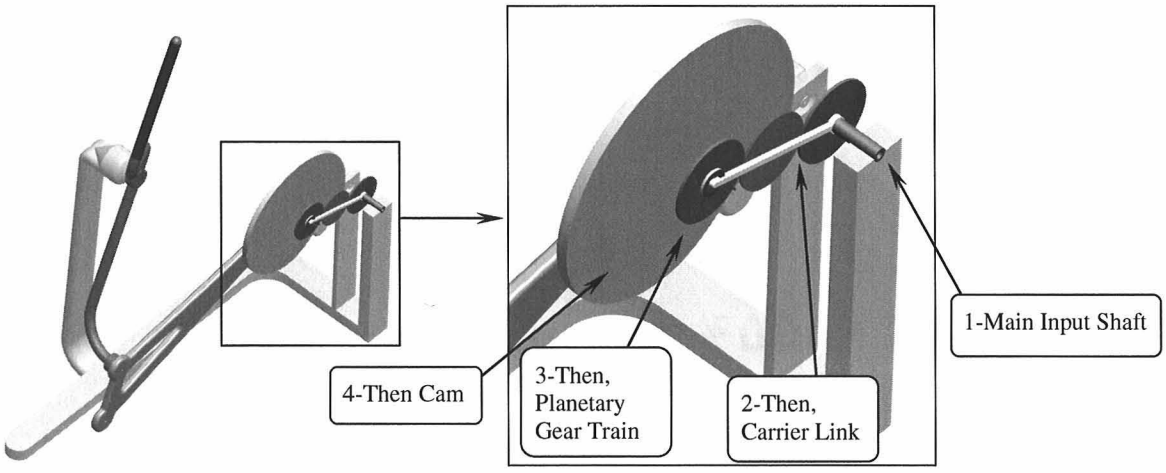

Figure 3.46 The order of the timing mechanism components arranged starting from the middle plane of the gait generation mechanism.

The components are arranged starting from the middle plane and going farther from it as follows: the carrier, then the planetary gear train set, and finally the cam. This order is necessary so that the cam will be at the end near the space where it can rotate freely without interfering with the main input shaft as shown in the below figure.

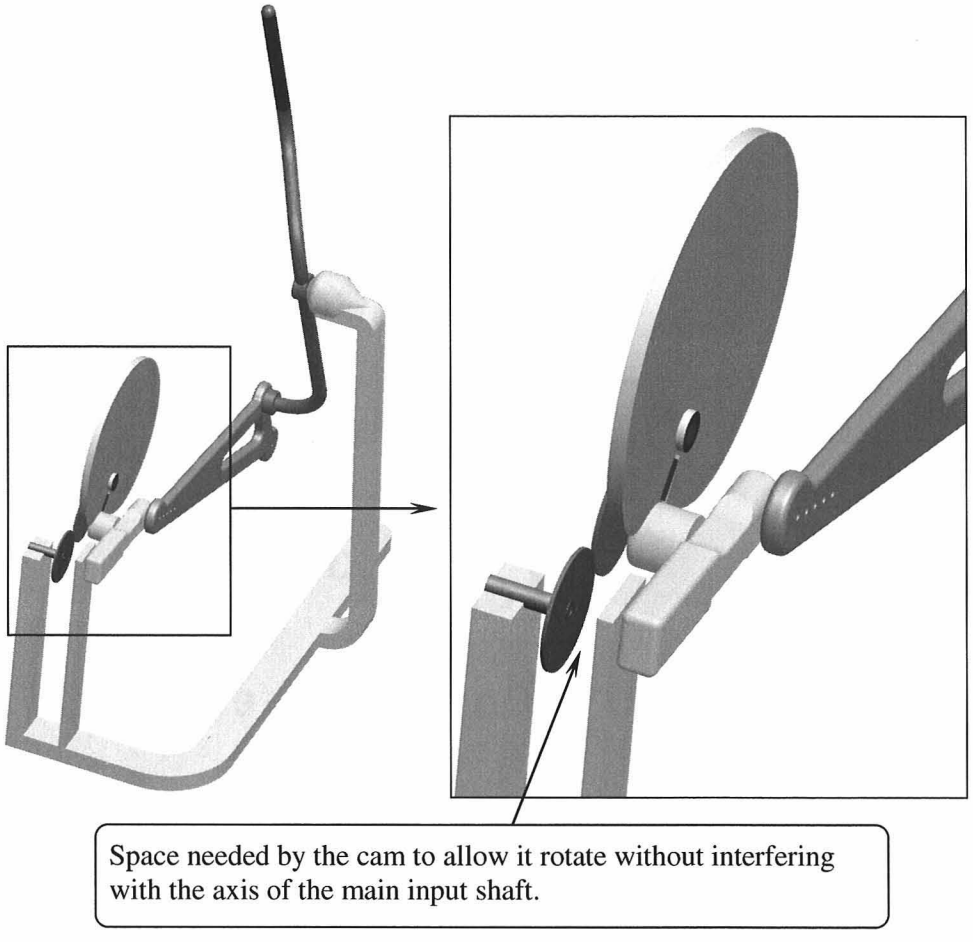

Figure 3.47 Another view of Figure 3.46 that shows the space for the right side.

The space width required should be larger than the cam's thickness to allow the cam to rotate freely. It should be kept in mind that the thickness of the roller-follower might need to be increased to allow it to reach the cam. The thickness of each of the cam and the roller-follower are not final designs and might be changed due to any later design requirements that might be appear in the design process. Using this recent configuration and arrangement, the cam will not interfere with the main input shaft.

Now that the movement of both sides has no interference problems, the way to obtain coordination between the right and left legs using the mechanical timing mechanism is shown.

First, coordination in *normal gait* for healthy persons must be understood. Throughout the gait cycle, the right foot goes through a series of events. The left foot goes through exactly the same series of events as the right foot, but **displaced in time approximately by half a cycle** [9]. Figure 3.1 that was shown previously is shown again here below. If the right foot is at the start of the gait cycle (or the initial contact event) for example, we can go back by half a cycle and over there is where the left foot should be approximately located.

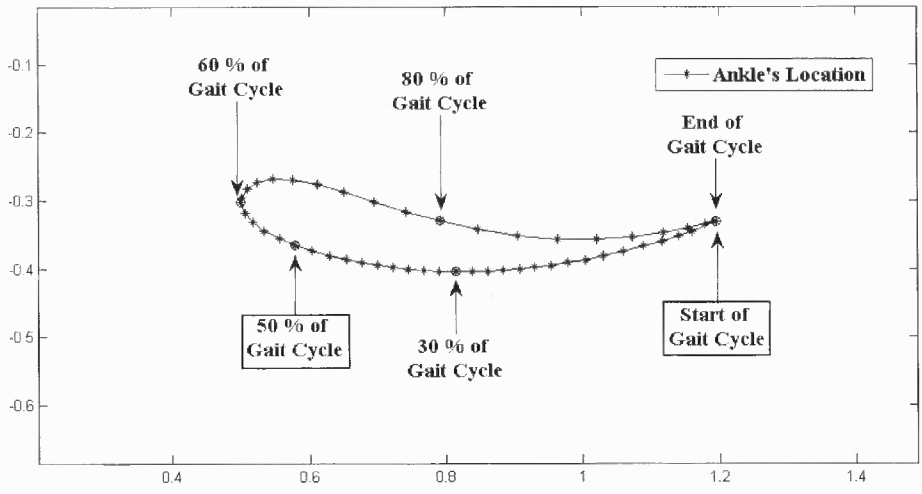

Figure 3.48 Desired timings of the ankle's location in one gait cycle projected on the desired ankle trajectory (units are in meter).

As a starting event in our gait generation mechanism, the right foot must be placed at the ***starting location*** of the gait cycle, and the left foot at the ***50% location*** of the gait cycle, shown in *boxes* in Figure 3.48. From there, the main input shaft starts rotating and the two cranks work accordingly. To be able to place the two feet there, two important things must be found. First one is *the corresponding crank angle* for these two locations and displaces the crank accordingly. The second one is the corresponding locations on the cam surface, since the correct compensation of the cam is needed, or the

correct contact surface of the cam. If the crank is placed at these two desired locations and is not attached to the right surface of the cam, we will NOT get the right compensation and the cranks will not go to the desired positions throughout the operation of the gait cycle.

The corresponding crank angles can be found from the work done previously in Section 3.3 where the crank angles θ_i that corresponds to the coupler curve points shown in Figure 3.48 were found. However, it was stated in Section 3.5.4 that the fitting for the discrete follower displacement points ***at the start of the gait cycle*** resulted in a fitting that is far from the desired location by around 11°. And it was concluded that the *position of the crank* of the four-bar mechanism after the cam's compensation will be ***exceeding the gait cycle starting position*** by around 11°, which means there is a **new gait cycle starting location**, and the **crank should be placed there** when initiating the movement of the gait generation mechanism. Otherwise, the amount of compensation for all the positions will be distorted and some of the resulted hip and knee joint angles will deviate far from the average patters and even exceed the accepted limits. With this new gait starting location, there will be a small deviation for the resulted hip and knee angles at that starting location. However, it will still be within the accepted limits as will be shown in a bit.

The vector θ_i has the desired values of the crank angles, which are $\theta_i(1)$ and $\theta_i(26)$. $\theta_i(1)$ is the value of the crank angle at the gait start position. To find the new gait cycle starting position, 11° are added to $\theta_i(1)$. $\theta_i(26)$ is the crank angle at the 50% gait location.

Since it is known that there are 2% between each two successive gait points, point number 26 has 25 intervals before it, or 50% period of the gait cycle. Hence, point number 26 is chosen to give the crank angle value at 50% of the gait cycle.

In our calculations, the new gait cycle starting position for the crank is around 355° and $\theta_i(26)$ is around 91.6° measured from the horizontal axis as shown in Figure 3.49.

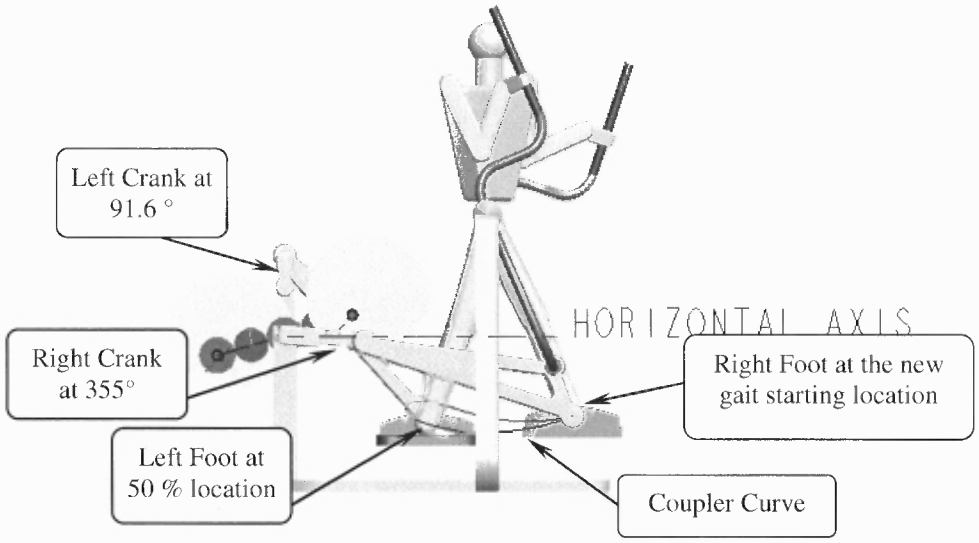

Figure 3.49 Starting positions for both cranks and both feet.

In this figure, the *coupler curve* is shown for comparison of the feet positions in this figure with Figure 3.48. The position of the left foot in this figure matches the 50 % gait position shown in Figure 3.48; hence the calculated crank angle is right. The right foot position in Figure 3.49 is still close to the original gait starting position shown in Figure 3.48, despite there is a new gait starting location.

The corresponding locations on the cam surface must be also found, since the correct compensation of the cam, or the correct contact surface of the cam is needed. For the first location, the cam base surface should be found and marked.

Then the cam must be aligned with the roller of the right crank where the right crank will be at the first desired location. The gears could then be installed to fix the movement of the cam.

For the second location, same procedure done to the right crank is repeated with the left crank. Then the gears are installed to fix the movement of the left cam.

We then rotate the left crank to the second desired location and the cam will be following it. And this is how we got the cam positions shown in Figure 3.49.

Now the two feet have been displaced by approximately half a cycle, shown next are different positions of the right foot when running the gait generation mechanism for one gait cycle. Then the instances that correspond to 0%, 30%, 50%, 60%, 80% and 100% of the gait cycle are captured to compare the right foot locations on the coupler curve with the *desired locations shown in Figure 3.48.*

The different positions are shown in Figure 3.50 below where the total time for this gait cycle is chosen to be 100 seconds. The instances at times: 0, 30, 50, 60, 80 and 100 seconds are captured to give the required percentages.

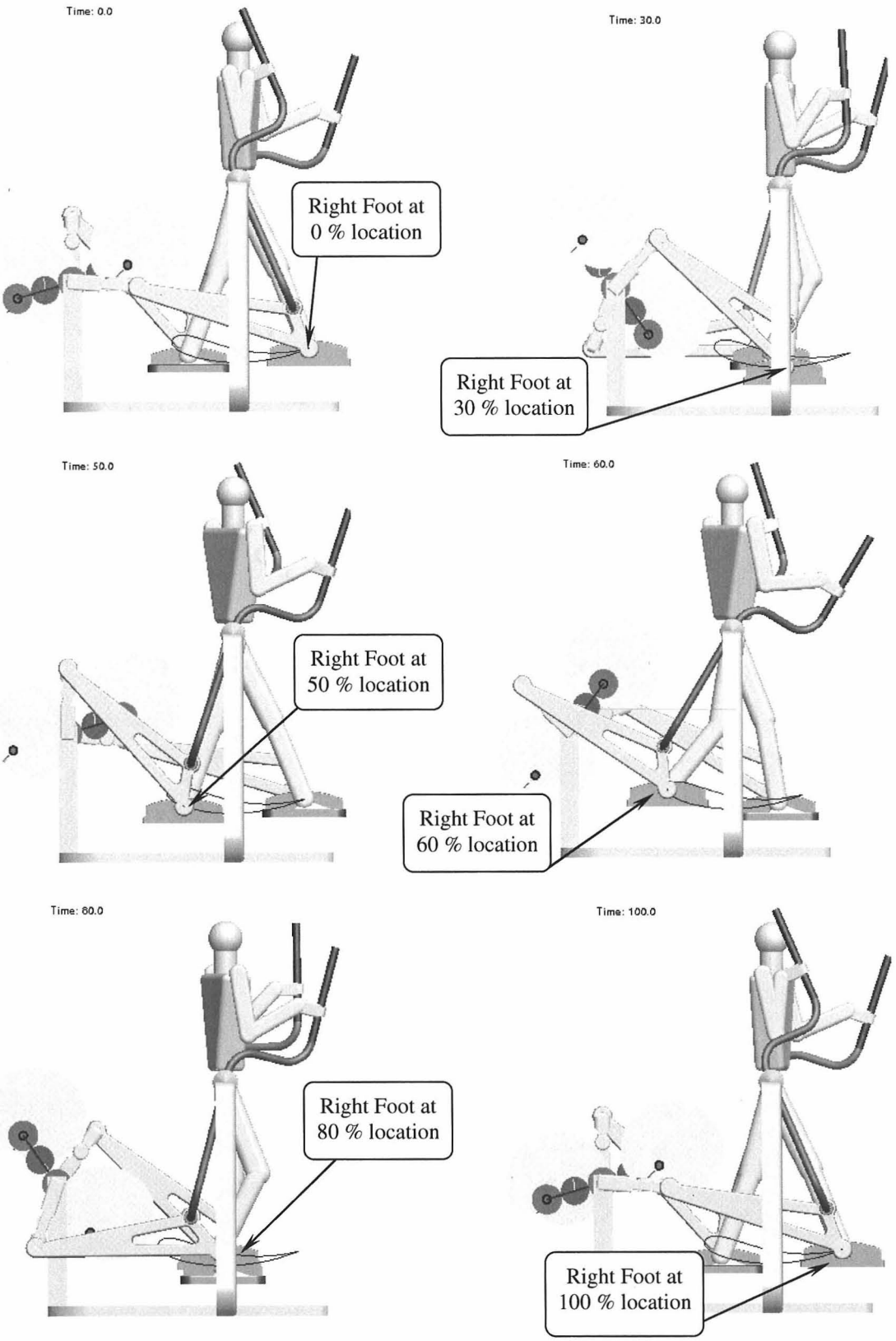

Figure 3.50 Different positions of the right foot when running the gait generation mechanism for one gait cycle (100 seconds in this figure).

It is clear that when the time is 30% of the gait cycle (30 seconds in this case), the right foot will indeed be at the 30% desired location on the coupler curve as in Figure 3.48. The same results will be obtained for the left foot as a similar mechanical timing mechanism is used.

Figure 3.50 shows also that both feet are displaced in time by half a cycle. At instance 50 seconds, it can be seen that the right foot is at 50 % gait location, and the left foot will be almost at the start of the gait cycle, which implies the half cycle displacement between the legs during the operation of the gait generation mechanism.

As mentioned in Section 3.5.3, the cam will *maintain a stationary orientation* while the carrier link is moving; this is because we chose to rotate the cam CW with respect to the carrier link. If an observer looks at Figure 3.50, he can see that the two cams for both sides *maintain a stationary orientation* in all figures. The cam in fact has a relative motion with respect to the carrier link; that if the observer sits on the carrier link, he will observe the cam rotating in a CW direction with respect to him.

The hip and knee joint angle profiles resulting from running the gait generation mechanism for one gait cycle (100 seconds in this case) for both the right and left legs are shown below in Figure 3.51. In the figure, the *average* hip and knee values for the left leg are the same as those for the right leg but *shifted in time by half a cycle*.

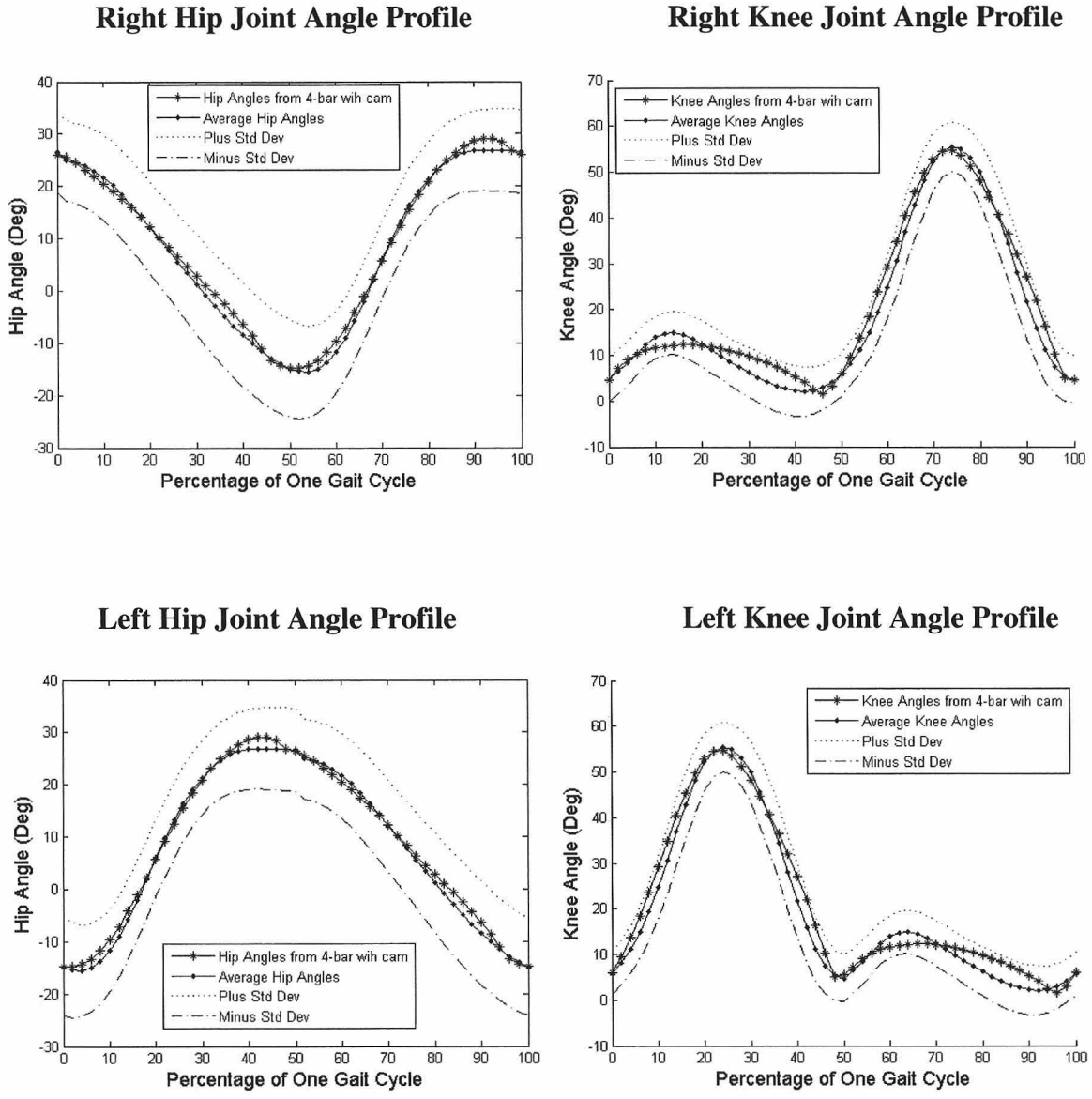

Figure 3.51 The resulted hip and knee joint angles profiles for both the right and left legs when having separate timing mechanism for each leg.

The hip and knee joint angle profiles resulting from running the gait generation mechanism for *three* gait cycles for the right leg are shown below in Figure 3.52. The total period was 300 seconds, where each gait runs for 100 seconds. The corresponding results for the left leg are shown in Figure 3.53.

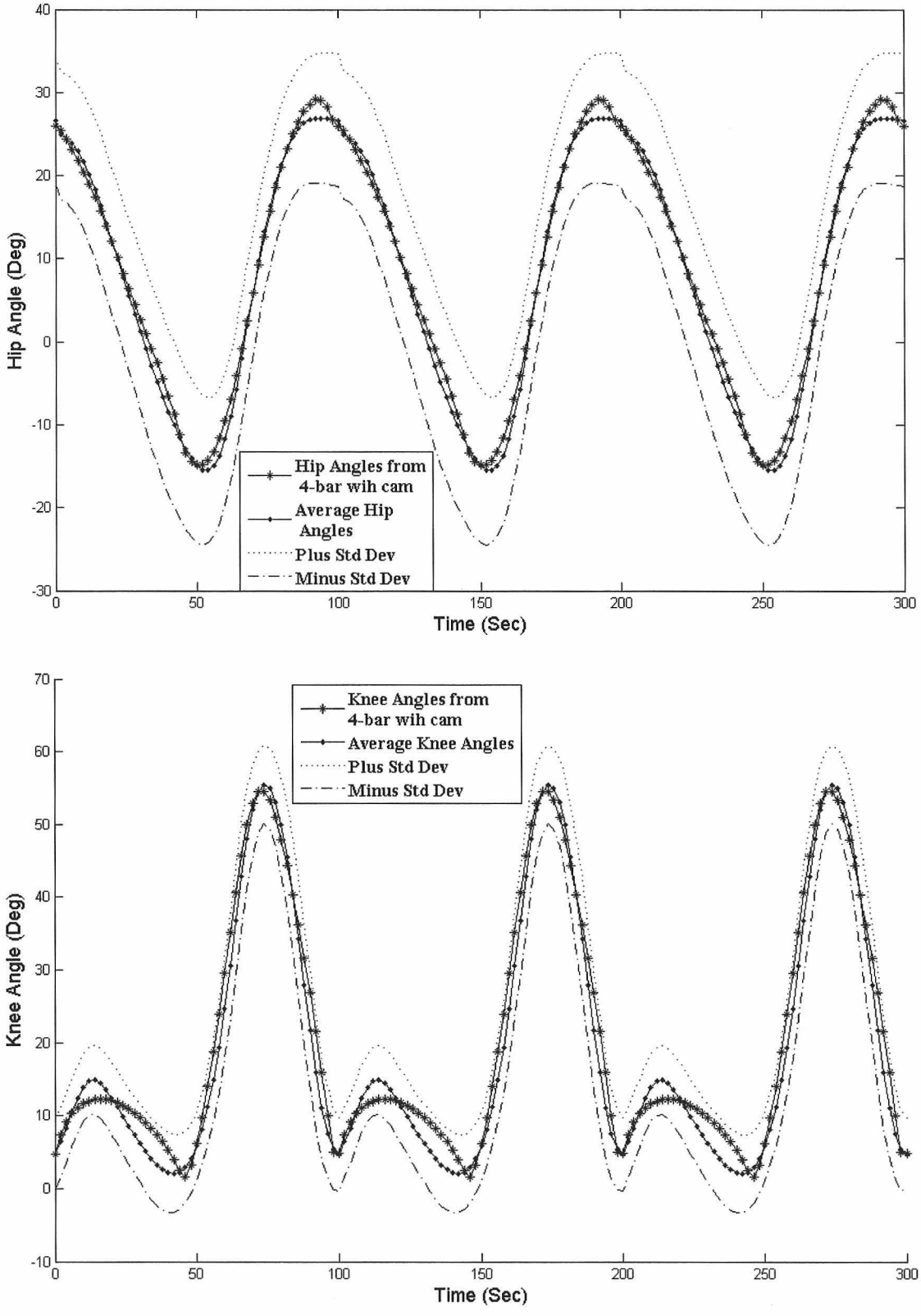

Figure 3.52 The resulted hip and knee joint angles profiles for the right leg when running the gait generation mechanism for three gait cycles.

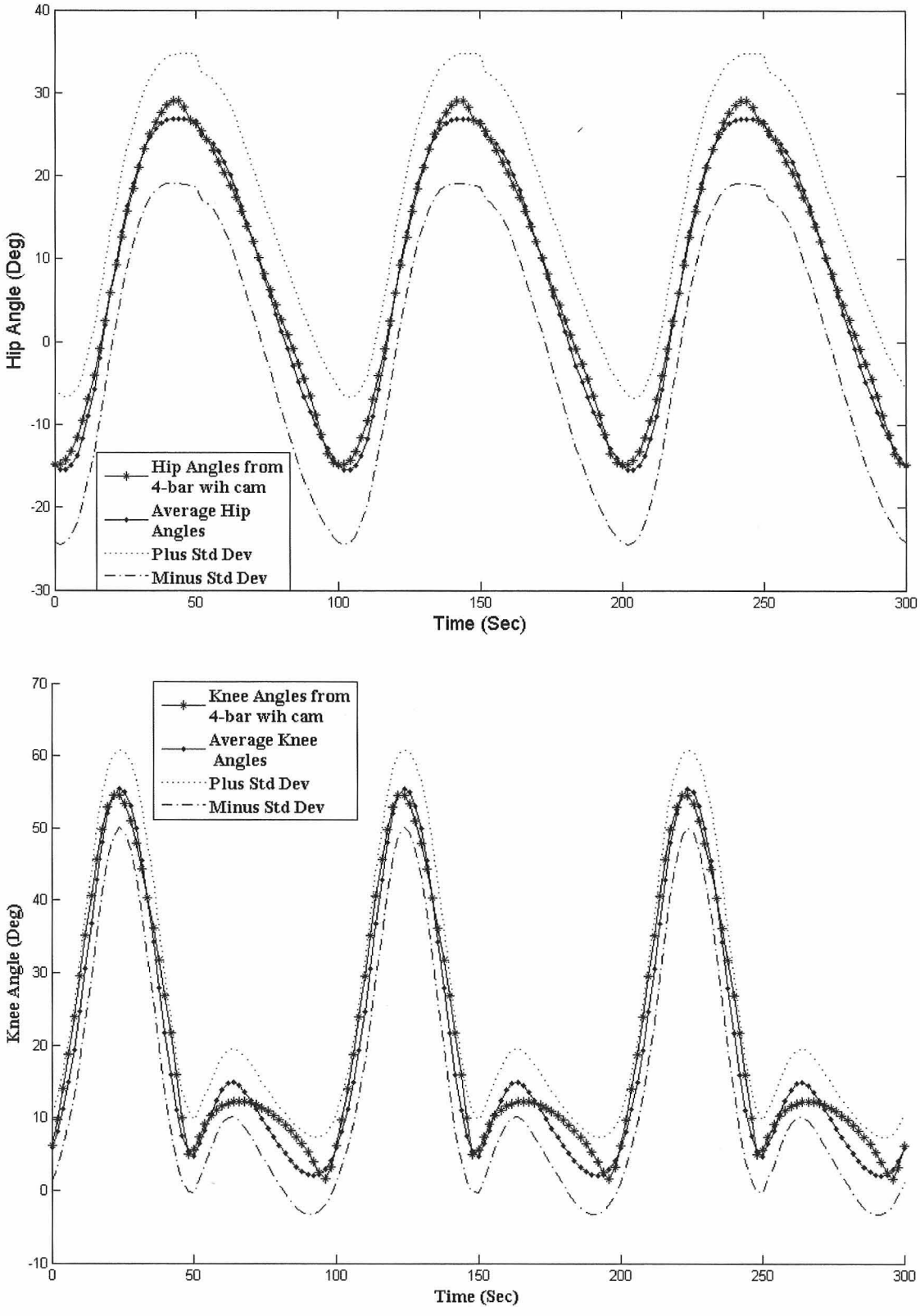

Figure 3.53: The resulted hip and knee joint angles profiles for the left leg when running the gait generation mechanism for three gait cycles.

The phase shift between the two results is around 50%, which means that our gait generation mechanism is providing the needed phase shift (half a cycle) between the two legs. Even though a *new gait starting location* is used because of the fitting result, the resulted hip and knee angles at that starting location are still within the accepted limits, and the fitting did not cause the resulted angles to deviate far.

The simulation illustrates that the proposed mechanical timing mechanism provides the input crank of the four-bar mechanism properly timed motion so that it can produce the properly timed hip and knee motion according to the normative gait data. It also shows that the coordination between the right and left legs can be achieved with a motor running at a constant speed.

Other inputs could also be used instead of the motor to move the timing mechanisms. A *handle-wheel*, for example, can be added and be rotated by the hands of the patient. This motion can be transmitted to the main input shaft to produce coordinated motion of the two legs, where the actual timing of the mechanism is, of course, dependent on the motion of the hands.

Although the use of a mechanical timing mechanism seems to make the system more complicated than the use of a pair of servo control devices, it is a very attractive option due to the reliability and low cost of the mechanical components, as well as the ease of use resulted from it.

Figure 3.54 shows the different views of total the gait generation mechanism including the four-bar mechanisms, the suspension and weight systems, and the mechanical timing mechanisms.

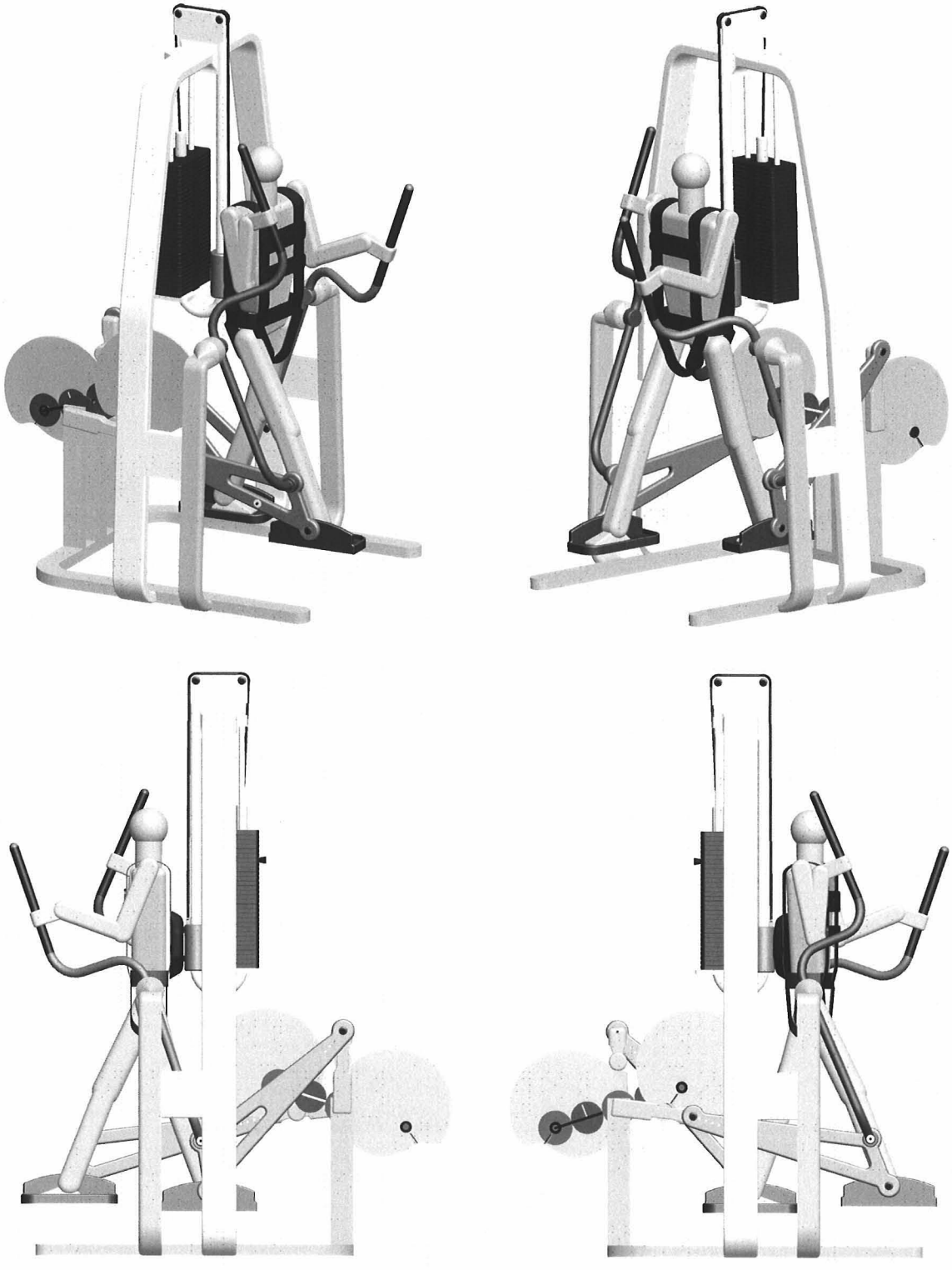

Figure 3.54 Different Views of the Gait Rehabilitation System.

CHAPTER 4

CONCLUSIONS AND FUTURE RESEARCH

4.1 Conclusions

A synthesis process is developed for the design of sagittal-plane gait generation mechanisms. The mechanism designed with this process is shown to generate a path that matches well with the desired ankle trajectory. When incorporated into a gait rehabilitation system, this mechanism will guide a user's ankles to produce coordinated motion of hip and knee joints during gait training. The closed path generated by the mechanism kinematically limits the range of motion (ROM) in the hip and knee joints, which improves gait training safety. The function needed for control of the timing of the mechanism is derived in order to ensure not only the 60/40 split between the stance and swing phases but also the proper timing within each phase in the physiological gait pattern. To further simplify the motion control and the coordination of the pair of mechanisms for the two legs, a combination of cam-follower mechanism and planetary gear system is designed. Computer aided motion simulation shows that the motion of the hip and knee joints generated with the mechanical timing mechanism closely resembles the normal profiles obtained by gait laboratories with healthy people. Although examples are based on certain gait data set and certain user stature to obtain the desired path and the desired timing profile, the methodology developed in this study can be used to design the gait rehabilitation system based on other desired data set or user information.

4.2 Recommendations for Future Research

The conceptual gait training system need to be fully designed and built for functional tests. A dynamic analysis of the user, the machine, and their interaction during training operation will be useful for the detailed design. Various actuation schemes should be designed and implemented to test active and passive modes of operation. The system should incorporate force sensors to measure interaction forces between the device and the user. A module to load and unload the patients for a training session needs to be incorporated into the system.

In the current research, the gait pattern is generated by guiding the ankle along the coupler curve of the linkage mechanism. If at the same time another mechanism can be added to guide the orientation of the legs while the torso is allowed to move slightly in the vertical direction, then the joints profiles can be generated to follow the normal gait profiles even better. Study of the feasibility and tradeoff of this approach might be of interest.

APPENDIX A

GAIT KINEMATICS DATA

The young group's data (from the file Young.gcd by Dr. Chris Kirtley [10]) for hip flexion and extension (hfe) angles, knee flexion and extension (kfe) angles, and ankle plantar flexion and dorsiflexion (apd) angles are shown, along with their standard deviations, in Tables A.1, A.2, and A.3, respectively.

Table A.1 Data for Hip Flexion and Extension (hfe) Angles

Data #	hfe (deg)	Standard Deviation	Data #	hfe (deg)	Standard Deviation
1	25.264	7.674	27	-15.417	9.081
2	24.899	7.687	28	-15.485	8.762
3	24.459	7.746	29	-14.962	8.418
4	23.849	7.853	30	-13.722	8.091
5	22.942	7.997	31	-11.715	7.836
6	21.706	8.177	32	-8.99	7.673
7	20.165	8.359	33	-5.68	7.573
8	18.362	8.514	34	-1.961	7.489
9	16.367	8.63	35	1.98	7.399
10	14.282	8.715	36	5.946	7.304
11	12.146	8.789	37	9.751	7.215
12	9.974	8.876	38	13.257	7.135
13	7.776	8.993	39	16.371	7.088
14	5.569	9.158	40	19.063	7.061
15	3.374	9.359	41	21.333	7.063
16	1.221	9.57	42	23.193	7.105
17	-0.874	9.759	43	24.645	7.182
18	-2.894	9.899	44	25.682	7.299
19	-4.833	9.977	45	26.343	7.443
20	-6.677	9.997	46	26.709	7.599
21	-8.424	9.968	47	26.868	7.734
22	-10.063	9.9	48	26.899	7.844
23	-11.567	9.806	49	26.854	7.918
24	-12.901	9.684	50	26.773	7.944
25	-14.029	9.536	51	26.632	7.94
26	-14.894	9.344			

Table A.2 Data for Knee Flexion and Extension (kfe) Angles

Data #	kfe (degrees)	Standard Deviation	Data #	kfe	Standard Deviation
1	5.375	4.867	**27**	8.167	4.777
2	6.416	4.777	**28**	11.149	5.104
3	8.289	4.729	**29**	14.844	5.611
4	10.476	4.659	**30**	19.335	6.2
5	12.443	4.596	**31**	24.625	6.78
6	13.899	4.615	**32**	30.556	7.234
7	14.735	4.685	**33**	36.788	7.437
8	14.88	4.757	**34**	42.803	7.305
9	14.431	4.837	**35**	48.029	6.835
10	13.578	4.934	**36**	52.015	6.174
11	12.443	5.002	**37**	54.51	5.604
12	11.163	5.042	**38**	55.473	5.384
13	9.846	5.083	**39**	54.961	5.566
14	8.557	5.151	**40**	53.069	6.065
15	7.333	5.25	**41**	49.894	6.728
16	6.181	5.378	**42**	45.561	7.393
17	5.11	5.509	**43**	40.286	7.913
18	4.139	5.598	**44**	34.294	8.226
19	3.301	5.624	**45**	27.951	8.321
20	2.633	5.578	**46**	21.679	8.18
21	2.186	5.47	**47**	15.907	7.76
22	2.032	5.31	**48**	11.053	7.074
23	2.252	5.112	**49**	7.467	6.225
24	2.929	4.902	**50**	5.38	5.5
25	4.113	4.736	**51**	4.722	5.076
26	5.839	4.668			

Table A.3 Data for Ankle Plantar Flexion and Dorsi-Flexion (apd) Angles

Data #	apd (degrees)	Standard Deviation	Data #	apd	Standard Deviation
1	3.029	3.914	**27**	11.882	5.52
2	1.896	3.886	**28**	9.473	6.46
3	0.886	3.767	**29**	5.947	7.583
4	0.353	3.582	**30**	1.612	8.537
5	0.54	3.396	**31**	-2.853	8.947
6	1.487	3.288	**32**	-6.689	8.729
7	2.905	3.252	**33**	-9.202	8.09
8	4.326	3.215	**34**	-10.11	7.353
9	5.546	3.154	**35**	-9.512	6.673
10	6.562	3.104	**36**	-7.789	6.037
11	7.408	3.057	**37**	-5.408	5.44
12	8.15	3.003	**38**	-2.77	4.918
13	8.843	2.969	**39**	-0.169	4.509
14	9.519	2.947	**40**	2.151	4.18
15	10.188	2.94	**41**	4.021	3.915
16	10.83	2.939	**42**	5.354	3.732
17	11.428	2.959	**43**	6.166	3.629
18	11.97	3.02	**44**	6.521	3.577
19	12.467	3.132	**45**	6.54	3.554
20	12.923	3.286	**46**	6.355	3.553
21	13.336	3.476	**47**	6.094	3.57
22	13.692	3.701	**48**	5.841	3.612
23	13.955	3.942	**49**	5.583	3.693
24	14.065	4.193	**50**	5.241	3.81
25	13.902	4.482	**51**	4.669	3.971
26	13.266	4.886			

APPENDIX B

DERIVATION OF SOLUTION FOR CURVE FITTING OF THE POLYNOMIAL TIMING FUNCTION

Having found the solutions for coefficients a_0, a_1, and a_n (see Equations 3.8, 3.10 and 3.22), their expressions are substituted into equation 3.5, the general expression for the polynomial function, to obtain the solutions for the remaining coefficients. First, an index "j"is assigned for every point of the input/output points. Thus, for any point with index "j", the value of the polynomial function at that index can now be expressed as:

$$y_j = \sum_{i=0}^{n} \left(a_i \times \left(\frac{x_j - x_0}{x_N - x_0} \right)^i \right) \tag{B1}$$

Extracting the 0^{th}, 1^{st}, and n^{th} terms from the summation term in Equation B1, we get:

$$y_j = a_n \times \left(\frac{x_j - x_0}{x_N - x_0} \right)^n + \sum_{i=2}^{n-1} \left(a_i \times \left(\frac{x_j - x_0}{x_N - x_0} \right)^i \right) + a_1 \left(\frac{x_j - x_0}{x_N - x_0} \right) + a_0 \tag{B2}$$

Substituting Equations 3.8, 3.17, and 3.22 in B2 yields:

$$y_j = \left(\sum_{i=2}^{n-1} \left(\frac{a_i \times i}{-n} \right) \right) \times \left(\frac{x_j - x_0}{x_N - x_0} \right)^n + \sum_{i=2}^{n-1} \left(a_i \left(\frac{x_j - x_0}{x_N - x_0} \right)^i \right) +$$

$$\left(y_N + \sum_{i=2}^{n-1} \left(\frac{a_i \times (i-n)}{n} \right) \right) \times \left(\frac{x_j - x_0}{x_N - x_0} \right) \tag{B3}$$

Equation B3 could be written as:

$$y_j = \left(\sum_{i=2}^{n-1}\left(\frac{a_i \times i}{-n}\right)\right)\times\left(\frac{x_j - x_0}{x_N - x_0}\right)^n + \sum_{i=2}^{n-1}\left(a_i\left(\frac{x_j - x_0}{x_N - x_0}\right)^i\right) +$$

$$\left(y_N \times \left(\frac{x_j - x_0}{x_N - x_0}\right)\right) + \sum_{i=2}^{n-1}\left(\frac{a_i \times (i-n)}{n}\right)\times\left(\frac{x_j - x_0}{x_N - x_0}\right) \qquad \text{(B4)}$$

Combining all the summation terms under one summation term and taking a_1 as a common factor outside square brackets gives:

$$y_j = \sum_{i=2}^{n-1}\left(a_i\left[\left(\frac{-i}{n}\right)\times\left(\frac{x_j - x_0}{x_N - x_0}\right)^n + \left(\frac{x_j - x_0}{x_N - x_0}\right)^i + \left(\frac{i-n}{n}\right)\times\left(\frac{x_j - x_0}{x_N - x_0}\right)\right]\right) + \left(y_N \times \left(\frac{x_j - x_0}{x_N - x_0}\right)\right) \qquad \text{(B5)}$$

Let

$$b_{ij} = \left[\left(\frac{-i}{n}\right)\times\left(\frac{x_j - x_0}{x_N - x_0}\right)^n + \left(\frac{x_j - x_0}{x_N - x_0}\right)^i + \left(\frac{i-n}{n}\right)\times\left(\frac{x_j - x_0}{x_N - x_0}\right)\right] \text{ and } \quad c_j = \left(y_N \times \left(\frac{x_j - x_0}{x_N - x_0}\right)\right)$$

Equation B5 can be re-written as:

$$y_j = \sum_{i=2}^{n-1}\left(a_i \times b_{ij}\right) + c_j \qquad j = 2, \cdots, N-1 \qquad \text{(B6)}$$

Substituting Equation B6 into the objective function, 3.6 yields:

$$F = \sum_{j=2}^{N-1}\left(\left(\sum_{i=2}^{n-1}\left(a_i \times b_{ij}\right) + c_j\right) - \zeta_j\right)^2 \qquad \text{(B7)}$$

It should be noted that although the summation term in Equation 3.6 is carried out from $j = 1$ to N, the summation term in Equation B7 is carried out from $j = 2$ to $N-1$ since the function at $j = 1$ and N is constrained using the two constraints in equations 3.2 and 3.3. Taking the partial derivative of Equation B7 with respect to the

coefficients a_k's for $k = 2,..., n-1$ and setting the results equal to zero, $n-2$ linear equations are obtained. The general expression for these equations can be given by:

$$\frac{\partial F}{\partial a_k} = 2 \times \sum_{j=2}^{N-1} \left(\sum_{i=2}^{n-1} \left(a_i \times b_{ij} \right) + c_j - \zeta_j \right) \times b_{kj} = 0, \qquad k = 2,..., n-1 \tag{B8}$$

In order to solve the above equations for the unknown coefficients, a_2 through a_{n-1}, Equation B8 is arranged to give:

$$\frac{\partial F}{\partial a_k} = \sum_{j=2}^{N-1} \left(\sum_{i=2}^{n-1} \left(a_i \times b_{ij} \times b_{kj} \right) \right) + \sum_{j=2}^{N-1} \left(\left(c_j - \zeta_j \right) \times b_{kj} \right) = 0, \qquad k = 2,..., n-1 \tag{B9}$$

which can be further rearranged as:

$$\sum_{i=2}^{n-1} \left(a_i \times \left(\sum_{j=2}^{N-1} \left(b_{ij} \times b_{kj} \right) \right) \right) - \sum_{j=2}^{N-1} \left(\left(\zeta_j - c_j \right) \times b_{kj} \right) = 0, \qquad k = 2,..., n-1 \tag{B10}$$

If $\sum_{j=2}^{N-1} \left(b_{ij} \times b_{kj} \right)$ is denoted as B_{ki} and $\sum_{j=2}^{N-1} \left(\left(\zeta_j - c_j \right) \times b_{kj} \right)$ as D_k, Equation B10 can be written as:

$$\sum_{i=2}^{n-1} \left(a_i \times B_{ki} \right) = D_k, \qquad k = 2,..., n-1 \tag{B11}$$

Or in a matrix form as

$$\mathbf{Bx} = \mathbf{d} \tag{B12}$$

where

$$\mathbf{B} = \begin{pmatrix} B_{22} & \cdots & B_{2(n-1)} \\ \vdots & \ddots & \vdots \\ B_{(n-1)2} & \cdots & B_{(n-1)(n-1)} \end{pmatrix}, \quad \mathbf{d} = \begin{pmatrix} D_2 \\ \vdots \\ D_{n-1} \end{pmatrix}, \text{ and } \quad \mathbf{x} = \begin{pmatrix} a_2 \\ \vdots \\ a_{n-1} \end{pmatrix}$$

Thus, the solution to the unknown coefficients, a_2 through a_{n-1}, can be expressed as

$$\mathbf{x} = \mathbf{B}^{-1}\mathbf{d} \tag{B13}$$

APPENDIX C

DERIVATION OF SOLUTION FOR CURVE FITTING OF THE FOLLOWER DISPLACEMENT PROFILE

Applying the first constraint in Equation 3.33 yields:

$$a_0 = 0 \tag{C1}$$

Applying the second constraint in Equation 3.33 yields:

$$\sum_{i=0}^{n}(a_i) = a_0 \tag{C2}$$

Extracting the " n^{th}" & the " 0^{th}" terms from the summation term gives:

$$a_n + \sum_{i=1}^{n-1}(a_i) + a_0 = a_0 \tag{C3}$$

From which, a_n can be written as:

$$a_n = -1 \times \sum_{i=1}^{n-1} a_i \tag{C4}$$

The general expression of the first derivative of Equation 3.33 taken with respect to x_c is given by Equation C5:

$$\frac{dP}{dx_c}(x_c) = P'(x_c) = \sum_{i=1}^{n}\left(a_i \times i \times \left(\frac{x_c - x_{c0}}{x_{cN} - x_{c0}}\right)^{i-1} \times \left(\frac{1}{x_{cN} - x_{c0}}\right)\right) \tag{C5}$$

Applying the third constraint in Equation C5 yields:

$$\frac{dP}{dx_c}(x_{c0}) = P_0' = a_1 \times \left(\frac{1}{x_{cN} - x_{c0}}\right) \tag{C6}$$

From which, a_1 can be written as:

$$a_1 = P_0^{'} \times (x_{cN} - x_{c0}) \tag{C7}$$

Applying the fourth constraint in Equation C5 gives:

$$\frac{dP}{dx_c}(x_{cN}) = \sum_{i=1}^{n} \left(a_i \times i \times \left(\frac{1}{x_{cN} - x_{c0}} \right) \right) = P_0^{'} \tag{C8}$$

Equation C8 can be written in the following form:

$$\sum_{i=1}^{n} (a_i \times i) = P_0^{'} \times (x_{cN} - x_{c0}) \tag{C9}$$

Extracting the " n^{th}" and the " 1^{st}" terms in the summation and noting that the right side of Equation C9 is equal to a_1 given by Equation C7 yields:

$$\sum_{i=1}^{n} (a_i \times i) = (a_n \times n) + \sum_{i=2}^{n-1} (a_i \times i) + (a_1 \times 1) = a_1 \tag{C10}$$

Cancelling a_1 in both sides, a_n can be written as:

$$a_n = \sum_{i=2}^{n-1} \left(\frac{a_i \times i}{-n} \right) \tag{C11}$$

Equations C4 and C11 are two different expressions for the same coefficient; a_n, which both could be equated to obtain the fourth coefficient:

$$a_n = \sum_{i=2}^{n-1} \left(\frac{a_i \times i}{-n} \right) = \left(-1 \times \sum_{i=1}^{n-1} a_i \right) \tag{C12}$$

After some manipulations of Equation C12, we get:

$$\sum_{i=2}^{n-1} (a_i \times (n-i)) + (n \times a_1) = 0 \tag{C13}$$

The above equation will be used to express coefficient a_2 in terms of the other terms as:

$$a_2 = \left(\frac{n \times a_1}{2-n}\right) + \sum_{i=3}^{n-1}\left(\frac{a_i \times (n-i)}{(2-n)}\right) \tag{C14}$$

It should be noted that the summation starting index starts from $i = 3$. When substituting the four coefficient equations in the general equation for the polynomial function, Equation 3.33, the starting index for the all summation terms in the four coefficient equations must be united. The summation term in Equation C11 starts from $i = 2$. Extracting the second term from the summation term in that equation yields:

$$a_n = \sum_{i=2}^{n-1}\left(\frac{a_i \times i}{-n}\right) = \left(\frac{a_2 \times 2}{-n}\right) + \sum_{i=3}^{n-1}\left(\frac{a_i \times i}{-n}\right) \tag{C15}$$

Substituting a_2 from Equation C14 in Equation C15 gives:

$$a_n = \left(\left(\left(\frac{n \times a_1}{2-n}\right) + \sum_{i=3}^{n-1}\left(\frac{a_i \times (n-i)}{(2-n)}\right)\right) \times \frac{2}{-n}\right) + \sum_{i=3}^{n-1}\left(\frac{a_i \times i}{-n}\right) \tag{C16}$$

Simplifying Equation C16 yields:

$$a_n = \left(\left(\left(\frac{2 \times a_1}{n-2}\right) + \sum_{i=3}^{n-1}\left(\frac{2 \times a_i \times (n-i)}{n \times (n-2)}\right)\right)\right) + \sum_{i=3}^{n-1}\left(\frac{a_i \times i}{-n}\right) \tag{C17}$$

Combining both summations into one term yields:

$$a_n = \left(\frac{2 \times a_1}{n-2}\right) + \sum_{i=3}^{n-1}\left(\left(\frac{2 \times a_i \times (n-i)}{n \times (n-2)}\right) + \left(\frac{a_i \times i}{-n}\right)\right) \tag{C18}$$

Taking a_i as a common term gives:

$$a_n = \left(\frac{2 \times a_1}{n-2}\right) + \sum_{i=3}^{n-1}\left(a_i \times \left[\left(\frac{2 \times (n-i)}{n \times (n-2)}\right) + \left(\frac{i}{-n}\right)\right]\right) \tag{C19}$$

The term inside the bracket could be simplified to give:

$$\left[\left(\frac{2\times(n-i)}{n\times(n-2)}\right)+\left(\frac{i}{-n}\right)\right]=\left(\frac{2-i}{n-2}\right) \tag{C20}$$

Thus, Equation C19 becomes:

$$a_n=\left(\frac{2\times a_1}{n-2}\right)+\sum_{i=3}^{n-1}\left(a_i\times\left(\frac{2-i}{n-2}\right)\right) \tag{C21}$$

The summation terms in the equations of coefficients a_2 and a_n start now from $i=3$. Denoting the $\left(\frac{x_c-x_{c0}}{x_{cN}-x_{c0}}\right)$ term as X for simplification, Equation 3.33 can be written as follows:

$$P(x_{cj})=a_n\times \mathrm{X}_j^n+\sum_{i=3}^{n-1}\left(a_i\times \mathrm{X}_j^i\right)+a_2\times \mathrm{X}_j^2+a_1\times \mathrm{X}_j+a_0 \tag{C22}$$

Substituting Equations C14 & C21 in Equation C22 gives:

$$P(x_{cj})=\left[\left(\frac{2\times a_1}{n-2}\right)+\sum_{i=3}^{n-1}\left(a_i\times\left(\frac{2-i}{n-2}\right)\right)\right]\times \mathrm{X}_j^n+\sum_{i=3}^{n-1}\left(a_i\times \mathrm{X}_j^i\right)+$$

$$\left[\left(\frac{n\times a_1}{2-n}\right)+\sum_{i=3}^{n-1}\left(\frac{a_i\times(n-i)}{(2-n)}\right)\right]\times \mathrm{X}_j^2+a_1\times \mathrm{X}_j+a_0 \tag{C23}$$

Combining all the summation terms yields:

$$P(x_{cj})=\left[\sum_{i=3}^{n-1}\left(a_i\times\left[\left(\left(\frac{2-i}{n-2}\right)\times \mathrm{X}_j^n\right)+\mathrm{X}_j^i+\left(\left(\frac{n-i}{2-n}\right)\times \mathrm{X}_j^2\right)\right]\right)\right]+$$

$$\left(\left(\frac{2\times a_1}{n-2}\right)\times \mathrm{X}_j^n\right)+\left(\left(\frac{n\times a_1}{2-n}\right)\times \mathrm{X}_j^2\right)+\left(a_1\times \mathrm{X}_j\right)+a_0 \tag{C24}$$

Equation C24 can be written as follow:

$$P(x_{cj})=\sum_{i=3}^{n-1}\left(a_i\times b(i,j)\right)+c(j) \tag{C25}$$

where: $b(i,j) = a_i \times \left[\left(\left(\frac{2-i}{n-2} \right) \times X_j^n \right) + X_j^i + \left(\left(\frac{n-i}{2-n} \right) \times X_j^2 \right) \right]$ and

$$c(j) = \left(\left(\frac{2 \times a_1}{n-2} \right) \times X_j^n \right) + \left(\left(\frac{n \times a_1}{2-n} \right) \times X_j^2 \right) + (a_1 \times X_j) + a_0$$

Substituting Equation C25 in the objective function's equation, 3.38 yields:

$$F_2 = \sum_{j=2}^{N-1} \left(\sum_{i=3}^{n-1} (a_i \times b(i,j)) + c(j) - \alpha_j \right)^2 \qquad \text{(C26)}$$

Although the summation in Equation 3.38 is carried out from $j = 1$ to N, the summation in Equation C26 is carried out from $j = 2$ to $N-1$ since the function at $j = 1$ *and* N is constrained using the constraints in Equations 3.34 and 3.35.

Taking the partial derivative of Equation C26 with respect to the coefficients a_i's for $i = 3, \ldots, n-1$ and setting the results equal to zero, $n-3$ normal linear equations are obtained.

The general expression for these normal equations can be given by:

$$\frac{\partial F_2}{\partial a_k} = 2 \times \sum_{j=2}^{N-1} \left[\sum_{i=3}^{n-1} (a_i \times b(i,j)) + c(j) - \alpha_j \right] \times b(k,j) = 0, \quad k = 3, \ldots, n-1 \qquad \text{(C27)}$$

Expanding Equation C27 gives:

$$\frac{\partial F_2}{\partial a_k} = \sum_{j=2}^{N-1} \left[\sum_{i=3}^{n-1} (a_i \times b(i,j) \times b(k,j)) \right] + \sum_{j=2}^{N-1} \left[(c(j) - \alpha_j) \times b(k,j) \right] = 0,$$

$$k = 3, \ldots, n-1, \qquad \text{(C28)}$$

Moving the inside summation of the first term in Equation C28 to the front of the outside summation gives:

$$\sum_{i=3}^{n-1}\left(a_i \times\left[\sum_{j=2}^{N-1}[b(i,j)\times b(k,j)]\right]\right)-\sum_{j=2}^{N-1}\left[\left(\alpha_j - c(j)\right)\times b(k,j)\right]=0\,,k=3,...,n-1 \qquad \text{(C29)}$$

If $\sum_{j=2}^{N-1}[b(i,j)\times b(k,j)]$ is denoted as B_{ki} and $\sum_{j=2}^{N-1}\left[\left(\alpha_j - c(j)\right)\times b(k,j)\right]$ as D_k, then

Equation C29 can be written as:

$$\sum_{i=3}^{n-1}\left[a_i \times B_{ki}\right]=D_k\,, \qquad k=3,...,n-1 \qquad \text{(C30)}$$

Equation C30 could be written in a matrix form that will make it easier to solve for the unknown coefficients:

$$\begin{pmatrix} B_{33} & \cdots & B_{3(n-1)} \\ \vdots & \ddots & \vdots \\ B_{(n-1)3} & \cdots & B_{(n-1)(n-1)} \end{pmatrix} \times \begin{pmatrix} a_3 \\ \vdots \\ a_{n-1} \end{pmatrix} = \begin{pmatrix} D_3 \\ \vdots \\ D_{n-1} \end{pmatrix} \qquad \text{(C31)}$$

Inverting the B_{ki} matrix gives:

$$\begin{pmatrix} a_3 \\ \vdots \\ a_{n-1} \end{pmatrix} = \begin{pmatrix} B_{33} & \cdots & B_{3(n-1)} \\ \vdots & \ddots & \vdots \\ B_{(n-1)3} & \cdots & B_{(n-1)(n-1)} \end{pmatrix}^{-1} \times \begin{pmatrix} D_3 \\ \vdots \\ D_{n-1} \end{pmatrix} \qquad \text{(C32)}$$

Thus, the unknown coefficients $a_i's$ for $i=3,...,n-1$ can be easily solved. Once the coefficients a_3 through a_{n-1} are found, these coefficients can be substituted in Equation C14 to find a_2. To find a_n, one can substitute in Equations: C4, C11, or C12. The above derivation was programmed in MATLAB to solve for the coefficients of the polynomial function.

REFERENCES

[1] Mayo Clinic web site. Retrieved October 1, 2009 from the World Wide Web: http://www.mayoclinic.com/health/spinal-cord-injury/DS00460.

[2] Volpe, B. T., Ferraro, M., Krebs, H. I., and Hogan, N., 2002, "Robotics in the Rehabilitation Treatment of Patients with Stroke". Current Atherosclerosis Reports, Vol. 4, 4, p. 270–276.

[3] Colombo, Gery, Joerg, Matthias, Schreier, Reinhard, and Dietz, Volker, November/December 2000, "Treadmill Training of Paraplegic Patients Using a Robotic Orthosis". Journal of Rehabilitation Research and Development, Vol. 37, No. 6, p. 693-700.

[4] Behrman, A., and Harkema S. J., 2000, "Locomotor Training After Human Spinal Cord Injury: A Series of Case Studies," Physical Therapy, Vol. 80, No.7, pp. 688-700.

[5] Schmidt, H., Hesse, S., Bernhardt, R., and Krüger, J., 2005, "Haptic Walker - A Novel Haptic Foot Device", ACM Transactions on Applied Perception, Vol. 2, 2, p. 166-180.

[6] Hesse, S., and Uhlenbrock, D., 2000, "A Mechanized Gait Trainer for Restoration of Gait". Journal of Rehabilitation Research and Development, Vol. 37, 6, p.701-708.

[7] Wilson, Michael S., Qureshy, Huma, Protas, Elizabeth J., Holmes, S. Ann, Krouskop, Thomas A., and Sherwood, Arthur M, July/August 2000, "Equipment Specifications for Supported Treadmill Ambulation Training: A Technical Note". Journal of Rehabilitation Research and Development, Vol. 37, No. 4.

[8] Jezernik, S., Colombo G., Keller T., Frueh H., Morari M., 2003, "Robotic Orthosis Lokomat: a Rehabilitation and Research Tool", Neuromodulation, Vol. 6(2), pp.108–115.

[9] Whittle, Michael W. "Gait Analysis: An introduction", fourth edition. ISBN-13: 978-0-7506-8883-3. Ch.2, p54 and p73.

[10] Clinical Gait Analysis Normative Gait Database. Retrieved April 1, 2005 from the World Wide Web: http://guardian.curtin.edu.au/cga/data/index.html and http://www.univie.ac.at/cga.

[11] Craig, John J., 1989. "Introduction to Robotics, Mechanics and Control", Third Edition, Pearson Education, Inc.

[12] Winter, David A., 1979, "Biomechanics of Human Movement", Wiley, New York, p. 48.

[13] Hrones , John A. and Nelson, George L., 1951, "Analysis of The Four Bar Linkage". Published jointly by The Technology Press of the Massachusetts Institute of Technology and John Wiley & Sons, Inc., New York.

[14] Waldron, Kenneth J. and Kinzel, Gray L., (1999). "Kinematics, Dynamics, and Design of Machinery". John Wiley & Sons, Inc.

[15] Ji, Zhiming and Manna, Yazan, Sep. 2008,"Synthesis of a Pattern Generation Mechanism for Gait Rehabilitation", Journal of Medical Devices, Volume 2, Number 3, Paper # 031004.

[16] Ullah, I. and Kota, S.,1997, "Optimal Synthesis of Mechanisms for Path Generation Using Fourier Descriptors and Global Search Methods" ASME J. Mech. Des., p. 119:504–510.

[17] Pletenetskyy, Andriy, 2007, "Design of Gait Rehabilitation Mechanism System", Master's Thesis, New Jersey Institute of Technology.

[18] Steven C. Chapra, Raymond P. Canale, 2002, "Numerical Methods for Engineers w*ith Software and Programming Applications*", Fourth edition. McGraw-Hill Higher Education.

[19] Asaithambi, N. S. , 1995, "Numerical Analysis, Theory and Practice". Saunders College Publishing.

[20] Ramsay, J.O, and Silverman, B.W. , 2005, "Functional Data Analysis", Second Edition, Springer Science Business Media, Inc.

[21] Milne, William Edmund, 1973, "Numerical Calculus", Seventh edition. Princeton University Press.

[22] Robinson, Enders A., 1981, "Least Squares Regression Analysis in Terms of Linear Algebra".

[23] Mosteller, Frederick , and Tukey, John W., 1997, "Data Analysis and Regression, A Second Course in Statistics". Addison-Wesley Publishing Company.

[24] Tutorial in National Instruments website, Retrieved Apr 9, 2009 from the World Wide Web: http://zone.ni.com/devzone/cda/tut/p/id/3367 and http://www.ni.com/swf/presentation/us/motion .

[25] Servomotor Handbook, Dr. Stephen O'Neil, Retrieved Apr 9, 2009 from the World Wide Web: http://www.micromo.com/n128948/n.html .

[26] Mabie, Hamilton H. and Reinholtz, Charles F., 1987, "Mechanisms and Dynamics of Machinery", 4th edition. John Wiley & Sons, Inc.

[27] Ji, Zhiming and Manna, Yazan A. "Size Minimization of Disk Cams with Roller-Followers under Pressure Angle Constraint", Dec. 2008, Journal of Mechanical Engineering Science, Vol. 222, No C12, ISSN 0954-4062.

[28] Mallik, Asok Kumar, Ghosh, Amitabha, and Dittrich, Gunter, 1994, "Kinematic Analysis and Synthesis of Mechanisms", Ch. 9, CRC Press, Boca Raton.